Chronic Dysregulation of the Cerebrovasculature in a Mouse Model of Repetitive Mild Traumatic Brain Injury

Thesis

Chronic Dysregulation of the Cerebrovasculature in a Mouse Model of Repetitive Mild Traumatic Brain Injury

Cillian E. Lynch, M.Sc.

A thesis submitted for the degree of Doctor of Philosophy

in the discipline of Neuroscience

Supervisors: Dr. Corbin Bachmeier

Dr. Benoit Mouzon

OU Affiliated Research Center (ARC):

Roskamp Institute

2040 Whitfield Avenue

Sarasota, Florida, 34243, USA

Declaration:

I hereby state that the work presented in this thesis is my own, except where otherwise stated, and that this work has not been submitted for any other professional qualification.

Acknowledgements:

I would like to extend my sincerest thanks to my supervisors, Dr Corbin Bachmeier and Dr Benoit Mouzon, and to my CEO and fellow Irish expatriate Dr Fiona Crawford, for their insight, support and guidance, and joviality throughout the course of my Ph. D studies.

I would also like to thank my fellow Ph. D. Students, current and past, for their help with and sometimes, much needed distraction from, my lab work and studies.

Publications:

1. Front Aging Neurosci. 2017 Dec 22;9:416. doi: 10.3389/fnagi.2017.00416. eCollection 2017.

   Negative Impact of Female Sex on Outcomes from Repetitive Mild Traumatic Brain Injury in hTau Mice Is Age Dependent: A Chronic Effects of Neurotrauma Consortium Study.

   Ferguson SA, Mouzon BC, Lynch C, Lungmus C, Morin A, Crynen G, Carper B, Bieler G, Mufson EJ, Stewart W, Mullan M, Crawford F.

2. Brain Injury

   Impact of age on acute post-TBI neuropathology in mice expressing humanized tau: A Chronic Effects of Neurotrauma Consortium Study.

   Benoit Mouzon, Nicole Saltiel, Scott Ferguson, Joseph Ojo, Cillian Lynch, Carlyn Lungmus, Moustafa, Algamal, Alexander Morin, Benjamin Carper, Gayle Bieler, Elliott J. Mufson, William Stewart, Michael Mullan, Fiona Crawford.

3. Brain Inj. 2016;30(12):1414-1427.

   Chronic cerebrovascular abnormalities in a mouse model of repetitive mild traumatic brain injury.

   Lynch CE, Crynen G, Ferguson S, Mouzon B, ParisD, Ojo J, Leary P, Crawford F, Bachmeier C.

4. J Neuropathol Exp Neurol. 2016 Jul;75(7):636-55. doi: 10.1093/jnen/nlw035. Epub 2016 May 31.

   Chronic Repetitive Mild Traumatic Brain Injury Results in Reduced Cerebral Blood Flow, Axonal Injury, Gliosis, and Increased T-Tau and Tau Oligomers.

   Ojo J, Mouzon B, Algamal M, Leary P, Lynch C, Abdullah L, Evans J, Mullan M, Bachmeier C, Stewart W, Crawford F

Abstract

There are over 2 million reports of Traumatic Brain Injury (TBI) every year in the United States alone, the majority of which are classified as a mild head injury. Incidences of mild TBI (mTBI), the kind of which are sustained most routinely by contact sports athletes, active military personnel, and by lesser extent, the general population, are now well accepted as being a definitive risk factor for development of chronic neurodegenerative disorders and debilitating illnesses, such as Chronic Traumatic Encephalopathy (CTE), thus leading to mild head injury being termed as a silent epidemic, and one desperately in need of further pre-clinical investigation and clinical therapeutics.

To date, the diagnosis of CTE has been based on late-stage, post-mortem neuropathological assessment of brain tissue, precluding the possibility of prophylactic or interventional therapy in human patients presenting with symptomatology too ambiguous for antemortem diagnosis, and ergo, appropriate clinical trial stratification. Moreover, the current pathognomonic neuropathological prerequisite feature for CTE diagnosis, diffuse aggregates of phosphorylated Tau protein (pTau), specifically pTau immune-positive subpial astrocytic scars in presence of perivascular foci of pTau positive neurons and astrocytes at the depths of the sulci, poses a difficult therapeutic target, even if a diagnostic were available for the pre-symptomatic stage of the disease.

Recently, it has been reported that military personnel and players of contact sports experiencing repetitive m-TBI (r-mTBI), as well as individuals suffering from chronic TBI-related illness, demonstrate a deficit in Cerebral Vascular Reactivity (CVR), the ability of the cerebral

vasculature to dilate in response to a vasoactive stimulus. This physiological impairment is non-invasively detected following repeat mTBI, and to be sustained at chronic time-points post-injury in both repetitive mTBI and moderate to severe TBI patients alike, implicating CVR detriment as an endophenotypic biomarker and possible *in vivo* diagnostic of TBI-related neuropathogenesis, and Traumatic Cerebral Vascular Injury (TCVI).

In this thesis, I developed and validated a preclinical *in vivo* imaging setup to examine CVR in our CTE-like neuropathology exhibiting mouse model of r-mTBI, with an aim to characterizing the evolving pathobiology of TCVI and concurrent neurobehavioral impairment, and their correlation to perturbed CVR. I demonstrated recapitulation of the CVR deficit seen in the human population in our animal model, alongside sustained memory and learning impairment, and signs of an underlying response of the cerebral vasculature to injury. These finding implicate measurement of CVR as a valid preclinical diagnostic, and the treatment of TCVI as a compelling parallel pathological target in r-mTBI.

Table of Contents

List of Tables

List of Figures

Chapter 1. Introduction

1.1. Background:

Traumatic brain injury (TBI) is a term used to describe a head trauma caused by an external physical force, which affects normal brain function. There are over two million clinically presented incidences of TBI per year in the United States alone, accounting for approximately 30% of all injury related fatalities[1], and an estimated 5.3 million American patients at present coping with chronic TBI-related disability[2,3]. A majority of reported head injuries (approximately 70%) falls in to the category of mild TBI (mTBI)[4], with a reported 15% of mTBI patients experiencing chronic symptoms following injury[5-9]. In comparison to a moderate-to-severe TBI, which is almost invariably accompanied by a prolonged loss of consciousness for greater than 30 minutes following injury, amnesia, or immediate physical damage to the brain[10], mTBIs are often more difficult to diagnose, due to the comparatively swift resolution of symptoms, and lack of evidence of injury on standard hospital imaging modalities[11]. Criteria for having sustained an mTBI include any confusion, loss of memory, transient and focal neurologic deficit, alteration in mental state, or loss of consciousness for thirty minutes or fewer; or for longer, but with an initial Glasgow Coma Scale (GCS) score of between 13 and 15[11-13]. While the term “concussion” is often used in unison and interchangeably with mTBI in both the clinic and the literature, a “sub-concussive” head injury may be defined as a cranial impact that does not result in a diagnosis of concussion/mTBI on the aforementioned criteria[14].

There has only relatively recently been heightened concern over repetitive mTBI (r-mTBI) acquired in professional and collegiate contact sports and military duty. Repetitive concussive and sub-concussive head injuries in the realm of athletics are now generally thought to be

associated with long and short term functional and neuropsychological impairments[15-19]. Congruently, the most frequent combat-related injuries seen in veterans and military personnel returning from Iraq and Afghanistan are mTBIs[20], acquired from blunt force head impact, motor vehicle accidents, and high pressure waves from explosive blasts[21,22]. Much like the functional and cognitive impairments exhibited by current and retired athletes, veterans returning from the theatre of war are now understood to have profound neurological and neuropsychological complications as a result of their history of warzone mTBIs[23-25].

The very clear burden of TBI on both the healthcare system and patient quality of life has begot extensive preclinical research and clinical trials aimed towards improving functional outcome following head trauma[26], however, all phase III clinical trials to this point have failed[27-29]. The almost schismatic success in treatment of TBI in animal models, versus failure in clinical trials, is in part due to the lack of any animal model recapitulating the diverse pathological and physiological sequelae of the human condition, and so, there is an incomplete understanding of the pathogenesis and evolution of r-mTBI related neurodegeneration. Treatment is curtailed still further by the inherent heterogeneity of TBI in the human population, for example, the aforementioned spectrum of (sub-)concussive to moderate to severe, and resultant erroneous recruitment and stratification of subjects in to clinical trial cohorts. As such, there is an ever-growing need for further scientific understanding of, and therapeutic intervention against the TBI phenotype.

1.2. Repetitive Head Trauma and CTE

The first known medical record of a history of repeat head trauma being linked to a neurodegenerative illness was described in a retired boxer as Dementia Pugulistica[30], and has since been given the name Chronic Traumatic Encephalopathy (CTE)[31]. The exact nature of the causal link between repetitive mTBI and development of CTE is much researched yet disproportionately unexplained. To date, the most accepted biological feature of CTE is the microtubule associated protein Tau (MAPT), which is expressed in both the peripheral and central nervous system[32], functioning to stabilize the microtubule[33] and mediate axonal transport[34-36]. CTE is characterized pathologically by diffuse deposition of hyper-phosphorylated tau (pTau) immune-reactive neurofibrillary and astrocytic tangles throughout the temporal and frontal cortices and propensity for accumulation of pTau species at perivascular locations at the depths of cerebral sulci[37]. While the aforementioned unique tau pathology, observable only at post-mortem, is a prominent feature of CTE, this disease can also be associated with a host of co-pathologies including, but not limited to, amyloid plaque formation, deposition of TAR DNA Binding Protein 43 (TDP-43), sustained microglial inflammatory profile, white matter axonal degeneration, and Lewy body neuritic inclusions[31,38].

CTE has only recently become fiercely researched, following many studies identifying the disorder in individuals with a history of r-mTBI, including reports documenting CTE in former National Football League (NFL) American football players[39,40], and further case reports confirming CTE pathology at postmortem in athletes[41], and military personnel exposed to blast shock wave (BSW) injury[37]. Indeed, from a critical review of 158 published case studies, of all CTE cases

diagnosed symptomatically in the past decade, 50% are seen in professional American football players[42], more than 20% of which did not show CTE pathology postmortem. Furthermore, 5% of cases showing classic CTE hallmarks postmortem despite being clinically asymptomatic for CTE[42]. Similarly, a recent report by Hazrati et al[43] mirrors the aforementioned review, showing non-CTE like pathology and absence of overt Tau hyper-phosphorylation and aggregation in post-mortem brains of retired athletes previously diagnosed with CTE, and instead presenting with pathologies likening those of vascular and motor neuron disease, and AD[43].

The postmortem diagnosis of CTE was initially based heavily on the Braak staging system[31,41], the neuropathological staging criteria used in the general diagnosis of tauopathy post-mortem[44], with the degree and topographical distribution of paired helical filamentous (PHF) Tau, as identified by the monoclonal antibodies against both Serine 202 and Threonine 205 of pTau (AT8), and against Serine 202 alone (CP13), with AT8 positive staining representing a hyperphosphorylated conformational form of pTau, and CP13 positive staining identifying a lower molecular weight pTau[42,45]. Pathology progression, as originally defined by Braak staging, increases in severity from Braak Stage I - IV. In the mildest of the Braak stages, Stage I, PHF Tau pathology is restricted to discrete foci throughout the cerebral cortex, and clustering around small blood vessels and at the depths of the sulci. Stage II CTE manifests as a multi-epicenter of PHF Tau staining at the depths of the cerebral sulci and spread of PHF Tau immune-reactive tissue to the superficial layers of the adjacent cerebral cortex. Stage III CTE pathology is much more widespread than Stages I and II, with the frontal, insular, temporal and parietal cortices, amygdala, hippocampal, and entorhinal cortex showing PHF Tau Neurofibrillary tangle (NFT) pathology. In Stage IV CTE, most regions of the cerebral cortex and temporal lobe exhibit

aggressive PHF Tau NFT immune reactivity throughout[31]. The graded increase and distribution of PHF Tau NFTs and astroglial tangles (ATs) from Stage I – IV CTE is accompanied by a concomitant rise in perturbed axonal profile, limited in Stage I and II CTE to the subcortical white matter and diencephalon, but found in Stages III – IV as more extreme axonal loss and pathology throughout the frontal and temporal lobes[37,41].

The above rather general pathologic diagnostic criteria have since been refined by a recent case report in which a team of seven neuropathologists evaluated 25 cases of already confirmed tauopathy, spanning CTE, Alzheimer's Disease, progressive supranuclear palsy (PSP), Argyrophilic Grain Disease (AGDA), Corticobasal Degeneration (CBD), primary age-related tauopathy, and Parkinsonism dementia complex of Guam[46]. The neuropathologists were blinded to the sample's diagnostic assignment, and any discrepancies were discussed and resolved in person following collective evaluation. This seminal consensus report concludes that there exists "a pathognomonic lesion of CTE that consists of an accumulation of abnormal Tau in neurons and astroglia distributed around small blood vessels at the depths of sulci in the cortex in an irregular pattern"[46]. Of notable deviation from the original Braak staging of the disease[31] is the prevalence of pTau immune-positive subpial astrocytic scars in presence of perivascular foci of pTau positive neurons and astrocytes at the depths of the sulci[46] as a specific diagnostic for CTE (see Figure 1.1).

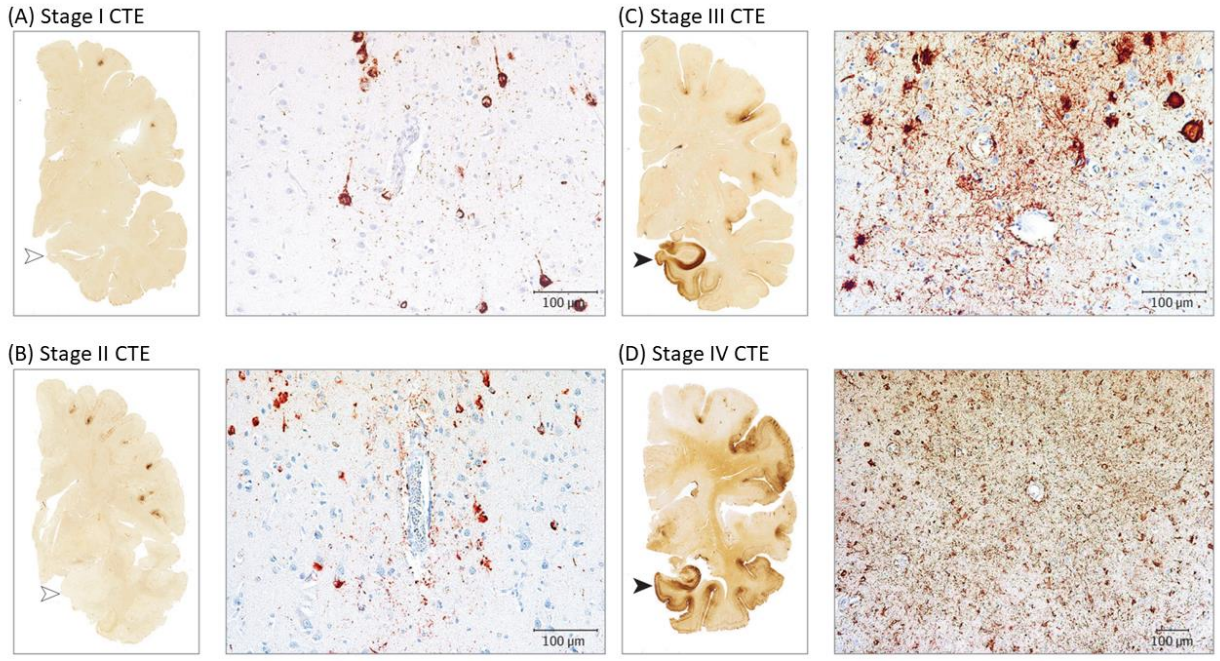

Figure 1.1. Neuropathological evaluation of CTE stages I – IV. Representative Images of phosphorylated Tau at CTE pathological stages I, II, III, and IV, in a convenience sample of 202 brains donated by deceased former players of American football, using the NINDS-NIBIB consensus criteria[46]. (A) Former college football player with stage I CTE, identified by the presence oftwo perivascular pTau lesions at the sulcal depths of the frontal cortex, in absence NFT in the temporal lobe (arrowhead), but with NFTs and neuritic foci encircling a small blood vessel. (B) Former NFL player diagnosed with stage II CTE, exhibiting pathognomonic pTau CTE lesions at the sulcal depths of both the frontal and medial cortices (open arrowhead), and perfunctory NFTs and dot-like and thread-like neurites encircling small blood vessels. (C) Former NFL player with stage III CTE, denoted by diffuse pTau and NFT pathology throughout the frontal and insular cortices and entorhinal hippocampus (black arrowhead), and perivascular CTE lesioning by NFTs and neuritic clusters around small blood vessels. (D) Stage IV CTE pathology in a former NFL player, identified by large and confluent CTE lesions throughout the frontal, temporal, and insular cortices, in combination with diffuse NFT pathology of the entorhinal cortex and amygdala (black arrowhead), and and aggressive perivascular NFT formation.

CTE denotes Chronic Traumatic Encephalopathy; NFT, Neurofibrillary Tangle; pTau, phosphorylated Tau. All microscopic images are taken from 10µm thick paraffin-embedded brain tissue sections, stained with the monoclonal mouse antibody AT8, directed against monoclonal mouse pTau. Positive pTau staining appears red. All hemispheric images taken from 50µm thick tissue sections, stained with monoclonal mouse antibody against phosphor-serine 202 of pTau, considered an early site of Tau phosphorylation in NFT formation. Positive pTau staining appears brown. Images modified from Mez et al, JAMA, 2017[45].

Using the afore mentioned collaborative consensus criteria, 177 of 202 post mortem brains of deceased American football players were since diagnosed as having had CTE[45], bolstering the implication of a history of contact sports being causal in the development of this neurodegenerative disease. The higher severity of CTE pathology (Stages III and IV) was

distributed across the more professional level of play, with the greater proportion of collegiate, semi-professional, Canadian Football League, and National Football League (NFL) players exhibiting severe pathology, compared to mild and infrequent perivascular lesions (Stage I and II) seen in former high school players[45]. The fact that the duration of play for mild cases was 13 years, in comparison to 15.8 years for severe CTE diagnosis, suggests that it is the frequency of head trauma, which may be higher at the more professional league, sooner than the length of exposure, that is most culpable in the pathogenesis of the disease[45]. Both mild and severe CTE patients were retrospectively recorded as having presented clinically with a host of behavior and mood symptoms including impulsivity, depression, apathy, anxiety, hopelessness, explosivity, suicidality, and physical and verbal violence[45]. Memory, executive function, and attention symptoms were seen in 73%, 73% and 69% of mild CTE cases, respectively, and 92%, 92% and 81% of severe CTE cases, respectively[45]. The insensitivity of clinical behavioral and memory assessments with relation to CTE diagnosis is again highlighted here, much as it was by Gardner[42] and Hazrati[43], as 25% of severe CTE cases in the current report by McKee and colleagues[45] were diagnosed with AD prior to death, and 85% of said severe cases were diagnosed by neuropathologists, blind to the case histories, as having dementia post mortem[45]. As big an improvement as the revised post mortem CTE diagnostic criteria is[46], there remains the issue of ambiguous symptomology between this and other neurodegenerative disorders[45]. Owing to these discrepancies in clinical presentation and neuropathological co-morbidity, a companion in-vivo diagnostic would be profoundly useful in the early detection and treatment of r-mTBI related neurodegenerative disease.

Model ***With Reference***	**Animal and Genotype**	**Number and Interval of Hits**	**Age at injury, to animal euthanasia**	**Effects on protein aggregate pathology**	**Additional Observations**
Momentum Exchange[47,48] (Single Mild)	Rat (Wistar)	1x, or 3x, at 1 per 6 hours	Adult, to 1d, 4d, or 10d	Neurofilaments	Axonal Injury, Astrogliosis, and Edema
Wayne State[49,50] (Repetitive Mild)	Mouse (C57BL/6)	1x, 5x, or 10x, at 1 per day, 95g or 30g weight drop	2m, or 1m, to 1m	Increased pTau Levels	Astrogliosis. Transient Locomotor Impairments, Anxiety and Depression-like Behavior,
Harvard Method[51,52] (Repetitive Mild)	Mouse (C57BL/6); ApoE4	5x, 7x, or 10x at various intervals	3m to various, 6m, 1y	No increase in $A\beta_{40}$, Tau, or Development of Amyloid Plaques or NFTs	Long Term Behavioral Deficits and Astrogliosis, No Cognitive Deficits in ApoE Groups
	Mouse (C57BL/6); T44 Tau; Tau KO	1x, or 7x, in 9d	2m -3m, to various timepoints	pTau Increase and Progressive Spread Throughout Brain over Time	Cellular Apoptosis, Disinhibited Behavior
Maryland[53] (Repetitive Mild)	Mouse, hTau; $hTau^{+/+}$, $hTau^{+/-}$, $hTau^{-/-}$	1x or 2x, 1 per 1d	4-6m, to 1 year	Absence of Tau expression aids behavior. Lower APP expression in KO	No difference in Astrogliosis or Microgliosis. Behavioral deficits.
Hit and Run[54,55] (Single Mild)	Mouse (C57BL/6)	1 Impact	2.5-3m, to 1h, 1d, 3d, 1w, 2w, 1m	Not Reported	Impaired Motor function, Astrogliosis, and Axonal Degeneration
Blast TBI[37,56] (Single Mild)	Mouse (C57BL/6)	1 Impact	3-4m, to 1d, 1m	Increased pTau, but no Difference in APP	Decreased Exploration
	Mouse (C57BL/6)	1 Impact	2.5m to 2w	Increased pTau and APP Levels	Astrogliosis and Microgliosis, Decreased Long Term Potentiation, Vascular Pathology
Blast TBI[57,58] (Repetitive Mild)	Mouse (C57BL/6); ($CX3CR1\text{-}GFP^{+/-}$)	1x, or 3x, 1 per 24h	3-4m, to 1h, 4h, or 14d	Rapid, but Transient, pTau and AT8-positive perivascular Tau Accumulation, Disappearing Within 4h	Astrogliosis and Microgliosis, Vascular Pathology, BBB Disruption, Increase in Inflammatory markers. No Behavior Data Reported.
	Mouse (C57BL/6)	1x, or 3x, 1 per 24h	3-4m, to 14d, or 30d	Cerebellar Neuronal Cell Loss, Increased APP,	Astrogliosis and Microgliosis Motor Function Impairment,
Controlled Closed Head Impact[59-63] (Repetitive Mild)	Mouse, hTau; $hTau^{+/+}$	5x, 1 per 48h	2-3m, 6-12m	No changes in pTau or $A\beta_{40}$. Progressive APP accumulation with injury. Thinning of the corpus callosum.	Astrogliosis and Microgliosis. Progressive and Long Term Behavioral Deficit. Disinhibited Behavior. No Long-Term Motor Deficit
	Mouse (C57BL/6)	5x, 1 per 48h	2-3m, to 24m	No changes in pTau or $A\beta_{40}$. Progressive APP accumulation with injury. Thinning of the corpus callosum.	Astrogliosis and Microgliosis. Progressive and Long Term Behavioral Deficit. No Long-Term Motor Deficit
	Mouse, hTau; $hTau^{+/+}$	2x per week, for 12w	2-3m, to 3m	Increased total and pTau. Progressive APP accumulation with injury. Thinning of the Corpus callosum.	Astrogliosis and Microgliosis. Progressive and Long Term Behavioral Deficit. Disinhibited Behavior. No Long-Term Motor Deficit
	Mouse (C57BL/6)	6x per day, for 7d	Adult Male, to 7d, 1m, or 6m	Increased pTau, AT8-positive Tau Accumulation	Astrogliosis and Microgliosis No Behavior reported.

Table 1.1. Animal models of head injury relevant to the dose, frequency, and neurobehavioral and pathological sequelae of that seen in the military and sports human population. h: hours; d: days; w: weeks; m: months. Elements of the table have been modified from Edwards et al, Biochem Biophys Res Commun, 2017[64].

1.3. Animal Models of Repetitive Mild Traumatic Brain Injury.

The heterogenous nature of mTBI in the human population makes it practically impossible for any one single animal model to recapitulate all of the pathological and behavioral sequelae of r-mTBI related neurodegeneration[64]. Current murine models of r-mTBI producing pathological and behavioral deficits most representative of the human TBI population are listed in *Table 1*. These include momentum exchange, whereby a ballistic impactor converges on an aluminum plate attached to the rodent's head[47,48]; the Wayne State and Harvard approaches, which institute a weight drop impact to the head, and preclude superfluous and unintentional impact[49-52]; the Maryland Model, in which a steel ball is rolled in to a coupling arm attached to the frontal portion of the animal's facial area, allowing for a frontal impact[53]; the "Hit and Run" paradigm, which uses a modified Controlled Cortical Impact (CCI) approach; single and repeat blast TBI, which uses a number of techniques to produce a blast wave that propagates through the brain matter, mimicking the form of injury endured by military personnel[37,56-58,65-67]; and numerous controlled closed head injury (CHI) models, typically relying on an electromagnetically driven piston with an impactor attached to the end, delivering a precisely calibrated insult[59-63,68-71].

In terms of mouse strains, both wild type (C57BL/6) and transgenic human tau (hTau) mouse models of r-mTBI have recapitulated many aspects of CTE-like pathology, alongside impairment in correlate behavioral indices. Wild type C57BL6 mouse brains almost exclusively express the isoform of tau with only 4 repeat microtubule binding domains (MTBs) located at the C-terminal, otherwise known as the 4R isoform of Tau, whereas human adults express approximately equal proportions of both 3R and 4R Tau isoforms throughout the CNS[72]. In an effort to mimic the

human condition more closely, many researchers have used hTau mice as animal models of r-mTBI. These mice express all six isoforms of human tau on a null murine tau background[73]. As can be seen in *Table 1*, the pathologies most robustly and unanimously reported across hit paradigms are the neuroinflammatory profile, axonal damage and white matter loss, and in a great proportion of cases, vasculopathy of varying degree. Reports of increases in pTau and higher oligomeric AT8-positive aggregates are mixed, with some studies reporting early yet transient ptau accumulation following r-mTBI in C57BL/6 mice[58,61], and others reporting a sustained increase in pTau and AT8-positive signal in hTau animals at chronic timepoints as late as 3 and 6 months post last injury[62,63]. The way in which impairments in the preclinical neurobehavioral paradigms for learning and memory, assessed by Barnes Maze (Figure 1.2, A and B), and in impulsivity or disinhibition, assessed via Elevated Plus Maze (Figure 1.2, C and D), show an injury-dependent effect in the absence of overt pTau expression in animal models (*Table 1*) mirrors the afore mentioned disjoint of clinical symptomology with CTE pathognomonic lesions in the human population, and questions the pathological role of pTau, beyond that of a physical signature hallmark, in animal models and the human condition alike.

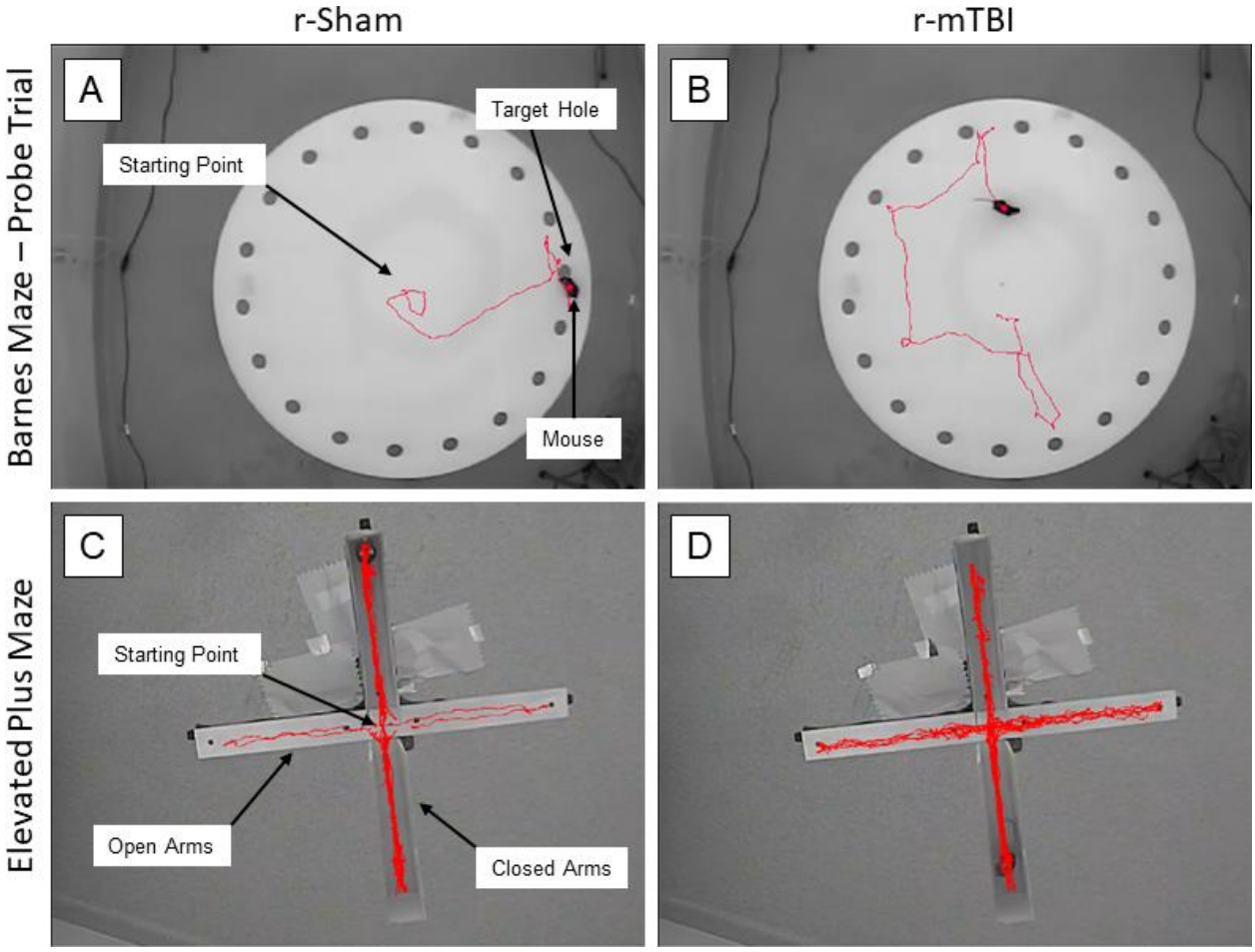

Figure 1.2. Behavioral paradigms for the evaluation of learning and memory deficit, and loss of in inhibition of mice following repeat mild head trauma. For assessment of learning, mice are given 90 seconds to locate and enter the target hole/box in the Barnes Maze (A) and required to remain in the target box for 30 seconds prior to retrieval, regardless of success. For a series of 6 consecutive days, 4 trials are given per day, with mice starting from one of four cardinal points on each trial. The inter-trial interval for each mouse on any given day of acquisition is approximately 40 minutes. The maze platform and retrieval box are both cleaned thoroughly between trials to limit the confounding effects of scent on performance of the mice during each trial. On the seventh day, a single probe trial lasting 60 seconds is performed (A and B), with the mouse starting from the center of the maze and the target box removed. The end-point behavioral metric of escape latency measured is the time taken for the mouse to locate the target hole where the escape box had been placed for the six consecutive days of learning. Panel (B) displays the dorsal plan view of the Barnes Maze apparatus, and the camera-tracked travelled by a r-mTBI mouse, highlighted in red, at 6 month post-injury during the first 30 seconds of the single 60 second memory probe trial. The r-mTBI mouse (B) is unable to locate the target hole within the first 30 seconds of the trial, indicating an impairment in spatial memory, as compared to an age-matched r-sham control animal (A), demonstrating the ability to locate the target hole within the first 30 seconds of probe, and travelling a significantly decreased distance to do so. In addition to assessment of learning and spatial memory via use of the Barnes maze, animals are also tested for anxiety-like behavior in the elevated plus maze. The apparatus consists of two open and two closed arms forming a plus shape (C and D). The arms are elevated approximately 80 cm from the floor. Each mouse is placed on the junction of the four arms of the maze, facing the open arm. The mouse is allowed to freely explore the maze for 5 minutes in a dimly lit ambient lighting (~1 lux). The percentage of time spent in the open arms was calculated using the Ethovision video tracking system. Panels (C) and (D) show the dorsal camera tracked paths of biological replicates of the r-sham and r-mTBI animals in (A) and (B), respectively. The r-mTBI animal (D) spends a much greater length of time in the open arms of the maze in proportion to the closed arms, relative to the r-sham mouse (C), indicating disinhibited behavior in the r-mTBI mouse at this time-point post-injury.

It is interesting to note that one of the few studies, by Huber et al[57], to report an increase in multiple phosphorylated forms of pTau in combination with accumulation of the CTE-defining AT8-positive Tau, did so by use of repetitive blast injury in wild type mice, and showed the accumulation of pTau to be perivascular in nature and accompanied by gross BBB disruption and vasculopathy[57]. However, this CTE-like pathology was transient, and AT8 immunoreactivity disappeared within 4 hours post-injury, a result the authors attribute to the use of anesthesia in their hit paradigm, and the potentiation effect that loss of consciousness has on rapid clearance of substances from the mouse brain[74]. The authors cited the AT8 signal as not being associated with any specific cell type or neuropil, and instead colocalizing with the glial limitans and Virchow-Robin Space, indicating that, even at this acute timepoint, the pTau was in transit out of the parenchyma proper, possibly by means of the augmented glymphatic clearance hypothesized by the authors[57]. Indeed, there is evidence for chronic disfunction of the glymphatic system in patients with a history of mTBIs[75], and work by Iliff et al[76] has demonstrated that impairment of the mouse glymphatic pathway via genetic knockout of the astrocytic water channel Aquaporin 4 (Aqp4) can promote extensive pTau pathology following a single "Hit and Run" mTBI[55] at the chronic 3 month post-injury time point[76]. Furthermore, the locus coeruleus, which positively regulates glymphatic clearance during sleep via noradrenergic input[75], is one of the first areas of the brain seen to be affected by astrocytic and neurofibrillary burden in mild CTE cases[45,46], at a stage when pTau is topographically limited to the cortex. These studies suggest that the relative lack of pTau accumulation across the myriad of animal models used may be due to a synergistic potentiation of pTau clearance by both lack of consciousness from anesthesia[57,74] and inherent

anatomical differences in the routes of drainage of metabolic waste, such as pTau, from the parenchyma in lissencephalic animals, such as mice, rats, and sheep, as compared to humans[75,77].

Despite these, and other, translational limitations in recapitulating perivascular pTau foci pathology alongside white matter degeneration and neuroinflammatory insult, the studies of Ojo et al[62] and Petraglia and colleagues[63] have demonstrated an increase of pTau in hTau and C57BL/6 mice, respectively, at 3-6 months post-last mTBI[62,63]. The former study showed accumulation of pTau and higher conformational pTau species in the cortex of injured hTau mice 3 months following the last of 26 mTBIs, delivered across a time-span of 3 months, and demonstrates marked deficits in neurobehavior and cerebral blood flow; the latter study also demonstrated increased pTau levels in the cortex, but did so following a much greater number of mTBIs, given at a much higher frequency, and to C57BL/6 mice, which do not express human Tau, and so have less of a proclivity towards exhibiting pTau aggregates. The juxtaposition of these reports further reiterates that, much like the observation of more aggressive CTE tauopathy seen in professional athletes in higher level of play[45], even non-transgenic mice exposed to higher dose of mTBI over a shorter time frame may develop CTE-like pTau burden. However, there has yet to be a study demonstrating evolution of pTau or AT8 load in to NFTs in non-transgenic preclinical models, and so, the investigation into the physiological relevance of pTau in general, and perivascular pTau in specific, remains elusive.

1.4. Diagnosis of TBI-related Pathology *In vivo*.

Magnetic Resonance Imaging (MRI), Diffuse Tensor Imaging (DTI), Single Photon Emission Computerized Tomography (SPECT), and Positron Emission Tomography (PET) MRI have been used for some time in the diagnosis and tracking of vascular dementia (VaD) and AD, amongst other neurodegenerative illnesses[78]. The most robust post-mortem pathological hallmarks of AD, such as atrophy of the cortical grey matter, and deposition of pTau NFTs and amyloid plaques throughout the parenchyma, are easily detectable *in vivo* via advanced neuroimaging techniques[79], and combined CT/MRI-based volumetric measurements of brain matter have been shown to provide much more diagnostic precision than visual evaluation alone[80].

DTI, which detects water molecule diffusion through axons, and so measures white matter integrity and anatomical connectivity, has not only been used in AD as both a diagnostic and prognostic for the disease[79], but has also recently shown promise in diagnosis of TBI related illness[81]. Single and serial DTI MRI studies have shown late and persistent cortical thinning and white matter loss in human patients following both moderate-to-severe TBI[82-84], and in those with a history of mTBI[24,85,86]. These recent points, and corroboration of longitudinal reports with the myelin loss and atrophy common to both CTE patient pathology[31,41,45,46] and animal models thereof (see *Table 1*) spell hope for DTI as an early indicator and possible prognostic of the disease. However, the modality is limited in this regard by the fact that white matter pathology is secondary in the NINDS consensus criteria for CTE[46], being a shared degenerative hallmark of multiple diseases, and so, more work and validation is required before DTI may be used as an *in vivo* biomarker for TBI.

PET imaging has proven indispensable in the detection of proteinic biomarkers, such as Aβ, by PET ligands[87], including ^{18}FDDNP[88], ^{11}CSB[89], and ^{11}C-PIB[90,91], and indeed, one such PET ligand,

^{18}F-Florbetapir has even been FDA-approved because of its imaging signal's correlation with Aβ load post-mortem[92]. The utility of neuroimaging as a diagnostic in AD, a disease the pathology of which is overlapping with TBI-related neurodegeneration, has led to recent research in to its clinical applicability in CTE. Preliminary research indeed suggests that imaging modalities may be a preferable approach to diagnosing and mapping CTE in the human population, as compared to neurocognitive and behavioral assessments, the insensitivity of which has been discussed earlier[31,41,42,93] in patients with a history of sports related mTBIs. To this end, the activity and pharmacokinetics of the Tau protein PET radioligand tracer ^{18}F-T807, otherwise known as ^{18}F-AV-1451, has recently been characterized in a study by Wooten et al[94]. The radiotracer was administered to four healthy control patients, three patients with a history of TBI, one of which sustained a severe TBI from an automotive accident, and two Mild Cognitive Impairment (MCI) patients[94]. Wooten and colleagues found that ^{18}F-AV-1451 exhibited fast uptake in to, and fast elimination from, the brains of the participants, and very little non-specific white matter binding[94], indicating its efficacy and safety as a potential PET tracer. Distribution of ^{18}F-AV-1451 was found to be uniform throughout the brain in control subjects, with no high sub-region accumulation, however, the patient with a severe TBI showed a high uptake in the posterior corpus callosum, extending in to the posterior cingulate gyrus[94]. Interestingly, both MCI subjects showed a separate, region-specific uptake of ^{18}F-AV-1451, one in the occipital cortex and the other throughout areas associated with the Braak staging of Tauopathy in AD[94,95]. Further to Wooten and colleagues' stratification of MCI from TBI patient antemortem by PET imaging[94], Dickstein et al[96] have reported PET recorded binding of ^{18}F-AV-1451 in a spatial pattern akin to established CTE neuropathological criteria[45,46], in the absence of ^{18}F-Florbetapir-positive

amyloidosis, in a 39 year old male retired professional American Football Player with clinicopathological diagnosis of mild to moderate CTE. Most interestingly, the subject had been recorded as having sustained 22 confirmed concussions over his career in sports, 4 of which were accompanied by loss of consciousness, and presented with mild CTE cognitive and emotional symptoms, suggesting PET ligand imaging may be sensitive enough for detection of the disease early on in its pathogenesis[96].

Although the above studies would posit Tau protein PET imaging as an attractive antemortem diagnostic for CTE and TBI-related illness in the human population, there are several caveats to this approach. Most presciently, as compelling as the PET studies by Dickstein[96], Wooten[94], and a handful of other researchers[97-99] are in gauging tauopathy non-invasively against case history, the aforementioned studies have not yet confirmed these PET findings against classical neuropathological analysis post-mortem.

Application of the afore-mentioned imaging modalities, as they pertain to pTau and white matter pallor in TBI-related co-morbidity, is clearly in its infancy. Furthermore, the above preliminary studies are reliant on having at least a tentative clinical diagnosis of dementia or CTE. Ergo, were PET and other approaches to be validated in post-mortem tissue analyses, prospective patients would have to already be symptomatic for the disease, depreciating the potential impact of the antemortem evaluation on interventional therapy. There is thus an urgent need for identification and validation of in-vivo hallmark sequelae, appearing prior to manifestation of clinical symptoms, and identifiable non-invasively, which would allow cataloging of molecular pathways upstream of behavioral and cognitive dysfunction.

1.5. Traumatic Cerebrovascular Injury in Mouse and Man.

The primary effects of mTBI involve not only mechanical insult to the neuronal milieu, and diffuse axonal shearing, but also extensive and diffuse damage to the vascular bed of the CNS, a form of TBI termed Traumatic Cerebral Vascular Injury (TCVI)[100]. Indeed, secondary injury following a mTBI, which results from the physiological cascade of molecular and cellular responses to the initial trauma, can perpetuate not only neuronal pathology, but also contribute further to TCVI[101-104]. The micro-domain connecting CNS vessels, regulation of CBF, vascular permeability, and angiogenesis, to neuronal metabolism and activity is known as the Neurovascular Unit[100] (NVU), and comprises a dynamic interaction between the cerebral blood vessel wall and adjacent pericytes, smooth muscle cells, perivascular astroglia and neurons[100], known as Neurovascular Coupling[105]. The gross macro-morphology of the cerebral vasculature and associated mechanisms of NVC and consequent increased CBF is depicted in Figure 1.2. The brain is critically dependent on a steady cerebral blood flow[106] (CBF), with physio-normal functioning of the NVU ensuring maintenance of a constant CBF irrespective of perturbation in peripheral mean arterial blood pressure[105,107], and so, any gross dysfunction of the NVU will have profound physiological consequences. There is much controversy regards which mural cell type, smooth muscle or pericyte, is most important for normal NVC functioning, with some groups stipulating the smooth musculature of arteries and arterioles as contributing the greatest towards changes in cerebral perfusion[106], and others ascribing this role to pericytes of the capillary bed[108]. While smooth muscle cells express appreciable amounts of the contractile protein αSMA[106], and so could be assumed to be responsible for bulk CBF response, pericytes have been shown to regulate CBF *in vivo*[108-110], initiate and maintain retrograde signaling

upstream to larger arterioles and arteries via sensing and conductance of hyperpolarizing potassium cation current (Figure 1.2, A)[111,112], and to contribute greatest to vascular resistance in the CNS[113]. It is also well accepted that the capillary strata of the cerebral vasculature responds and dilates first in mouse imaging studies[114,115] and the initial BOLD MRI signal in humans emanates from localized parenchymal areas[116], suggesting engagement of the capillaries, and perhaps by default pericytes, first in physio-normal Neurovascular coupling. Given the hypothesized importance of pericytes in healthy coupling of neuronal metabolic demand to adequate cerebral blood supply, it is perhaps not surprising that many groups have reported a decrease in pericyte vessel coverage following TBI in animal models[117-122], coincident with impaired resting state CBF. The above data implicates a cellular and functional contribution of pericytes of the CNS to development of TCVI.

As opposed to neurodegenerative hallmarks, such as pathognomonic pTau and NFT/amyloid pathology, the causal link to, and time of appearance alongside, neuronal dysfunction is still speculative, cerebrovascular pathology is known to not only appear in tandem with clinical symptomatology in tauopathies, such as AD, and downstream of primary TCVI and neuronal injury, but also to precede said neuronal pathology in these disease states[100]. Such is the case with the small vessel disease 'Cerebral Autosomal Dominant Arteriopathy with Subcortical Infarcts and Leukoencephalopathy (CADASIL)', the most common form of hereditary stroke and vascular dementia[123], in which early and aggressive micro-vasculopathy does, by itself, cause neurodegeneration[123]. CADASIL is characterized by pre-symptomatic osmophylic accumulation in, and thickening of, the walls of small penetrating arteries and leptomeningeal vessels, and is similar in clinical presentation to vascular dementia and AD[123,124], conditions for the development

of which a history of r-mTBI has been posited as a predisposing factor[42,125-127]. Concomitantly, one physiological correlate of vascular degeneration, cerebral hypoperfusion, has also been noted as a definitive risk factor for development of AD[128,129], and a rapid conversion of mild cognitive impairment (MCI) to AD with reduced CBF has been reported in human patients[130].

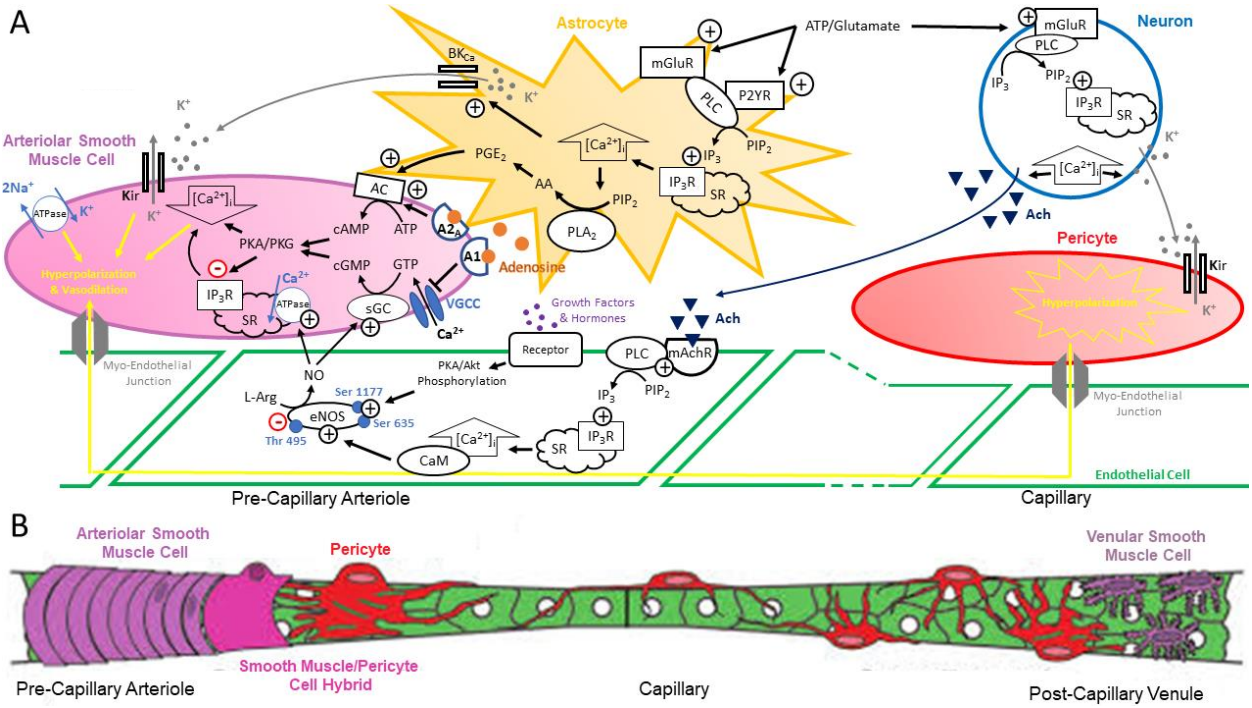

Figure 1.3. Anatomy and Function of the Neurovascular Unit. Neurovascular coupling is mediated by a variety of neurotransmitters and pathways (A), including, but not limited to, local release of vasodilators such as Adenosine and Prostoglandin E_2 (PGE_2) from astrocytes, and their direct hyperpolarizing action on the smooth musculature of the cerebral vasculature, resulting in cerebral vasodilation, and increased cerebral blood flow (CBF). Neuronally derived Acetylcholine (Ach) and growth factors and hormones, can also act on the endothelial layer of the cerebral vasculature, resulting in an increase in intracellular calcium concentration, and a calcium-dependent activation of endothelial Nitric Oxide Synthase (eNOS) through the activation of Calcium-Calmodulin complex (CaM) and release of endothelium-derived Nitric Oxide (NO), which increases activity of soluble Gaunalyl Cyclase, activating intracellular protein kinases, which promote reuptake of cytosolic calcium in to intracellular stores, causing smooth muscle cell hyperpolarization, relaxation, and vasodilation (A). Generation of eNOS is positively regulated by phosphorylation of the enzyme at Serine 1177, and Serine 635, and negatively regulated by dephosphorylation at Threonine 495. The pericytes and endothelium of the capillary bed are also involved in sensing of, and functional hyperemic response to, neuronal activity. Local increases in extracellular concentration of K^+, resulting from increased activity-dependent neuronal depolarization, activate inwardly rectifying K^+ channels resident on both pericytes and endothelial cells, initiating a net efflux of positive current, and hyperpolarization of the endothelium, which is retrogradely transmitted upstream to the endothelium of larger arterioles, and hyperpolarizes the smooth muscle cells through myo-endothelial junctions. The general morphology and mural cell distribution of the cerebrovasculature is shown in (B), with larger arteries and arterioles (greater than 10µm in diameter) being encompassed by circumferential band-like smooth muscle cells and pericytes. The surface of capillaries (of less than 6µm in diameter) are mostly covered by pericytes with a "bump on a log" morphology, with astrocytic end-feet making up the difference in vessel coverage. The capillary bed terminates in to the venules of the cerebral vasculature, which are wrapped in both pericytes and stellate-shaped smooth muscle cells.

AA, Arachidonic Acid; AC, Adenylyl Cyclase; Ach, Acetylcholine; Akt, Serine/Threonine-Specific Protein Kinase B; ATP, Adenosine Triphosphate; A1, Adenosine A1 Receptor; A2A, Adenosine A2 Receptor; BK_{CA}, Big Potassium Channel; CaM, Calmodulin; cAMP, cyclic Adenosine Monophosphate; cGMP, cyclic Guanidine Monophosphate; eNOS, endothelial Nitric Oxide Synthase; GTP, Guanosine Triphosphate; IP_3, Inositol Triphosphate; IP_3R, Inositol Triphosphate Receptor; K_{ir}, inwardly rectifying Potassium channel; L-Arg, L-Arginine; mAchR, muscarinic Acetylcholine Receptor; mGluR, metabotropic Glutamate Receptor; PIP2, Phosphatidyl Inositol 4,5 Bisphosphate; PLA2, Phospholipase A2; PLC, Phospholipase C; PGE_2, Prostoglandin E_2; P2YR, Purinergic P2Y Receptor; sGC, soluble Guanylyl Cyclase; SR, Sarcoplasmic Reticulum. Figure modified from Hartmann et al[131], Neurophotonics, 2015.

TCVI of varying degree is seen in almost all reported cases of severe TBI post-mortem[100], and also in the brains of patients dying in the acute phase of hours to days following a mTBI[132]. TCVI typically manifests as extensive pericyte pathology postmortem in the acute and subacute phase following a severe TBI[133,134], as brain contusion and capillary compression by astrocytic end-feet[135], and signs of blood brain barrier (BBB) penetrance[136]. These sequelae, such as BBB permeability, are not monogamous for severe TBI however, but also for lesser intensities of head trauma, as Gill et al[137] have recently shown plasma measurement of the astroglial marker Glial Fibrillary Acid Protein (GFAP), the neuronal cytoplasmic protein Neurofilament (NFL), and Tau to be sufficient to discriminate between mTBI patients and controls in the acute phase following injury and emergency room admission[137]. Changes in both regional and global CBF are observed in human patients following a single severe TBI, with vasospasm accompanying reduced flow in the acute period post-injury, before normalization of CBF to basal levels[135]. As with BBB disruption, neuroimaging implicates global and regional CBF disruption in much milder forms of TBI, and at more chronic timepoints post-injury, as is the case with a recent study by Siobounov and colleagues[138], demonstrating differences in both global and regional CBF via Arterial Spin labelling (ASL), and Susceptibility Weighted Imaging (SWI), between collegiate football athletes and control participants over the course of a single season of football[138]. These perfusion-specific mTBI effects have also been recapitulated in animal models, with just a single cortical impact mTBI sufficient to cause reduced CBF and behavioral deficit in mice[139], and work from our own institute has demonstrated a separate r-mTBI closed head impact model emulating a professional football-like frequency of mild impacts resulted in global CBF impairment as late as 3 months

post-last hit in hTau mice[62]. These data indicate a potential role for cerebrovascular dysregulation and resting state cerebral perfusion in the pathophysiology of TBI-related disease.

As with resting state cerebral perfusion deficit and BBB permeability, Cerebrovascular Reactivity (CVR), the ability of the cerebral vasculature to produce a change in CBF in response to a vasoactive stimulus, and a direct measure of cerebral vascular health and reserve[140], is known to be compromised across the spectrum of human head trauma intensity[141-146]. CVR deficit may not only be physiological proxy of TCVI, but is also seen in other neurodegenerative disorders, such as CADASIl[147-149], MCI[150] and AD[150]. Much like resting state CBF, CVR is often tested in the clinic using imaging modalities such as ASL, MRI, and NIRS, with BOLD MRI being the preferred imaging technique, and a transient increase in arterial partial pressure of CO_2 ($paCO_2$) via facemask inhalation of CO_2-subsidized air being the vasoactive stimulus of choice and termed a hypercapnic challenge. Under physiological conditions, CVR may be said to be incumbent for NVC, as many mediators, including CO_2, are generated by neurons during neuronal metabolism and depolarization (Figure 1.2), however, the CBF signal in response to the robust, supra-physiological CO_2 level used during hypercapnic challenge (pre)clinically is regarded as a more vascular-specific readout, by virtue of the fact that it is hypothesized to largely bypass neuronal input. Although the mechanisms underlying hypercapnic challenge-evoked CVR in health are incompletely understood, recent studies have shown this cerebral vascular function to be compromised in patients suffering from mild-to-moderate head trauma, and in animal models of moderate-to-severe TBI, positing CVR as a potential in vivo diagnostic, and possibly a therapeutic target, of chronic TBI related illness.

Owing to the prevalence of TCVI in the pathogenesis of both genetic and sporadic neurodegenerative illness, as above, and the perivascular nature of the pathognomonic pTau lesioning as a prerequisite for diagnosis of CTE, TCVI is implicated as a *de facto* hallmark of repetitive mTBI related neurodegeneration in general, and CTE in particular. Furthermore, vascular pathology appears to be the most universally recapitulated CTE-like pathological phenotype in animal models of r-mTBI (see Table 1), alongside inflammation and white matter damage. As such, investigating the integrity and function of the cerebrovasculature post-injury is an attractive preclinical research endeavor, which may lead to a meaningful therapeutic outcome measure. Despite the plethora of in-vivo neuroimaging modalities clinically available for the serial monitoring of patients following mTBI, and the emerging prevalence of cerebrovascular associated biomarkers in the human mTBI population, there is a stark paucity of pre-clinical CBF imaging conducted alongside correlative behavioral and vascular pathological analyses in relevant animal models of r-mTBI related neurodegeneration. This thesis will comprehensively examine the state of the cerebrovasculature at chronic time-points post-injury in a validated murine model of repetitive mild head trauma.

1.6. Hypothesis.

The data here outlined implicate cerebrovascular dysfunction as a contributory factor in pathophysiology following repetitive head trauma in animal models and the human population. However, preclinical information regarding r-mTBI and the cerebrovasculature chronic time-points post-injury is lacking. As such, the purpose of this thesis is to characterize the pathological and physiological state of the cerebrovasculature in an already-validated mouse model of repetitive mild traumatic brain injury. I hypothesize there is chronic dysregulation of the cerebrovasculature following r-mTBI, accompanied by a gross deficit in cerebrovascular physiological response. The work to test this hypothesis is detailed in the following Chapters as outlined below:

1. Chapter 2: Adult mice subject to a high dose and frequency of mild head trauma, analogous to that received by a professional athlete over the course of a career in sports, will exhibit learning and memory impairments and reduced cerebral blood flow at a chronic time-point post-injury.

2. Chapter 3: Sustained neurobehavioral deficits seen following r-mTBI are accompanied by progressive dysregulation of cerebrovascular markers throughout the cortex.

3. Chapter 4: Cerebrovascular reactivity is impaired in r-mTBI mice post-injury.

4. Chapter 5: General discussion of findings.

Chapter 2. Characterization of chronic memory and cerebral blood flow in a mouse model of repetitive mild traumatic brain injury.

2.1. Introduction.

Despite recent attempts to limit concussion in collegiate and professional contact sports, the incidence of r-mTBI and consequent acute and chronic neurocognitive symptoms among players remains high[151]. Almost all retrospective neuropathological post-mortem analyses of brains from former contact sports players, spanning the recreational and professional realms of American football, Hockey, Soccer, and Rugby, indicate that there is a causal link between a history of concussion and development of CTE-like pathology[41,45,46,152,153]. However, current and concise diagnosis of CTE can only be made post-mortem[46], and recent neuroimaging techniques directed at the pathognomonic pTau spatial distribution throughout the diseased brain[94,96-99] also necessitate enrollment of subjects based on clinical symptoms synonymous with having sustained repeat head trauma. Ergo, an established ante-mortem phenotype diagnostic approach to identify individuals in the pathogenic infancy of repetitive mTBI-related neurodegeneration is needed to circumvent clinicians' dependency on insensitive behavioral assessments and self-reported, and often erroneous, testimony of time and severity of injury.

The *in vivo* diagnoses of neurodegenerative disorders such as AD and vascular dementia have relied heavily upon detection of accumulation of misfolded and aggregated protein throughout brain regions of culpability. These regions are defined post-mortem across thousands of patients

at various stages of disease onset and pathology[78]. Therapeutic intervention based upon removing, or halting accumulation of, these aggregates has been unsuccessful, with exception of the recent Biogen Phase II clinical trial[154], which demonstrated a modest slowing of progression of AD symptoms in patients receiving a passive antibody-based clearance of amyloid from their brain, as detected by PET, compared to control placebo-treated subjects. However, although the progression of the disease was described as being slowed by approximately 30% in the subset of patients given the highest dose of drug, compared to placebo treated group, individuals still exhibited symptom progression with time across the 18 months of treatment[154]. This result would suggest that for amyloid in AD, and possibly pTau in CTE, identification and enrollment of patients at a stage when the signature proteinaceous lesions have already formed may be too late in the pathobiology of the disease for feasible intervention.

For these reasons, there is an unmet need in the field to identify clinical biomarkers and diagnostic tools, which can be detected and administered non-invasively following head trauma, for those patients at risk of chronic r-mTBI-related illness.

To date, ample evidence exists for a role of vascular pathology and cerebrovascular dysregulation in the human mTBI population, with separate groups both reporting aberrant regional and global CBF in athletes[138,141], however, very few studies have examined CBF in relevant mouse models of r-mTBI[62,155,156]. We have recently reported a chronic reduction in global CBF in tandem with a trend towards neurobehavioral impairment, occurring alongside accumulation of pTau throughout the cerebral cortex, with marked inflammatory marker expression and white matter loss, in 9-month-old hTau mice at 3 months post-injury, in our novel chronic r-mTBI mouse model, consisting of one hit administered twice a week, approximately 72

hours apart, for 12 weeks[62]. This hit paradigm used in the studies herein is thus different in frequency to another also previously characterized by our group, which consisted of 5 mTBIs administered at an interval of 48 hours apart[60]. As our first approach, we aimed to more rigorously assess learning and memory-related neurobehavior, as opposed to solely the disinhibition-like and exploratory/locomotor activity examined in our previous report, in 12-month-old adult C57BL/6 mice, subjected to the same r-mTBI paradigm, and to examine the state of the cerebrovasculature at a chronic time-point post-injury. Furthermore, for this study, adult wild type, rather than hTau transgenic mice were used to establish whether sustained CBF impairment and cognitive dysfunction can occur in the absence of detectable differences in levels of pTau, allowing for a more cerebrovascular-associated assessment of TBI phenotype in this r-mTBI mouse model.

2.2. Materials and Methods

2.2.1. Animals.

Male and female C57BL/6 mice were housed under standard laboratory conditions (23 ± 1ºC, 50 ± 5% humidity, and 12 hour light/dark cycle) with free access to food and water throughout the study. All procedures were carried out under Institutional Animal Care and Use Committee approval, and in accordance with the National Institute of Health Guide for the Care and Use of Laboratory Animals.

2.2.2. Injury Schedule.

12-month-old mice were randomly assigned to one of two groups: repetitive mild Traumatic Brain Injury (r-mTBI, delivered twice each calendar week i.e., 1 hit approximately every 72 hours, over a period of 3 months) or repetitive Sham (r-Sham; animals underwent the same duration and frequency of anesthesia as r-mTBI animals). An electromagnetic impactor (Leica Instruments) was used to generate a midline mTBI, using a 5.0mm diameter flat face tip, 5m/s strike velocity, 1.0mm strike depth, and a 200msec dwell time, as previously characterized[59]. The mice were euthanatized 7 months after the final injury/anesthesia (i.e., 22 months of age).

2.2.3. Assessment of Cognitive Function

Cognitive function was assessed at 1 and 6 months after the final injury/anesthesia (15 months of age and 21 months of age, respectively) by use of the Barnes maze, as described previously by our group[59]. Researchers conducting the experiments were blind to grouping, and the Ethovision XT System (Noldus) was used to track and record the movement of each animal. Mice were given 90 seconds to locate and enter the target box and required to remain in the target box for 30 seconds prior to retrieval, regardless of success. For a series of 6 consecutive days, 4 trials were given per day, with mice starting from one of four cardinal points on each trial. The inter-trial interval for each mouse on any given day of acquisition was approximately 40 minutes. The maze platform and retrieval box were both cleaned thoroughly between trials to limit the confounding effects of scent on performance of the mice during each trial. On the seventh day, a single probe trial lasting 60 seconds was performed, with the mouse starting from

the center of the maze and the target box removed. Escape latency measured the time taken for the mouse to enter the box.

In addition to assessment of learning and spatial memory via use of the Barnes maze, animals were tested for anxiety-like behavior in the elevated plus maze (EPM)[157]. The apparatus consists of two open and two closed arms forming a plus shape. The arms are elevated approximately 80 cm from the floor. Each mouse was placed on the junction of the four arms of the maze, facing the open arm. The mouse was allowed to freely explore the maze for 5 min in a dimly lit ambient lighting (~1 lux). The percentage of time spent in the open arms was calculated using the Ethovision video tracking system[158].

2.2.4. Histology

Following CBF measurements at 22 months of age, the animals were anesthetized with isoflurane and perfused trans-cardially with phosphate-buffered saline (PBS), pH 7.4, the brain was removed from the skull, and one hemisphere was dissected to separate the brainstem, cerebellum, and ophthalmic bulbs from the rest of the hemisphere for biochemical analysis. The other hemisphere was post-fixed in 4% paraformaldehyde solution at 4ºC for 48 hours, and paraffin-embedded for Immunohistochemistry as previously described[60]. For each group, sagittal sections were cut at 6µm in thickness (lateral 1 in 10 series, 0.1–0.2mm), with the first 10 consecutive sections cut mounted one by one on to 10 separate consecutive slides, and the next 10 sections below these, resulting in 10 slides, each with two sections, per animal. Sections were deparaffinized with Histoclear (Fisher Scientific) followed by re-hydration via decreasing ethanol

gradient. Sections were then incubated in 3% hydrogen peroxide in order to quench endogenous peroxidase activity, and then underwent citrate buffer (pH 6.0) antigen retrieval for 7 minutes. Following antigen retrieval, sections were blocked in 2.5% normal serum at room temperature for approximately 30 minutes, and then incubated with primary antibody overnight at 4ºC. Sections were stained with primary antibodies against glial fibrillary acid protein (GFAP; DAKO, rabbit anti-GFAP polyclonal, ZO334, 1:10000 dilution), and ionized calcium binding adaptor protein 1 (Iba1; Abcam, goat anti-Iba1 polyclonal, Ab5076, 1:2500 dilution), either anti-rabbit or anti-goat secondary antibodies, using respective Vector ABC rabbit IgG or goat IgG Vectastain reagent kits (Vector Laboratories) and revealed using the Avidin-Biotin peroxidase DAB substrate solution (Vector DAB peroxidase substrate kit, Vector Laboratories, SK4105). Sections were counter-stained with Mayer's Hematoxylin (Sigma). Slides were visualized with a bright field microscope (BX60), and digital images were visualized and acquired using a MagnaFire SP camera (Olympus). At least 2 sections (one slide) were stained per animal for either Iba1 or GFAP immunohistochemistry, with at least 5 non-overlapping 40x magnification images of cortex analyzed per brain section, and at least 2 non-overlapping 60x magnification images of the Cornu Ammonis 1 (CA1), and at least 6 non-overlapping 60x images of the body of the Corpus Callosum (CC) regions of interest analyzed per brain section. The percentage area of image positive for either GFAP or Iba1 immunoreactivity was then analyzed by Zeiss Software following manual thresholding of image. The percentage area of individual regions of interest across sections for each mouse were averaged and then analyzed as biological replicates per group using unpaired student t-test.

2.2.5. Biochemistry

Western Blot analysis was carried out on brain tissue homogenates, following homogenization of tissue by sonication in HALT Protease and Phosphatase Inhibitor Cocktail mPER-containing lysis buffer. Equivalent total protein amounts were analyzed on sodium dodecyl sulfate-polyacrylamide gel electrophoresis under denatured and reduced, and denatured and non-reduced, conditions using 4-20% Bis-Tris precast Gels (Biorad), and electro-blotted on to a polyvinylidene difluoride (PVDF) membrane overnight at 90mA constant current. Membranes were then washed in de-ionized water, before being blocked for 1 hour at room temperature with 5% non-fat milk in tris buffered saline (TBS). Membranes were then incubated with primary antibodies overnight (12-16 hours at 4°C). The following primary antibodies were used at the given concentrations; GFAP (DAKO, rabbit anti-GFAP polyclonal, ZO334, 1:10000 dilution), laminin (Sigma, rabbit anti-mouse laminin, L9393, 1:50 Dilution), platelet derived growth factor receptor β (PDGFRβ; Abcam, rabbit anti-PDGFRβ monoclonal, ab32570, 1:1000 Dilution), alpha smooth muscle actin (αSMA; Millipore, mouse anti-αSMA monoclonal, ASM-1, 1:1000 dilution), Iba1 (Abcam, goat anti-Iba1 polyclonal, Ab5076, 1:2500 dilution) and rabbit anti-GAPDH, glyceraldehyde 3-phosphate dehydrogenase (Sigma-Aldrich, 1:1000 dilution). Membranes were washed with deionized water, incubated with their respective secondary antibody for 1 hour at 4°C, washed once more, and then developed using ECL chemiluminescent detection reagent (GE Life Sciences). Membranes were imaged using a Biorad ChemiDoc Wetern Blot Imager, and densitometry results of individual bands were collected using ImageLab 5.2 (Biorad) software. Target protein values for each lane were normalized against densitometry values for GAPDH for their respective lane. Target protein values were also normalized against the total protein stain

for their respective lane using a coomassie blue stain (data not shown) to validate the GAPDH-normalized results.

2.2.6. Determination of Regional Cerebral Blood Flow by Laser Scanner Doppler Imaging

For CBF measurements, 22 month-old r-Sham and r-mTBI wild type mice (at 7 months post injury) were anesthetized with a gas mixture of 3% isoflurane and 0.5 L/min oxygen, immobilized on a mouse stereotaxic table (Kopf Instruments). Body temperature was monitored via rectal probe and maintained at 37ºC using a mouse homeothermic blanket system (Harvard Apparatus). An incision was made through the scalp, and the skin retracted to expose the skull. The periosteal connective tissue, which adheres to the skull, was removed with a sterile cotton swab. Cortical perfusion was measured with the Laser Doppler Perfusion Imager from Moor Instruments as previously described[159]. A computer-controlled optical scanner directed a low-powered He–Ne laser beam over the exposed cortex. The scanner head was positioned parallel to the cerebral cortex at a distance of 26 cm. The scanning procedure took 1 min 21 s for measurements of 5538 pixels covering an area of 0.8 x 0.8 cm, and six replicate images per mouse were collected. At each measuring site, the beam illuminated the tissue to a depth of approximately 0.5 mm. An image color-coded to denote specific relative perfusion levels was displayed on a video monitor. All images were stored in computer memory for subsequent analysis. For each animal, a square area of 0.05 cm^2 (360 pixels) equally distributed between the right and left hemispheres was defined and applied to each image of the series in order to measure the CBF in the entire, frontal, and occipital cortex using the Moor LDI Image Processing

V3.0h software. CBF was also measured by manually delineating for each mouse the cortex area (0.51– 0.54 cm^2 corresponding to 3504–3714 pixels). Relative perfusion values for each area studied were expressed as arbitrary units.

2.2.7. Statistical Analysis

All data were assessed as if they were coming from a normally distributed population, using skewness and kurtosis of the distribution. If there were statistically significant kurtosis and skewness, the data was transformed using log2, or square root transformation. When transformation did not yield a normally distributed data set, the non-parametric Kruskal-Wallis test was used.

For Barnes Maze, normally distributed data was analyzed using parametric methods. If a given dataset was normally distributed and variances were equal, One-way ANOVA (for probe) or repeated measures ANOVA (for acquisition) were used to assess significant changes due to injury. Mauchly's sphericity test was used to evaluate sphericity in repeated measures ANOVA, and, if it was statistically significant, degrees of freedom were corrected with Greenhouse-Geisser estimates of sphericity. Two-way ANOVA was used to assess significant differences between groups on only day 6 of acquisition trials.

For the measurement of cerebral blood flow, the data were first tested for unequal variances using the O'Brien test for homogeneity of variance. If the variances were not equal Welch's test was used. For the analysis of CBF measurements, two-way ANOVA of values was run on a one

way ANOVA platform, selecting the replicate values as block, i.e. X and Y variables were analyzed via two way ANOVA to reveal statistical differences in X. Both Western Blot and Immunohistochemistry data were analyzed using unpaired student t-test. A given effect was considered significant at $p<0.05$, and indicated by asterisks in the figures. Error bars represent the standard error of the mean. Statistical analyses were performed using JMP 11.1.1 (SAS) and graphs were created using GraphPad Prism 5.0.

2.3. Results

2.3.1. Barnes Maze Acquisition

At both the 1 month and 6 month time-points following the final injury/anesthesia, r-mTBI mice travelled a significantly greater cumulative distance than their r-Sham controls (Figure 2.1, A and B, $P<0.001$). Additionally, we observed a distinct effect of injury on cumulative distance travelled over time, reflected by a progressive separation of cumulative distance travelled by r-mTBI mice, compared to r-sham controls, across the 6 consecutive days of acquisition at 1 month post-injury (Figure 2.1, A, r-Sham vs r-mTBI; $P=0.0028$) and a non-significant effect of treatment on cumulative distance with time at 6 months (Figure 2.1, B, r-Sham vs r-mTBI; $P=0.07$). We observed a time-dependent effect of injury across the 6 days of acquisition at 1 month post-injury (Figure 2.1, C, $P=0.08$), however, this injury by time interaction was not significant at 6 months post-injury (Figure 2.1, D, $P<0.001$), with the average velocity of r-mTBI mice being statistically greater than that of r-Sham controls on day 6 of acquisition at 6 months (Figure 2.1, D, $P<0.001$) but not at 1 month (Figure 2.1, C, $P=0.2$) post-injury.

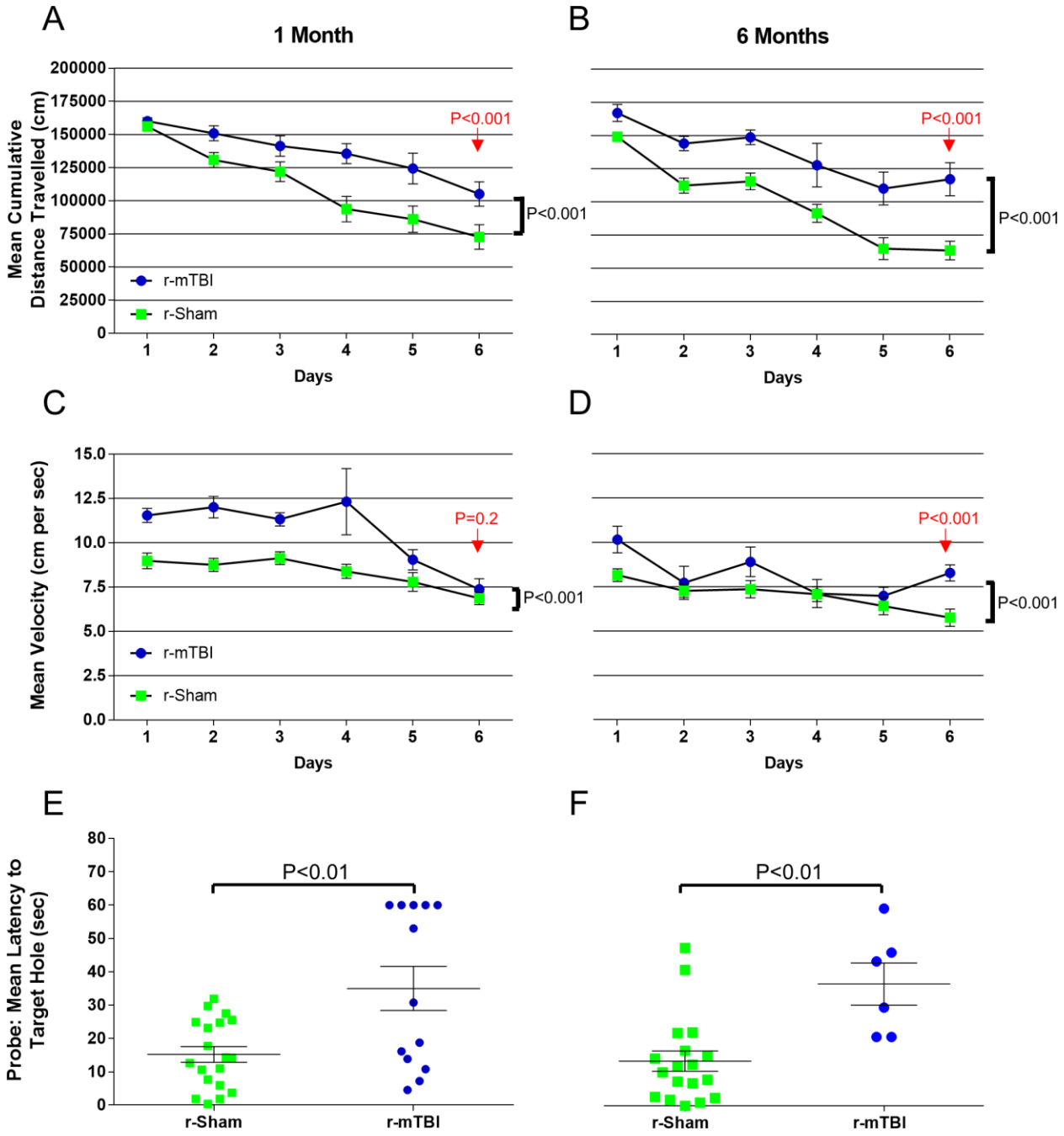

Figure 2.1. Evaluation of learning (acquisition) and retention of spatial memory of wild type mice using the Barnes maze at 1 and 6 months following repetitive mild traumatic brain injury. Mice were tested in the Barnes maze for their ability to locate a black box at the target hole. During the course of the 6 days of acquisition at both the 1 month sub-acute, and 6 month chronic time-points post-injury, the r-mTBI mice travelled a greater mean cumulative distance to reach the target hole, compared to sham controls (A and B, P<0.001, repeated measures ANOVA). In cumulative distance data, the injury by time interaction term was statistically significant across the 6 days of acquisition at the 1 month post-injury time-point (P<0.01, Repeated Measures ANOVA), however, this was not seen at the 6 month time-point (P=0.07, repeated measures ANOVA). There was also a significant effect of injury on mean velocity between groups across all 6 days of acquisition at both the sub-acute 1 month and the chronic 6 Month time-point (C and D; P<0.001, repeated measures ANOVA) with a significant increase in velocity of r-mTBI mice vs r-

Sham controls on day 6 of acquisition at 6 months post-injury (D; P<0.001, Two Way ANOVA). There was no significant effect of injury with time on mean velocity at 1 month post-injury (C; P=0.08, repeated measures ANOVA), and no significant difference in velocity between groups on day 6 of acquisition at 1 month post-injury (C, P=0.2, two way ANOVA). Evaluation of spatial memory retention (Probe) of wild type mice using the Barnes maze, at 1 and 6 months following r-mTBI (Figure 2, E and F, respectively). For the probe trial (the day immediately following the 6 consecutive days of acquisition testing), the target box was removed and mice were placed in the middle of the table for a single, 60-second trial. Probe test performance was significantly impaired in the r-mTBI mice at 1 month (A, P<0.01, Welch's Test) and 6 months (B, P<0.01, one-way ANOVA), compared to r-Sham controls. *Data are presented as Mean ± Standard Error of the Mean (SEM); 19 r-Sham, and 13 r-mTBI at 1 Month; 18 r-Sham, and 6 r-mTBI at 6 Months. Statistical P values on figure represent statistical analysis only for day 6 of acquisition. The injury by time interaction values are not shown in the figure.*

2.3.2. Barnes Maze Probe

Probe test performance was profoundly impaired in r-mTBI mice, compared to sham controls, at both 1 month (Figure 2.1, E, P<0.01) and 6 months (Figure 2.1, F, P<0.01) post-injury. There was no statistically significant difference in mean velocity, distance travelled, or total errors made between groups during the probe trial at either 1 month or 6 months post-injury (P<0.05, data not shown).

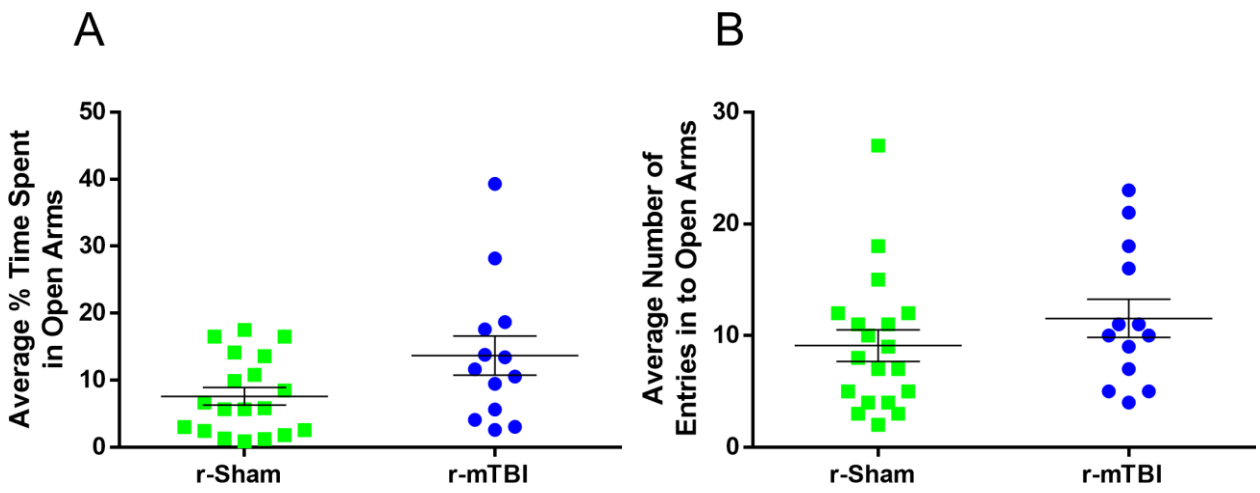

Figure 2.2. Evaluation of anxiety using the elevated plus maze (EPM) at 1 month post-injury. (A) Injured animals spent on average 79% more time in the open arms of the EPM compared to r-Sham controls, however, this trend in behavior was not statistically significant (P>0.05, unpaired student t-test). Additionally, r-mTBI animals exhibited approximately 26% greater frequency of entries in-to the open arms of the maze, compared to r-Sham controls, however, this result was not significant (B, P>0.05, unpaired student t-test). *Data are presented as mean ± standard error of the mean (SEM); 19 r-Sham, and 13 r-mTBI at 1 month.*

2.3.3. Elevated Plus Maze

Following probe testing at 1 month post-injury, r-mTBI and r-Sham mice were assessed for anxiety-like behavior via the Elevated Plus Maze (EPM, Figure 2.2). There was no significant difference in percentage time spent in the open arms by r-mTBI mice, compared to r-Sham controls (Figure 2.2, A, P>0.05), and so, similar levels of anxiety between both r-Sham and r-mTBI animals at this time-point. Additionally, there was no significant difference in the number of entries of r-mTBI mice in to the open arms (Figure 2.2, B, P>0.05), compared to r-Sham controls.

2.3.4. GFAP Immunostaining and Biochemistry

Immunohistochemical analysis of glial fibrillary acidic protein (GFAP) immunostaining was carried out on the brain regions underlying the impact site, specifically the somatosensory and primary motor cortices, Corpus Callosum (CC), and Cornu Ammonis 1 (CA1) of the Hippocampus, of the r-Sham and r-mTBI mice from which Cerebral Blood Flow recordings were obtained. There was no statistically significant difference in the percentage area of GFAP-positive labelling in images taken of the cortices of r-Sham (0.1523% ± 0.05%) vs r-mTBI (0.1234% ± 0.03%) animals (Figure 2.3, A, P = 0.89). The lack of injury-effect on GFAP labelling in the cortex was not accompanied by the presence of hypertrophic GFAP-positive cells, but instead by a morphologically quiescent GFAP-positive cell phenotype in both r-Sham and r-mTBI mice (Figure 2.3 A, the boxed insets being magnifications of the cells indicated by arrows). There was a noticeable increase in astrogliosis in the CC of r-mTBI mice (Figure 2.5, D, 9.05% ± 0.68% of area) compared to that of r-Sham controls (Figure 2.5, C, 5.69% ± 1.14% of area), however, this was not significant (Figure 2.5 J, P=0.0519). Pursuant to the immunopathological GFAP labelling in the cortex, western blot analysis of the contralateral brain homogenate did not demonstrate a statistically significant difference in GFAP expression between r-Sham and r-mTBI mice at 7 months post-injury (Figure 2.3, B, P=0.57). Immunohistochemical analysis of the CA1 revealed no significant difference in GFAP immunoreactivity between r-Sham and r-mTBI animals (Figure 2.5, A and B; I, P=0.41).

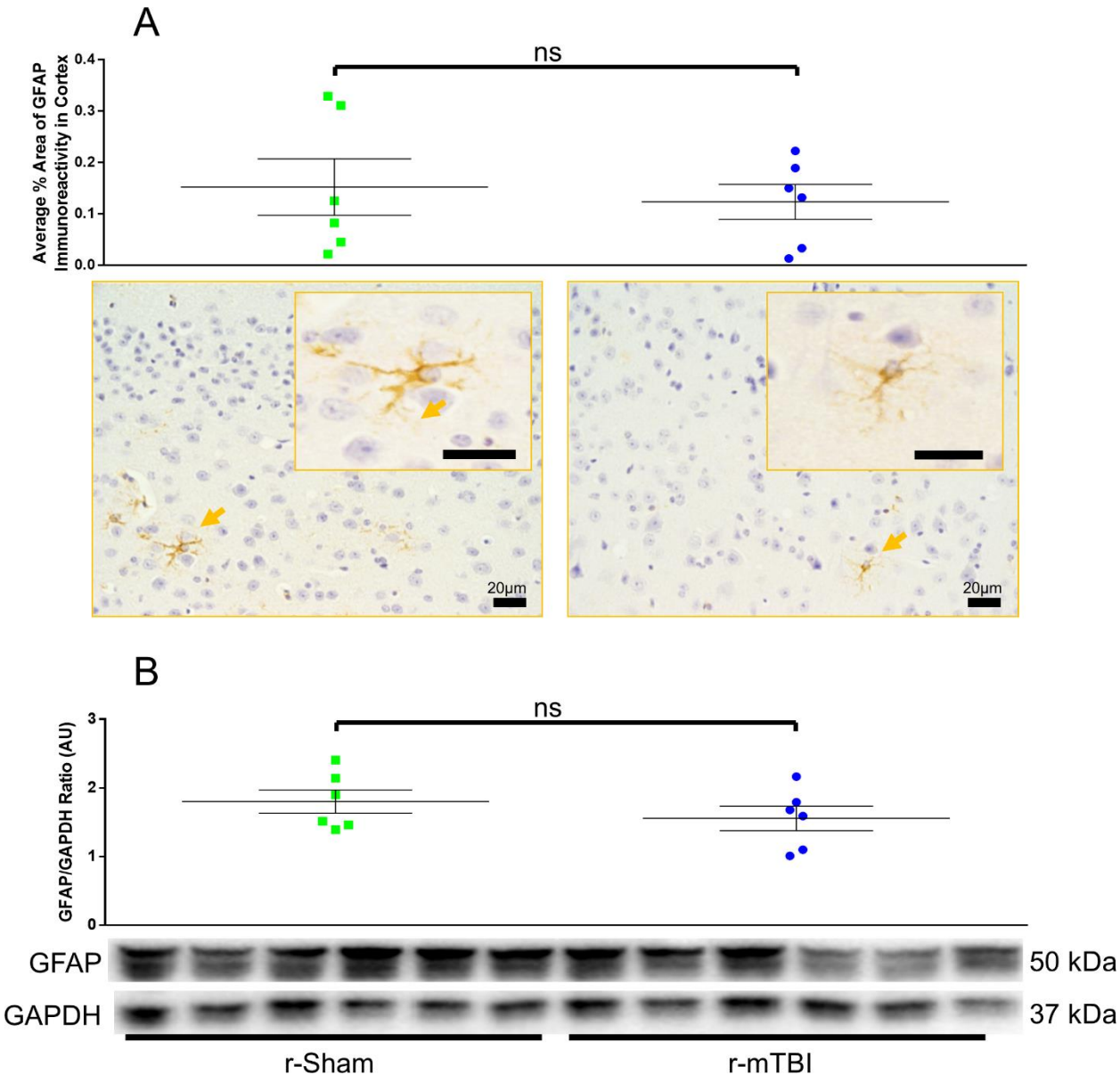

Figure 2.3. Astrogliosis in the cortex of animals 7 months following r-mTBI. (A) There was no difference in expression of GFAP within the cortex of the r-mTBI group when compared to their sham counterpart (P=0.89, unpaired student t-test). (B) Western Blot analysis of brain homogenates showed no significant difference in GFAP expression between groups at 7 months post-injury (P=0.57, unpaired student t-test). Boxed inset in (A) shows 60x magnification of area indicated by the arrow. Astrocytes in the superficial layer of cortex of both r-sham and r-mTBI animals appeared to be morphologically quiescent, and opposed to hypertrophic, in shape. *Immunohistochemistry: 6 r-Sham, 6 female; and 6 r-mTBI, 3 male, 3 female. Values represent percentage area of image analyzed. Error bars represent ± SEM, scale bars in images represent 20μm in length.*

2.3.5. Iba1 Immunohistochemistry and Biochemistry

The degree of glial reactivity throughout the superficial layers of the cortices, the CA1 and the CC of all mice from which the CBF recordings were taken was assessed via immunostaining of brain sections with a macrophage/microglial marker antibody specific to ionized calcium binding adaptor molecule 1 (Iba1). Immunohistochemical analysis of the Cortex (Figure 2.4, A) revealed no significant difference in Iba1 staining between the cortices of r-Sham (0.48% ± 0.04%) and r-mTBI (0.67% ± 0.09%) mice (Figure 2.4, A, P=0.065). Furthermore, it appeared that cells positive for Iba1 in the superficial layer of cortex of either r-Sham or r-mTBI animals were rounded, but not amoeboid in shape, displayed long thin processes and a spherical shaped cell soma (Figure 2.4, A, boxed inset of cell in magnified areas indicated by arrows), indicating an unreactive phenotype. There was a significant increase in Iba1 levels in the CC of r-mTBI mice (Figure 2.5, H, 1.25% ± 0.01% of area) compared to that of r-Sham (Figure 2.5, G, 0.88% ± 0.07% of area) control mice (Figure 2.5, L, $P<0.01$). Immunohistochemical evaluation of Iba1 expression in the cortex of these animals was confirmed by western blot analysis (Figure 2.4, B), which showed no significant difference in brain homogenate Iba1 levels between r-Sham and r-mTBI mice (Figure 2.4, B, P=0.67) at 7 months post-injury. Immunohistochemical analysis of the CA1 revealed no significant difference in Iba1 immunoreactivity between r-Sham (Figure 2.5, E) and r-mTBI (Figure 2.5, F) animals (Figure 2.5, K, P=0.89).

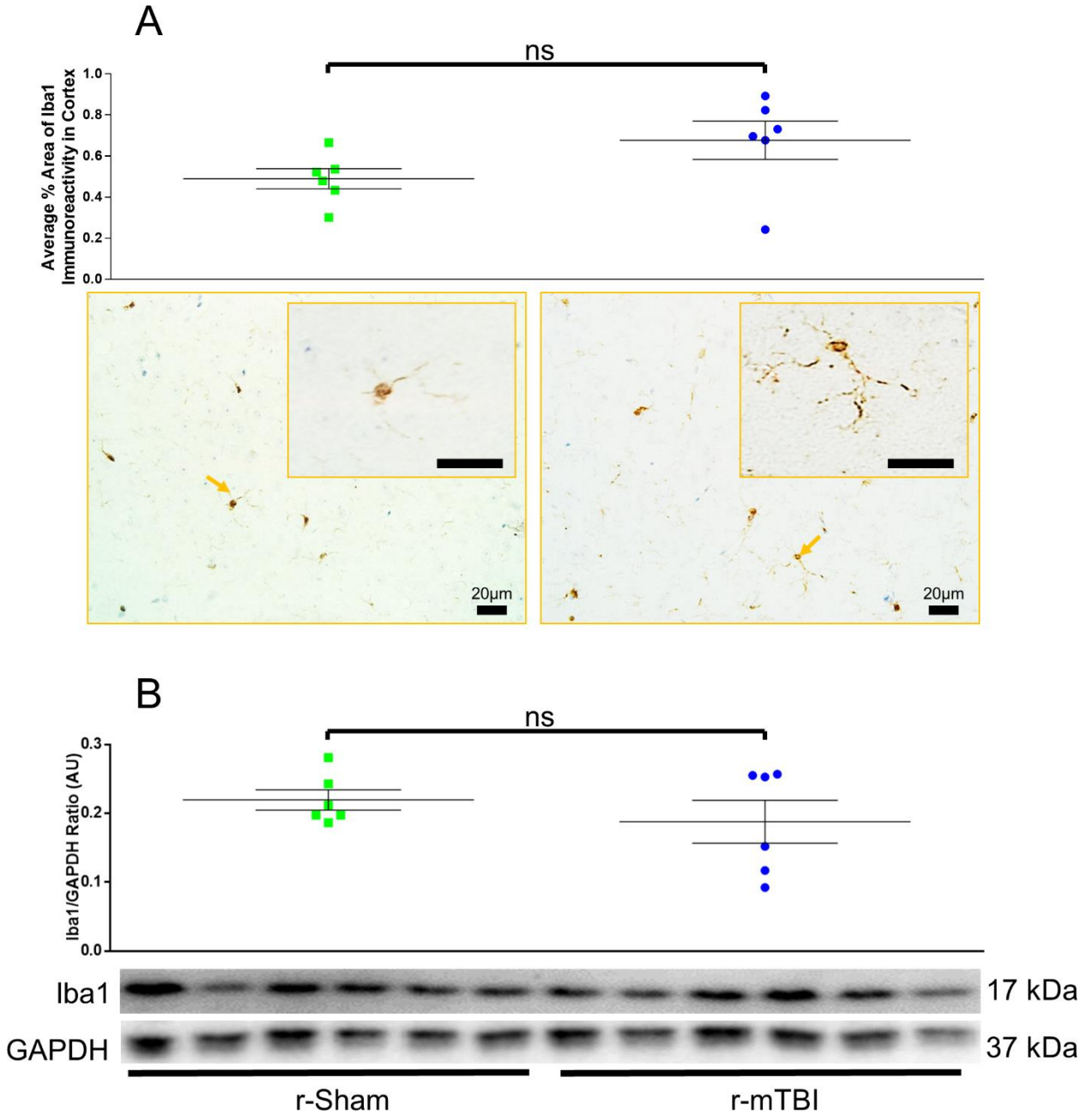

Figure 2.4. Assessment of glial cell reactivity in the cortex of animals 7 months following injury. (A) Immunohistochemistry of brain sections did not reveal a significant difference in glial cell count, as assessed by Iba1 immunostaining, between the cortices of injured animals and sham controls post-injury (P=0.065, unpaired student t-test). (B) Western Blot analysis of brain homogenates showed no significant difference in Iba1 expression between groups at 7 months post-injury (P=0.67, unpaired student t-test). Boxed inset in (A) shows 60x magnification of area indicated by the arrow. Glia in the superficial layer of cortex of both r-sham and r-mTBI animals appeared to be small and rounded, but not amoeboid in shape, with long, thin processes, indicative of a non-reactive microglial state. *Immunohistochemistry: 6 r-Sham, 6 female; 6 r-mTBI, 3 male and 3 female. Biochemical analysis: 6 r-Sham, 6 female; 6 r-mTBI, 3 male and 3 female. Values expressed as percentage of area of image analyzed. Error bars represent ± SEM, Scale bars in images represent 20μm in length.*

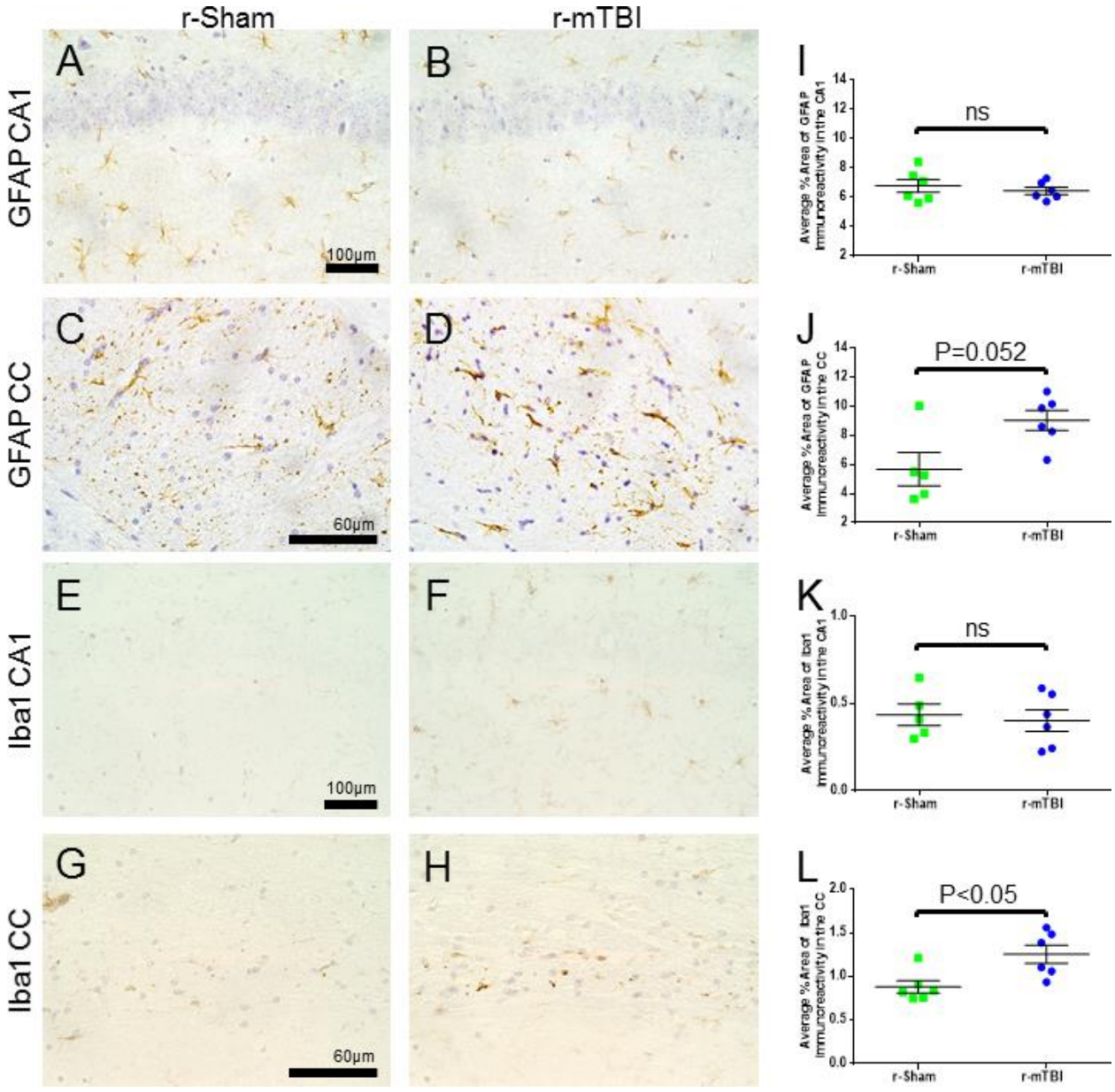

Figure 2.5. Evaluation of astrogliosis and micro-glial cell reactivity by expression of glial fibrillary acidic protein (GFAP) and ionized calcium binding adaptor protein 1 (Iba1), respectively, in the CA1 and corpus callosum (CC) of r-Sham and r-mTBI mice at 7 months post-injury (GFAP, A, B, C, & D; Iba1; E, F, G, & H). There was no significant difference in expression of GFAP-positive cells between r-Sham (A) and r-mTBI (B) mice in the CA1 of the hippocampus at 7 months post-injury (I, P=0.78, Unpaired Student t-test), however, analysis of GFAP immunoreactivity in the CC revealed a moderate increase in astrogliosis in the CC of r-mTBI mice (D, 9.05% ± 0.68% of area) compared to that of r-Sham controls (C, 5.69% ± 1.14% of area), though this was not significant (J, P=0.0519, unpaired Student t-test). Analysis of Iba1 expression in the CA1 (E and F) and CC (G and H) of mice 7 months post injury revealed no significant difference in the degree of gliosis in the CA1 (K, P>0.05, Unpaired Student t-test), however, there was a significant increase in the degree of Iba1 immuno-positive staining in the CC of r-mTBI mice (1.25% ± 0.01% of area) compared to r-Sham controls (0.88% ± 0.07% of area) at 7 months post-injury (L, P<0.05, unpaired student t-test). *GFAP Immunohistochemistry: 6 r-Sham and 6 r-mTBI. Iba1 Immunohistochemistry: 4 r-Sham, 4 Female; 6 r-mTBI, 3 Male and 3 Female. Values expressed as percentage of area of image analyzed. Error bars represent ± SEM, Scale bars in*

images represent 60µm in length for images taken at 40x magnification, and 100µm in length for images taken at 20x magnification.

2.3.6. Biochemical Analysis of Vascular Markers

Immunoblot analysis of the blood vessel markers laminin, PDGFRβ, and αSMA was carried out in r-Sham and r-mTBI mice. The antibody chosen for the experiments herein (Rabbit Anti-laminin, Sigma-Aldrich, L9393) was raised against the α (440 kDa) and β/γ (220 kDa) chains of purified mouse laminin, however, this antibody does not detect the α1 chain on western blots, and so, immunoblot analysis detected a 200-220 kDa protein band appropriate to be the size of β/γ chains. Western analysis of wild type brain homogenate revealed a statistically significant increase in levels of Laminin, PDGFRβ, but not αSMA, in r-mTBI mice, compared to r-Sham controls (Data not shown, $P<0.01$; PDGFRβ, $P<0.01$; αSMA, $P=0.3$). However, as mural cell expression is dependent on vessel density, PDGFRβ and αSMA expression was normalized to the laminin/GAPDH ratio for each lane in the gel, which is portrayed in the graphs seen in Figure 2.6, B and C). The values for PDGFRβ and αSMA, when normalized to their respective Laminin proportions, showed a statistically significant decrease in PDGFRβ and αSMA r-mTBI cortex of 30% and 33%, respectively, compared to r-Sham controls (Figure 2.6, B, $P<0.01$; αSMA Figure 7, B, $P<0.05$).

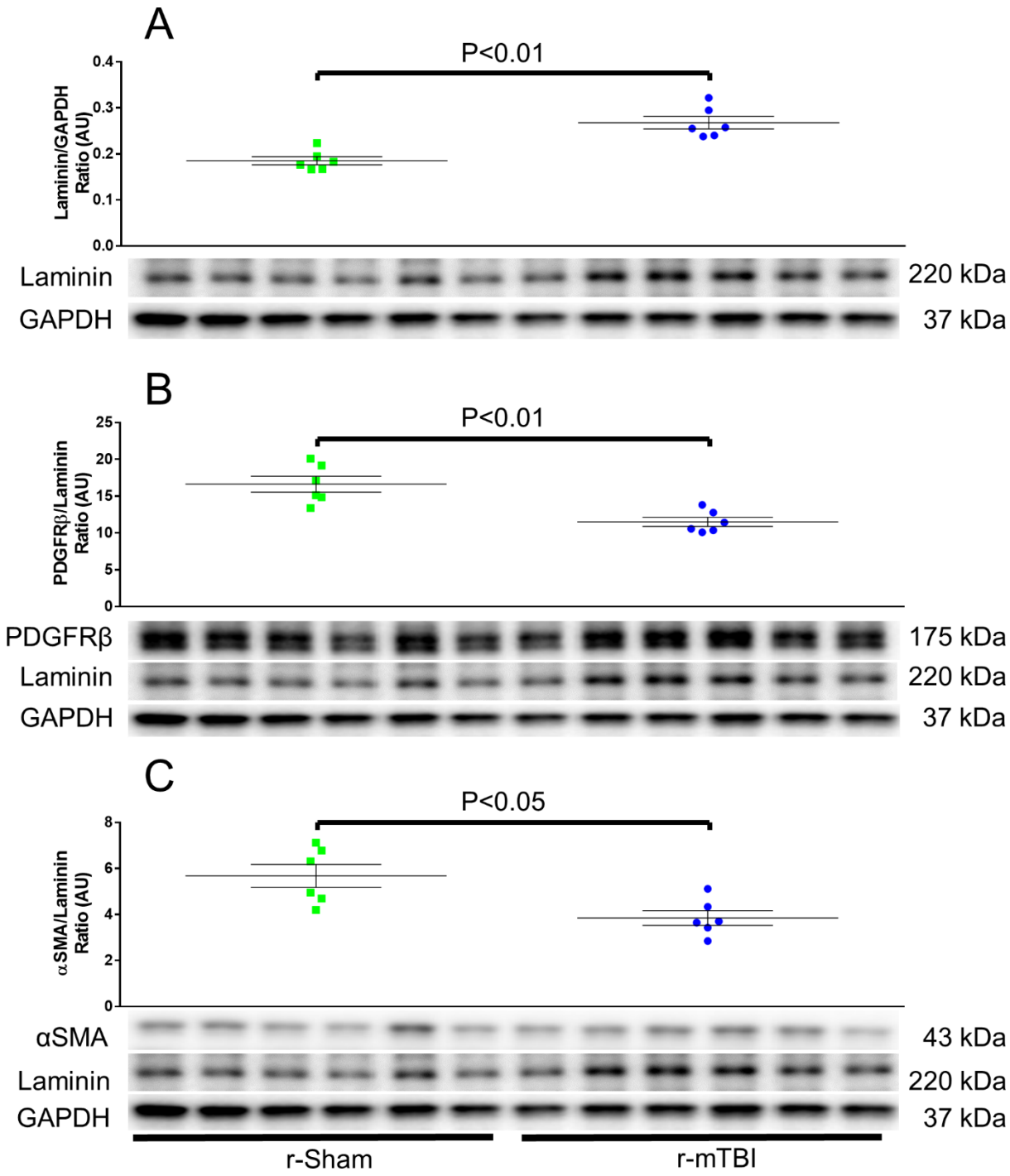

Figure 2.6. Western Immunoblot analysis of brain homogenates of r-Sham and r-mTBI mice. (A) Expression of the neurovascular-associated base-membrane protein laminin was significantly increased in the brains of r-mTBI mice (0.18 ± 0.02, Arbitrary units (AU)) compared to r-Sham controls (0.26 ± 0.03, AU, P<0.01, unpaired student t-test). (B) Levels of platelet derived growth factor receptor β (PDGFRβ) were significantly decreased in the cortex of r-mTBI mice compared to that of r-Sham controls (r-mTBI; 11.52 ± 0.61 AU vs r-Sham; 16.63 ± 0.07, P<0.01, unpaired student t-test) when normalized to laminin expression throughout the brain. (C) Expression of the contractile-associated protein α-smooth muscle actin (αSMA) was significantly lower in r-mTBI cortex compared to r-Sham control cortex (5.67 ± 0.49 AU for r-Sham, vs 3.85 ± 0.32 for r-mTBI, P<0.05, unpaired student t-test), when normalized to laminin

expression throughout the brain. *6 r-Sham and 6 r-mTBI. Values expressed as AU. Error bars represent ± SEM. All densitometry values for laminin for individual bands were normalized to the glyceraldehyde 3-phosphate dehydrogenase (GAPDH) value for their respective lane and this ratio used for statistical analysis. Values for individual lanes for PDGFRβ and αSMA were both normalized to the laminin/GAPDH ratio of the same lane for statistical analysis and generation of graphs (B) and (C).*

2.3.7. Assessment of Cerebral Blood Flow

Average global or entire cortex CBF was markedly decreased in r-mTBI mice compared to their respective r-Sham controls (Figure 2.7, D, wild type r-mTBI vs r-Sham, 10.66% ± 2.04%, $P<0.001$). When analyzed by brain region, there was no significant difference in average CBF between the frontal cortices of r-mTBI and r-Sham mice (Figure 2.7, E, $P>0.05$), however, there was a significant decrease in average CBF in the occipital cortex of r-mTBI mice, compared to r-Sham controls (Figure 2.7, F, $P<0.001$) indicating that the decrease in average global CBF readings in the r-mTBI mice is being driven by the decrease in CBF in the occipital, and not frontal, cortical regions.

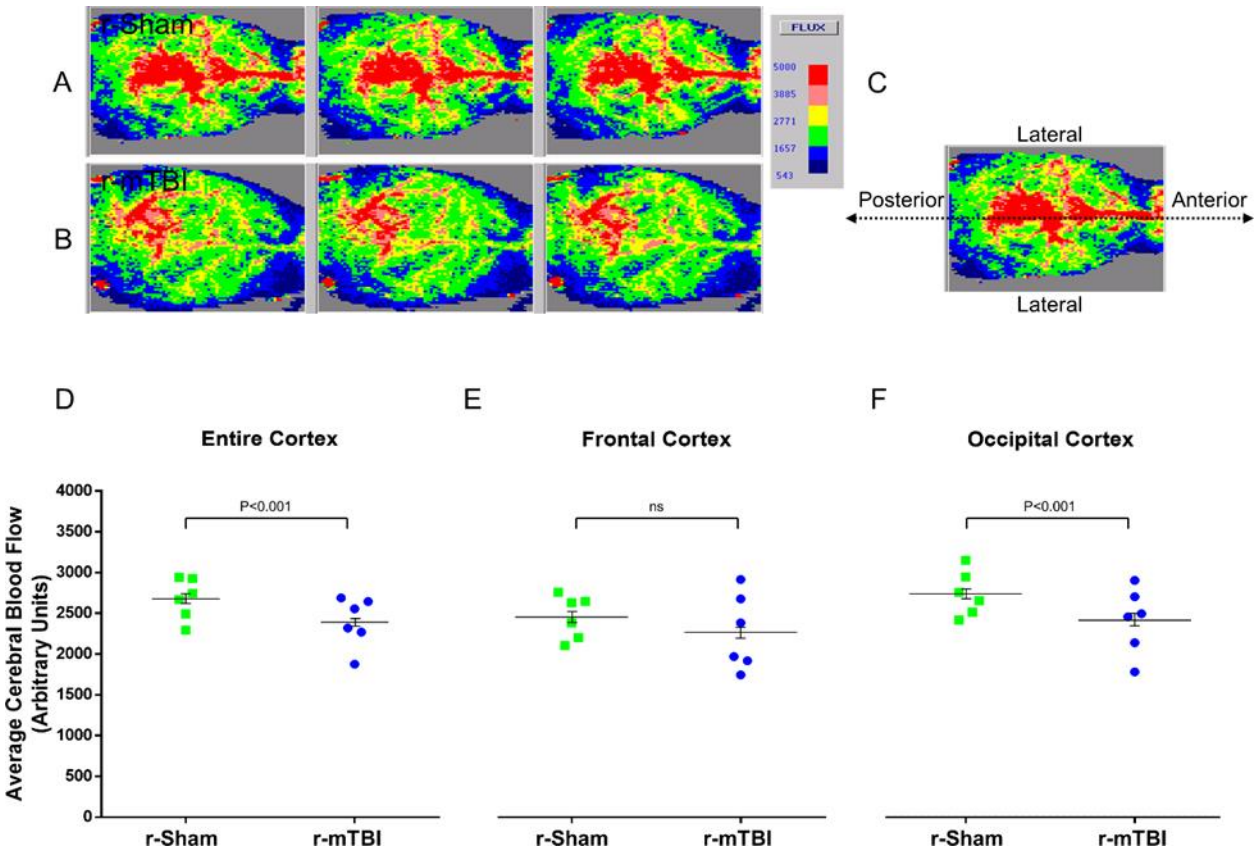

Figure 2.7. Representative replicate images (3 per mouse) of two-dimensional color-coded microvasculature flow maps of both sham and injured aged wild-type mice (A, and B, respectively) obtained using a Moor Instruments® Laser Doppler Imager. Orientation of a representative dorsal view of a microvasculature flow map along the posterior-anterior axis is shown in C. Mouse skull was exposed under isoflurane anesthetic and a bright-field image taken before every repeat scan to allow for future subdivision of the entire cortex reading in to frontal and occipital regions of interest relative to Bregma and Lambda. Six replicate scans per mouse were analyzed to give the average cerebral blood flow for the entire cortex, occipital cortex, and frontal cortex for each group (n=6), represented here as scatter dot plot figures D, E, and F, respectively. The cerebral blood flow recordings were analyzed using a two-way Analysis of Variance (ANOVA) mixed model ANOVA, selecting the replicate values as block (n=6 for each group). At 7 months post-injury, r-mTBI mice show a statistically significant decrease in average cerebral blood flow recordings in the entire cortex of 10.66% ± 2.04%, compared to age matched r-Sham controls. A statistically significant difference in cerebral blood flow is not seen between the frontal cortices of r-Sham and r-mTBI mice, however, a statistically significant and injury-dependent decrease in occipital cortex CBF of 11.87% ±2.33% for r-mTBI mice, compared to their r-Sham controls is evident several months following injury (Figure 1, F). *Mice: 6 r-Sham, 6 r-mTBI. Statistical analysis was conducted using two-way ANOVA. Error bars represent mean ± SEM.*

2.4. Discussion

Understanding the initial primary injuries and evolving secondary injury cascades behind repetitive head trauma is paramount to the development of new therapies to combat disorders like CTE in the human population. Using a mouse model of repetitive injury, we here demonstrate that repetitive mild injury, given at a frequency intended to mimic that endured by professional athletes or military personnel over the course of a career, results in profound impairment of global cerebral blood flow. This impairment in CBF was associated with persistent cognitive deficits evident at 1 month and 6 months post-injury, as demonstrated by impaired acquisition and consolidation of spatial memory in the Barnes Maze. The diminished CBF recordings and behavioral effect we identified here following r-mTBI are in accordance with CBF impairment observed following a single mTBI[139] in the rodent, and prior reports from our lab describing neurobehavioral deficits at chronic time-points following repetitive injury[60,62]. A further advantage to the behavioral analyses conducted here is that that the Barnes Maze acquisition and probe, and the Elevated Plus Maze test, were repeated at both time-points on the same cohorts of mice. The results are thus truly representative of the persistent and evolving nature of cognitive impairment described, and not confounded by any potential cohort-to-cohort experimental error or biological replicate variability. There are fewer r-mTBI mice analyzed and depicted at the 6 month post-injury time-point, as compared to the 1 month post-injury time-point, due to four r-mTBI mice having to be euthanized in compliance with animal welfare and ethics guidelines, and also because of several injured mice having been excluded from probe test as they failed to poke their nose in a single target hole during the 60 seconds of trial.

Perhaps the most prominent of the secondary injury cascades implicated in chronic mild and moderate-to-severe TBI neuropathology in the human population to date is CNS inflammation, seen following even just a single acute severe TBI[160], and persisting up to years following a mild head injury[161]. Indeed, pTau astrogliopathy is a hallmark of CTE[45,46]. Furthermore, recent findings in human CTE patients, by Hsu et al[162], show a phenotype termed 'astrocytic degeneration' in both gray and white matter, with no correlation between pTau immunoreactivity in the sulcal depths and astrogliosis and astrocytic degeneration in white matter adjacent to the sulcal depths. These observations suggest that the neuroinflammatory component of CTE-like pathology may be a CTE signature hallmark of its own[162]. Animal models of r-mTBI readily recapitulate neuroinflammation, with microgliosis and astrogliosis and accompanied white matter degeneration observed up to two years following r-mTBI in mice[59-61,163]. The hit paradigm used in this present study has been shown to induce CBF impairment and neuroinflammatory insult of the white matter in hTau mice aged 9 months, at 3 months post last hit. To validate our current findings as being representative of the white matter microgliosis and astrogliosis demonstrated throughout our previous chronic survival studies in mice at various ages, we examined the Iba1 and GFAP positive immunoreactivity in the superficial gray matter of the cortex, the CA1 of the hippocampus, and the body of the corpus callosum. In line with our previous studies, we observed a significantly greater area of immunoreactivity throughout the white matter at 7 months post-injury in r-mTBI mice, compared to r-sham control animals, with no neuroinflammation evident throughout the gray matter.

Laser Doppler Flowmetry (LDF) is a non-invasive method to estimate the relative blood perfusion in the microcirculation. The LDF technique used here is not only useful in that it is a

real-time measurement of blood flow in these mice, but also pertinent due to the recent use of a similar technique (transcranial Doppler ultrasonography) investigating sports-related injuries in humans, a TBI demographic which our animal model emulates in terms of the frequency of hits sustained over a prolonged period of time. Owing to the failure of many animal models of repetitive injury to recapitulate the kind of extensive p-tau immunoreactivity, neurofibrillary tangles (NFTs), and amyloid burden seen in the human population, and indeed the fact that, as mentioned, tau/amyloid pathology post-mortem may not fully reflect the processes contributing to the development of CTE, the recapitulation of CBF impairment in both athletes and retired military personnel by our r-mTBI mouse model may be of great translational significance. Adding further credence to the diagnostic and preclinical relevance of CBF impairment in repetitive injury-induced pathogenesis, a recent report by Amen et al[141] demonstrated global and regional CBF impairments in National Football League (NFL) players, as measured by Single Photon Emission Computed Tomography (SPECT) imaging, compared to healthy control individuals. Our perfusion studies coincide with these findings, as we observed both a global reduction of CBF in r-mTBI mice, compared to control animals, and brain region-specific alterations in the aftermath of brain trauma. One caveat regards our implemented laser doppler imaging approach is that the whole brain CBF flux maps are two-dimensional image compilations of an approximate 500µm depth of brain tissue beneath the skull, and so, will presumably have incorporated the perfusion of the sagittal sinus and leptomeningeal constituents of the sub-dural anatomy of each mouse, in addition to the pial and parenchymal arteriolar and capillary blood flow. It is known that even a single mild TBI can result in Traumatic Meningeal Injury (TMI)[164,165], characterized in human patients as an abnormal enhancement on post-contrast MRI[164], and seen to lead to cytotoxic

neuronal cell death, oxidative stress, and meningeal vasculature remodelling in animal models of experimental mTBI[165-167]. There is, to the best of our knowledge, no data concerning the effects of TBI on sinus or meningeal flow in human or mouse, however, we cannot ignore the possibility that, given the incidence of TMI following mTBI, the decreased CBF described in the r-mTBI mice in the present study could have been in part due to injury-related perfusion deficit in these vessels. Future studies will incorporate a more zealous positioning of the regions of interest to be analyzed, in order to exclude potentially confounding supra-cortical vessels.

In order to ascertain whether the observed changes in CBF in our mouse model of r-mTBI were due to alterations in vessel status, we conducted biochemical analysis of the protein laminin, a known component of the vascular basement membrane[168]. We observed significant increases in laminin expression at 7 months following injury in r-mTBI mice. Recent studies describe angiogenesis and vasculogenesis in both human patients and animal models following TBI and stroke[169]. Angiogenesis involves the proliferation of endothelial cells and sprouting of micro-vessels, both culminating in a gross increase in intra-cerebral vascular density[170]. Indeed, neovascularization at a chronic time-point post-injury has been seen at as late a time-point as 9 months post-injury in a Lateral Fluid Percussion injury mTBI model in the rat[171]. This evidence of chronic increases in vascularization (upwards of 28% as detected using arterial spin labelling MRI) are not unlike our own observations of increased expression of laminin in r-mTBI mice.

Pursuant to determining the importance of changes in vessel density as a cause of reduced CBF, we also investigated the possibility of cerebrovascular mural cell involvement. Leptomeningeal arteries and precapillary arterioles are covered by Smooth Muscle Cells (SMCs,

which express the contractile component αSMA), which wrap around the vessel with a band-like circumferential morphology, and are thought to be principally responsible for vasomotion and regional CBF flux[106]. Capillaries are bereft of SMCs, and are instead predominantly covered by pericytes, expressing high constitutive levels of PDGFRβ[106]. The involvement of SMCs and pericytes in CBF regulation[106,108,109,121,172-177] has been well characterized and, as such, we have chosen these markers for interrogation of mural cell involvement in r-mTBI induced CBF dysregulation. In order to represent the observed mural cell marker changes as a function of vessel density, the values of PDGFRβ and αSMA were normalized to the relative amount of laminin in each sample and we observed a significant decrease in levels of both PDGFRβ and αSMA in r-mTBI mice, compared to r-Sham animals. It may be worth noting that we examined whole-brain homogenate, and thus it is impossible to surmise whether the reductions in mural cell markers seen herein are confined to either large leptomeningeal and intraparenchymal arteries, smaller arterioles, or both. With the exception of aforementioned work by Dore-Duffy et al[121], the expression of αSMA has not been extensively researched with respect to mTBI. However, it has been demonstrated that intracerebral and leptomeningeal SMCs taken from AD patient brains express significantly greater levels of αSMA, compared with age-matched control subject samples, when normalized to β-tubulin[178], a housekeeping protein whose expression is found not to be altered by the AD phenotype[178]. The same study[178] reported an increase in αSMA, as opposed to the decrease catalogued by our present observations, however, this group did not normalize αSMA expression to the associated vasculature, as has been done in the current report, but instead to the individual vesicular SMC β-tubulin levels, thereby expressing αSMA as a function of the cell on which it is ubiquitously expressed, rather than in proportion to the

vasculature as a whole. Furthermore, recent studies by Merlini et al[179] demonstrated an early-onset Braak Tau-dependent, amyloid pathology-independent decrease in large leptomeningeal artery αSMA expression in the brains of human AD patients, with smaller arterioles exhibiting a significant decrease in αSMA at later disease progression. Akin to our approach, the relative αSMA expression was obtained by normalization to vessel wall levels[179]. These results may in part explain the hypoperfusion deficits seen with early AD[128-130], as larger arterioles are implicated as being more regulative of CBF[106], and so, the above studies provide rationale for how the reduced αSMA expression observed in this report may be causative of the reduced CBF noted in our r-mTBI mouse model.

Although some studies have designated capillaries, and by default pericytes, as the principal contributors to regional CBF both in normal physiology[108,109,118] and following cerebral ischemia[108,175,176], others[106,173,174] have catalogued pericytes as unimportant in these regards. However, as mentioned earlier, pericytes have been implicated in TBI-induced hypoperfusion in both human patients[135] and also in animal model studies, one such being a recent report by Dore-Duffy et al[121], showing the release of endothelin-1 (ET1), a potent vasoconstrictor, from damaged pericytes 4 hours following a closed head injury. Inhibition of ET1 *in vivo* has also been shown to both alleviate impairment in autoregulation in the piglet cerebrovasculature[180], and to restore CBF levels in the rat[181] following mTBI, and elevation of ET1 levels in CSF is shown to be correlated with unfavorable outcomes in children following severe TBI[182]. DeGracia et al[183] have shown a robust stress response, identified by Heat Shock protein 70 (HSP-70) immunofluorescence, confined to the capillary bed of the mouse microvasculature, and coinciding with endothelial and pericyte cell death, following a single mTBI. Using quantitative autoradiography, Bell et al[172] have

demonstrated that knockdown in PDGFRβ signaling leads to pericyte deficiency-induced impairments in CBF and BBB integrity in adult mice, in addition to age-dependent neuronal degeneration and novel object recognition memory deficits. As opposed to the 10% reduction in global CBF recorded in r-mTBI mice, compared to r-Sham controls, in our study, Bell and colleagues observed CBF reductions of up to 50% in the cortex and hippocampus of 14-16 month old mutant heterozygous $PDGFRB^{+/-}$ deficient mice[172]. However, the decrease in PDGFRβ expression and any consequent effects on CBF seen in our study are not directly relatable to those seen by Bell et al[172], as theirs was an aging, and not an injury, study. Firstly, the increases in laminin expression in the r-mTBI mice in our study may reflect injury-induced angiogenesis and/or thickening of laminae, whereas Bell et al[172] documented significant decrease in microvessel length, and decreased laminin expression, as a result of PDGFRβ deficiency. Secondly, the mice used in the Bell study exhibited impaired PDGFRβ signaling from birth, as opposed to an injury-induced depletion later in life as with our animals. However, despite these caveats, it is clear the disruption of pericytes, be it through direct ablation of the cells, or encroached PDGFRβ activity, can dramatically impair CBF in mouse models. Further research is merited to discover whether the decrease in PDGFRβ following r-mTBI reflects reduced pericyte density, or mere alterations in the expression of this receptor.

These findings, alongside our observations of reduced mural cell marker expression following r-mTBI, indicate a role for mural cells in the pathophysiological profile following brain trauma. Select representative images from the superficial layers of cortex of our r-Sham and r-mTBI mice show non-hypertrophic astroglia, and microglia with small and round cell bodies and many dendritic processes, indicative of a resting or unreactive state of both astrocytes and microglia[184].

There is also an increase in GFAP and Iba1 immunoreactivity in the CC, data in agreement with previous studies from our group investigating astrocytic and glial immunoreactivity at this time-point post injury[60]. The fact that there is also a r-mTBI-induced increase in GFAP/Iba1 immunoreactivity in the cortex, nor a reactive phenotype of these cells would suggest that glial-associated neuro-inflammation may not be a factor with regards to the injury-induced hypoperfusion seen at 7 months post-injury in our studies. Instead, the reduced CBF we observe following r-mTBI is more likely due to changes in the expression profile of the cerebrovascular mural cell markers.

A previous report from our laboratory demonstrated r-mTBI pathology in conjunction with marked and persistent behavioral deficits at chronic time-points following 5 repetitive injuries[60] in wild type mice. Another pursuant study from our lab, using an identical hit intensity, but at a greater frequency, occurring over a longer period of time, and carried out in hTau mice, showed diverse CTE-like pathology at a chronic time-point post-last injury, in tandem with marked CBF impairment, but with only modest neurobehavioral effects[62]. This current study bridges the gap in reporting between the last two studies mentioned, showing an injury-dependent effect of r-mTBI on global CBF readings and a down-regulation in mural cell markers several months after the final injury, which taken together suggest a causal role for CBF dysregulation and the emergent neurocognitive deficit in this r-mTBI animal model. Moreover, we demonstrate neuroinflammatory hallmarks consistent with the pathology observed in other mouse TBI models and human TBI cases. In the next Chapter, I will explore these concepts further to characterize the nature of the cerebrovasculature following brain trauma and elucidate the association between vascular dysfunction and brain pathology after repetitive injuries to the brain.

Chapter 3. Sustained neurobehavioral deficits and progressive cerebrovascular marker dysregulation throughout the cortex at chronic time-points post-injury.

3.1. Introduction

The greater proportion of reports cataloging Traumatic Cerebrovascular Injury (TCVI) in the human population have been within the acute survival window for patients suffering severe head trauma and expiring shortly thereafter[185-188]. The very few case studies investigating TCVI and the response of the vascular bed of the CNS to more modest injury have only been feasible due to fatal complications not related to the initial trauma following concussion, or analysis of cerebral tissues removed during lobectomy or hematoma as surgical intervention following injury[100,132,185,186,188]. Two separate studies by Rodriguez-Baeza and colleagues[186], and Castejon et al[133,134], investigating ultimately fatal severe TBI, at 1 to 20 days post-injury, and 7 to 30 days post-injury, respectively, have demonstrated vessel wall morphological and cellular changes in the brains of traumatized patients, compared to non-TBI control samples. This early remodeling of the cerebrovasculature following a severe insult, which is invariably coupled with impaired CBF, might be a shared pathogenesis of the CBF perturbations seen in repetitive mild head trauma. Our recent findings in Chapter 2 support this hypothesis, demonstrating a robust dysregulation in vascular marker expression in the brains of head-injured mice many months following r-mTBI, in tandem with gross perfusion deficits.

Our work is the first to characterize vascular pathology, and correlate CBF infringement, at such a chronic time-point post-r-mTBI in a preclinical animal model, however, there is little

post-mortem data with which to compare these findings with the time-course of TCVI progression after mild injury in human patients. The preclinical TBI field must instead rely on human imaging studies of resting state CBF in those afflicted with a history of mTBI as phenotypic for the underlying pathology easily quantifiable across murine studies. However, this approach is far from ideal, as post-mortem human studies have identified both apoptotic and regenerative features occurring alongside one another at sites of TCVI in human tissue weeks following a severe TBI[189], and repetitive high magnitude head acceleration r-mTBI is linked to transient vascular perfusion deficit in asymptomatic female soccer athletes[145,146], suggesting that TCVI phenotypes may be biphasic in nature. Ergo, point-in-time measurements of CBF, such as our work in chapter 2, in both clinical and preclinical studies may not be fully representative of the evolution of TCVI over time. Instead, a longitudinal and serial imaging approach, such as the aforementioned study by Svaldi and colleagues[145,146], would be more suitable in elucidation of the cerebrovasculature's changing structural plasticity and manifest physiological signal in response to head trauma.

Another caveat of our study in Chapter 2 is the fact that, while r-mTBI at an adult age of 12 months in mice may be representative of the more tenured professional athlete and military demographic in the human population, it might also be too advanced a time of first injury to be reflective of the larger proportion of human mTBI patients. In fact, recent work by Alosco and McKee[190] has shown younger age of first tackle in contact sports to predict earlier cognitive and neuropsychological symptom onset across both CTE and CTE-like neuropathological brains of former athletes, and without correlation with increased CTE neuropathological staging[190]. Indeed, recent work from our lab has demonstrated a pre-clinical parallel of the afore mentioned

findings by Alosco and colleagues[190], demonstrating differential age-dependent neuropathological effects following an identical r-mTBI in young and aged hTau mice, with the microglial and neuronal injury profile showing greatest ferocity in younger 3 month old mice, compared with 12 month old adult mice[191]. While the injury paradigm and survival time studied were of lesser intensity and more acute length, respectively, than those in chapter 2, juxtaposition of both above works by Mouzon[191] and Alosco[190] compel us to ask whether there is an optimal time at which to administer r-mTBI in our, and other, animal models, and to look at the chronic TCVI aspect thereafter.

With all of this in mind, and owing to the possible biphasic mechanism of TCVI in mouse and man, in this chapter, we aimed to study the biological basis of TCVI across two chronic time-points following r-mTBI, using the same model as described in Chapter 2, but instead administering the mTBIs at an earlier age, more relevant to the human athlete and military collective of r-mTBI patients.

3.2. Materials and Methods

3.2.1. Injury Schedule

3-month-old male mice were randomly assigned to one of two groups: repetitive mild Traumatic Brain Injury (r-mTBI, delivered twice each calendar week i.e. 1 hit approximately every 72 hours, over a period of 3 months) or repetitive Sham (r-Sham; animals underwent the same duration and frequency of anesthesia as r-mTBI animals). An electromagnetic impactor (Leica Instruments) was used to generate a midline mTBI, using a 5.0mm diameter flat face tip, 5m/s strike velocity, 1.0mm strike depth, and a 200msec dwell time, as previously characterized. The mice were euthanatized at either 3 months or 9 months after the final injury/anesthesia (6, and 15 months of age, respectively), with euthanasia preceded by behavioral testing and evaluation of cerebrovascular reactivity (Chapter 4). The "9 month" cohort was initiated first, and was originally intended as a 6 months post-injury cohort; hence the behavioral testing was carried out at 6 months post-injury. However, development and optimization of the CVR procedure was extremely labor intensive and was not ready for implementation until the animals were 9 months post-last injury/anesthesia, hence the delay between behavior and CVR/euthanasia. The "3 month" cohort underwent behavioral assessment, CVR analysis, and euthanasia on schedule.

3.2.2. Biochemical Analyses of vascular markers in vascular-enriched fractions.

Western blot analysis was carried out on vascular-enriched fractions from whole cortical brain tissue dissected from sacrificed r-sham and r-mTBI mice. The cerebrovasculature from mouse brain tissue was isolated using a methodology previously established by our group[192]. For

the murine samples, fresh cortices were collected (minus the cerebellum, brain stem, and hippocampus). The mouse cortex was minced with a blade prior to being ground with 6–8 passes of a Teflon pestle in a glass Dounce homogenizer. Brain material was homogenized in fivefold excess of ice-cold Hank's balanced salt solution (HBSS) containing 10 mM HEPES. A sample of the brain homogenate was collected as a representation of the whole cortex. An equal volume of 40% dextran solution was added to the brain homogenate for a final concentration of 20% dextran and immediately centrifuged at 6000g for 15 min at 4˚C. This procedure results in a pellet at the bottom of the container (cerebrovasculature) and a compact mass at the top of the solution (parenchyma) separated by a clear dextran interface (soluble fraction). The cerebrovascular and parenchymal pellets were washed with ice-cold HBSS and resuspended in lysis buffer consisting of M-PER reagent (Pierce Biotechnology) supplemented with Halt protease and phosphatase inhibitor cocktail (Thermo Scientific). All the fractionated mouse brain samples were stored at −80˚C until further analysis. Our cerebrovascular preparation consists of capillary micro-vessels and small cerebral vessels, as we are interested in studying the role of both brain vascular pericytes and smooth muscle cells in r-mTBI. Equivalent total protein amounts were analyzed on sodium dodecyl sulfate-polyacrylamide gel electrophoresis under denatured and reduced conditions using 4-20% TGX Stain-free precast Gels (Biorad), and electro-blotted on to a low fluorescence polyvinylidene difluoride (PVDF) membrane for 2 hours at 90mA constant current. Membranes were then washed in de-ionized water, before being blocked for 1 hour at room temperature with 5% non-fat milk in tris buffered saline (TBS). Membranes were then incubated with primary antibodies overnight (12-16 hours at 4°C). The following primary antibodies were used at the given concentrations; laminin (Sigma, rabbit anti-mouse laminin,

L9393, 1:50 Dilution), platelet derived growth factor receptor β (PDGFRβ; Abcam, rabbit anti-PDGFRβ monoclonal, ab32570, 1:1000 Dilution), alpha smooth muscle actin (αSMA; Millipore, mouse anti-αSMA monoclonal, ASM-1, 1:1000 dilution), rabbit ant-mouse β-Actin (Cell Signaling Technology (CST), 13E5, 1:1000 dilution), goat anti-mouse Aminopeptidase-N (CD13; R&D Systems, AF2335, 1:1000 dilution), rabbit anti-CD31 (PECAM-1, R&D Systems, D8V9E, 1:1000 dilution), mouse anti-cycloxygenase-1 (COX1, Abcam, ab695, 1:500 dilution), mouse anti-endothelial nitric oxide synthase (eNOS, Abcam, ab76198, 1:500 dilution). Membranes were washed with deionized water, incubated with the appropriate secondary antibody for 1 hour at 4°C, washed once more, and then developed using ECL chemiluminescent detection reagent (GE Life Sciences). Membranes were imaged using a Biorad ChemiDoc Western Blot Imager, and densitometry results of individual bands were collected using ImageLab 5.2 (Biorad) software. Target protein values for each lane were normalized against densitometry values for either the β-Actin value, or the Laminin/β-Actin ratio, for their respective lane. Target protein values were also normalized against the total protein stain for their respective lane using a stain-free total protein stain (data not shown) to validate the β-Actin-normalized results.

3.2.3. Biochemical Analysis of BBB Integrity

Western blot analysis of vascular endothelial tight junction proteins was carried out on the same vascular-enriched immunoblots as were analyzed for mural cellular and functional markers as above, and under the same experimental conditions. The following primary antibodies were used at the given concentrations; rabbit polyclonal anti-Occludin (Santa Cruz Technology, H279,

1:1000 dilution), rabbit anti-Zonnula Occludens 1 (ZO-1) antibody (Santa Cruz Technology, H300, 1:1000 dilution).

3.2.4. Assessment of Cognitive Function

Cognitive function was assessed at 3 and 6 months after the final injury/anesthesia (9 months of age and 12 months of age, respectively) by use of the Barnes maze, as described previously by our group[59]. Researchers conducting the experiments were blind to the grouping, and the Ethovision XT System (Noldus) was used to track and record the movement of each animal. Mice were given 90 seconds to locate and enter the target box and required to remain in the target box 30 seconds prior to retrieval, regardless of success. For a series of 6 consecutive days, 4 trials were given per day, with mice starting from one of four cardinal points on each trial. The inter-trial interval for each mouse on any given day of acquisition was approximately 40 minutes. The maze platform and retrieval box were both cleaned thoroughly between trials to limit the confounding effects of scent on performance of the mice during each trial. On the seventh day, a single probe trial lasting 60 seconds was performed with the mouse starting from the center of the maze and the target box removed. Escape latency measured the time taken for the mouse to enter the box. In addition to assessment of learning and spatial memory via use of the Barnes maze, animals were tested for anxiety-like behavior in the elevated plus maze (EPM)[158]. The apparatus consists of two open and two closed arms forming a plus shape. The arms are elevated approximately 80 cm from the floor. Each mouse was placed on the junction of the four arms of the maze, facing the open arm. The mouse was allowed to freely explore the maze for 5 min in a

dimly lit ambient lighting (~1 lux). The percentage of time spent in the open arms was calculated using Ethovision video tracking system[158].

3.2.5. Validation of Vascular-Enriched Fraction Preparation.

Laser confocal microscopy of a vascular-enriched fraction from the cortical tissue of a naïve, 9 month old wild type mouse was carried out in order to confirm the presence of intact vessels in these vascular-enriched preparations. Immediately following dextran filtration centrifugation, the vascular pellet was resuspended in ice-cold 4% Paraformaldehyde (PFA) and fixed for 24 hours at 4 degrees Celsius. Following PFA fixation, the vessel preparation was centrifuged at 2000g for 30 seconds, the pellet was cleaned once with ice cold PBS, and the pellet was resuspended in 200µL PBS containing 10% Bovine Serum Albumin and 0.5% Triton X 100 detergent and blocked for 2 hours at room temperature. After blocking, 200µL of PBS containing 1:1000 dilution of fluorescent Dylight Lectin, and the primary antibodies CD13, at 1:1000 dilution, and the nuclear stain 4',6-diamidino-2-phenylindole (DAPI), at 1:2000 dilution, were added to the 200µL fixed and resuspended vascular pellet solution, and the vessels incubated overnight at 4 degrees Celsius. The vessel fraction suspension was then centrifuged at 2000g for 30 seconds, and washed twice with PBS, before incubation with the respective fluorescent secondary antibody to CD13 for 1 hour at room temperature. Following secondary antibody incubation, the vessel preparation suspension was once more centrifuged at 2000g for 30 seconds, washed twice in PBS, and resuspended in 200µL aqueous fluorescent mounting media. 50µL of the vessel fraction containing aqueous mounting media was then pipetted on to a glass slide, and covered with a cover slip. The vessels were the n imaged using a Carl Zeiss Laser Scanning Confocal Microscope.

3.3. Results

3.3.1. Barnes Maze Acquisition and Probe

At both 3 and 6 months following the final injury/anesthesia, r-mTBI mice travelled a significantly greater cumulative distance than their r-Sham controls (Figure 3.1, A and B, $P<0.001$). Additionally, we observed a distinct effect of injury on cumulative distance travelled over time, reflected by a progressive separation of cumulative distance travelled by r-mTBI mice, compared to r-sham controls, across the 6 consecutive days of acquisition at 3 month post-injury (Figure 3.1, A, r-Sham vs r-mTBI; $P=0.0118$), and also a significant effect of treatment on cumulative distance with time at 6 months (Figure 3.1, B, r-Sham vs r-mTBI; $P<0.001$). The mean velocity of r-mTBI mice was statistically significantly greater at both 3 and 6 months post-injury (Figure 3.1, C and D, $P=0.0046$ & $P=0.0119$, respectively), with the average velocity of r-mTBI mice being statistically greater than that of r-Sham controls on day 6 of acquisition at both 3 months (Figure 3.1, C, $P<0.05$) and 6 months (Figure 3.1, D, $P<0.05$) post-injury.

Spatial memory was analyzed at 3 and 6 months following final injury/anesthesia, at 9 and 12 months of age, respectively. Probe test performance was profoundly impaired in r-mTBI mice, compared to r-sham controls, at both 3 months (Figure 3.1, E, $P<0.01$) and 6 months (Figure 3.1, F, $P<0.05$) post-injury.

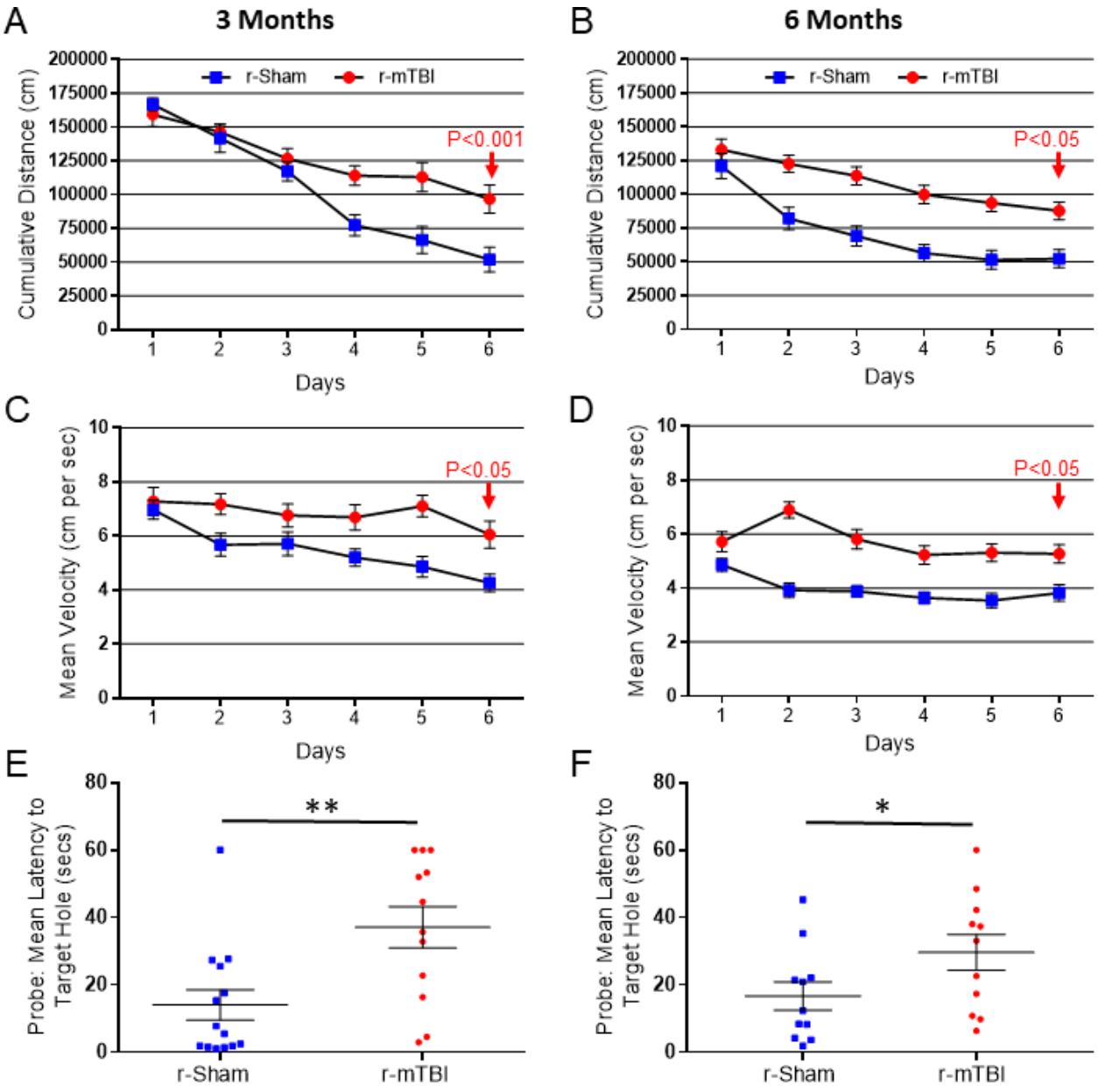

Figure 3.1. Evaluation of learning (acquisition) and retention of spatial memory of wild type mice using the Barnes maze at 3 and 6 months following repetitive mild traumatic brain injury. Mice were tested in the Barnes maze for their ability to locate a black box at the target hole. During the course of the 6 days of acquisition at both the 3 and 6 months chronic time-points post-injury, the r-mTBI mice travelled a greater mean cumulative distance to reach the target hole, compared to sham controls (A and B, $P<0.001$, repeated measures ANOVA). In cumulative distance data, the injury by time interaction term was statistically significant across the 6 days of acquisition at the 3 month post-injury time-point ($P<0.0001$, Repeated Measures ANOVA), however, this was not seen at the 6 month time-point ($P=0.08$, repeated measures ANOVA). There was also a significant effect of injury on mean velocity between groups across all 6 days of acquisition at both the 3 month and the 6 month time-points (C and D; $P<0.05$, repeated measures ANOVA) with a significant increase in velocity of r-mTBI mice vs r-Sham controls on day 6 of acquisition at both 3 and 6 months post-injury (D; $P<0.05$, Two Way ANOVA). Evaluation of spatial memory of wild type mice using the Barnes maze at 3 and 6 months following repetitive mild traumatic brain injury. Mice were tested in the Barnes

maze for their ability to locate a black box at the target hole. During the course of the 6 days of acquisition at both the 3 and 6 month chronic time-points post-injury, the r-mTBI-treated mice travelled a greater mean cumulative distance to reach the target hole, compared to sham controls (A and B, $P<0.001$, repeated measures Two Way ANOVA). Evaluation of spatial memory retention (Probe) of wild type mice using the Barnes maze, at 3 and 6 months following r-mTBI (Figure 3.1, E and F, respectively). For the probe trial (the day immediately following the 6 consecutive days of acquisition testing), the target box was removed, and mice were placed in the middle of the table for a single, 60-second trial. Probe test performance was significantly impaired in the r-mTBI mice at 3 months (A, $P<0.01$, one-way ANOVA, student t-test) and 6 months (B, $P<0.01$, one-way ANOVA, student t-test), compared to r-Sham controls. *Data are presented as Mean ± Standard Error of the Mean (SEM); 12 r-Sham, and 12 r-mTBI at 3 Month; 11 r-Sham, and 11 r-mTBI at 6 Months.*

3.3.2. Cerebrovascular Marker Dysregulation, Normalized to β-Actin, at 3 , Months Post-Injury

The biochemical analysis of vascular fractions of wild type r-sham and r-mTBI cortical tissue revealed a statistically significant decrease in expression of both platelet derived growth factor receptor-β (PDGFRβ) (Figure 3.2, B, $P<0.01$, unpaired student t-test) and endothelial nitric oxide synthase (eNOS) (Figure 3.2, B, $P<0.05$, unpaired student t-test) at 3 months post last mTBI (9 months of age). There was no apparent change in the expression level of any other cerebrovascular-associated marker, except for expression of cyclo-oxygenase-1 (COX-1), which displayed a modest increase in expression following r-mTBI, compared to the r-sham group, however, this change was not statistically significant (Figure 3.2, B, $P = 0.0532$, unpaired student t-test). The average density of the loading control bands (β-Actin) was not different between groups at 3 months post-injury, indicating that the vasculature of both r-mTBI and r-sham mice exhibited proportionately similar cellularity at this time-point (Figure 3.2, C, $P>0.05$, unpaired student t-test).

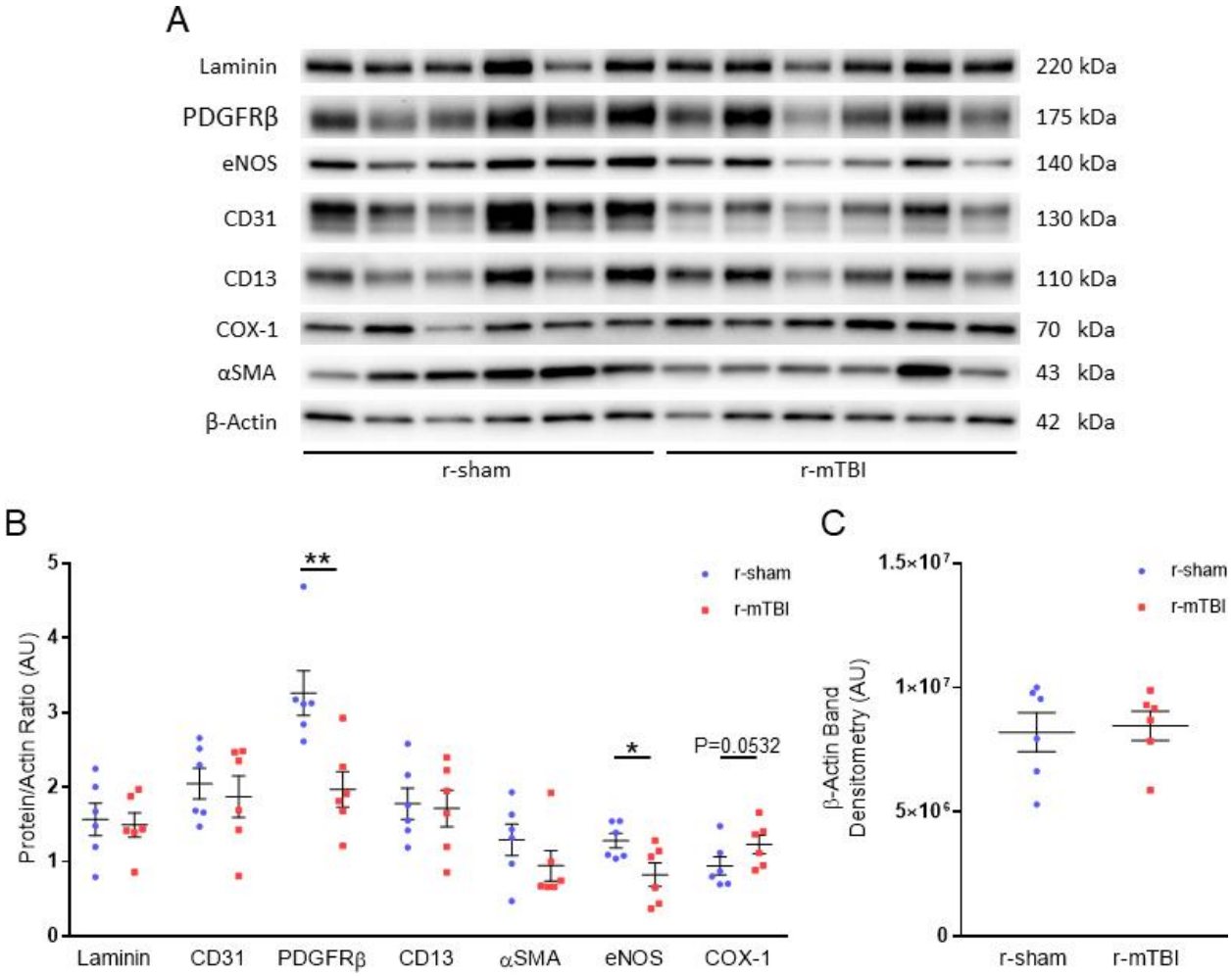

Figure 3.2. Western immunoblot analyses of cerebrovascular cellular and functional markers in cortical vascular-enriched fractions at 3 months following r-mTBI. Representative images of western blot bands shown in (A) were analyzed via densitometry to compile the graphs shown in (B) and (C). Expression of laminin, CD31, CD13, αSMA, and COX-1 were not altered in cortical vascular fractions of r-mTBI mice, as compared to r-sham, at 3 months post-injury (B, P>0.05, unpaired student t-test), however, the expression of the receptor complex PDGFRβ, and endothelial nitric oxide synthase (eNOS) were significantly decreased in r-mTBI cortical vasculature, compared to the vascular fractions of r-sham controls (B, P<0.05, unpaired student t-test). There was a trend toward increase in levels of cyclo-oxygenase 1 (COX-1) in the cortical cerebrovasculature of r-mTBI mice, versus that of r-sham controls, however, this change was not significant (C, P = 0.0532, unpaired student t-test). The mean density of the β-Actin bands did not differ across groups (C, P>0.05, unpaired student t-test). *Wild type mice; 6 r-Sham and 6 r-mTBI. Values expressed as AU. Error bars represent ± SEM. All densitometry values for individual bands in (A) were normalized to the β-Actin value for their respective lane and this ratio used for statistical analysis in (B). Values for individual lanes for β-Actin in (C) were not normalized to any other band. No statistical significance between groups unless otherwise stated by horizontal bars and text. Error bars represent ± SEM.*

3.3.3. Cerebrovascular Marker Dysregulation, Normalized to the Laminin/β-Actin ratio, at 3 Months Post-Injury

When normalized to their respective Laminin/β-Actin ratio for each lane, the biochemical analysis of vascular fractions of wild type r-sham and r-mTBI cortical tissue revealed a statistically significant decrease in expression of both platelet derived growth factor receptor-β (PDGFRβ) (Figure 3.3, B, $P<0.05$, unpaired student t-test) and endothelial nitric oxide synthase (eNOS) (Figure 3.3, B, $P<0.05$, unpaired student t-test) at 3 months post last mTBI (9 months of age). There was no apparent change in the expression level of any other cerebrovascular-associated marker, except for expression of cyclo-oxygenase-1 (COX-1), which displayed a modest increase in expression following r-mTBI, compared to the r-sham group, however, this change was not statistically significant (Figure 3.3, B, $P>0.05$, unpaired student t-test). The average density of the loading control (Laminin/β-Actin ratio) was not different between groups at 3 months post-injury, indicating that the vasculature of both r-mTBI and r-sham mice exhibited proportionately similar cellularity at this time-point (Figure 3.3, C, $P>0.05$, unpaired student t-test).

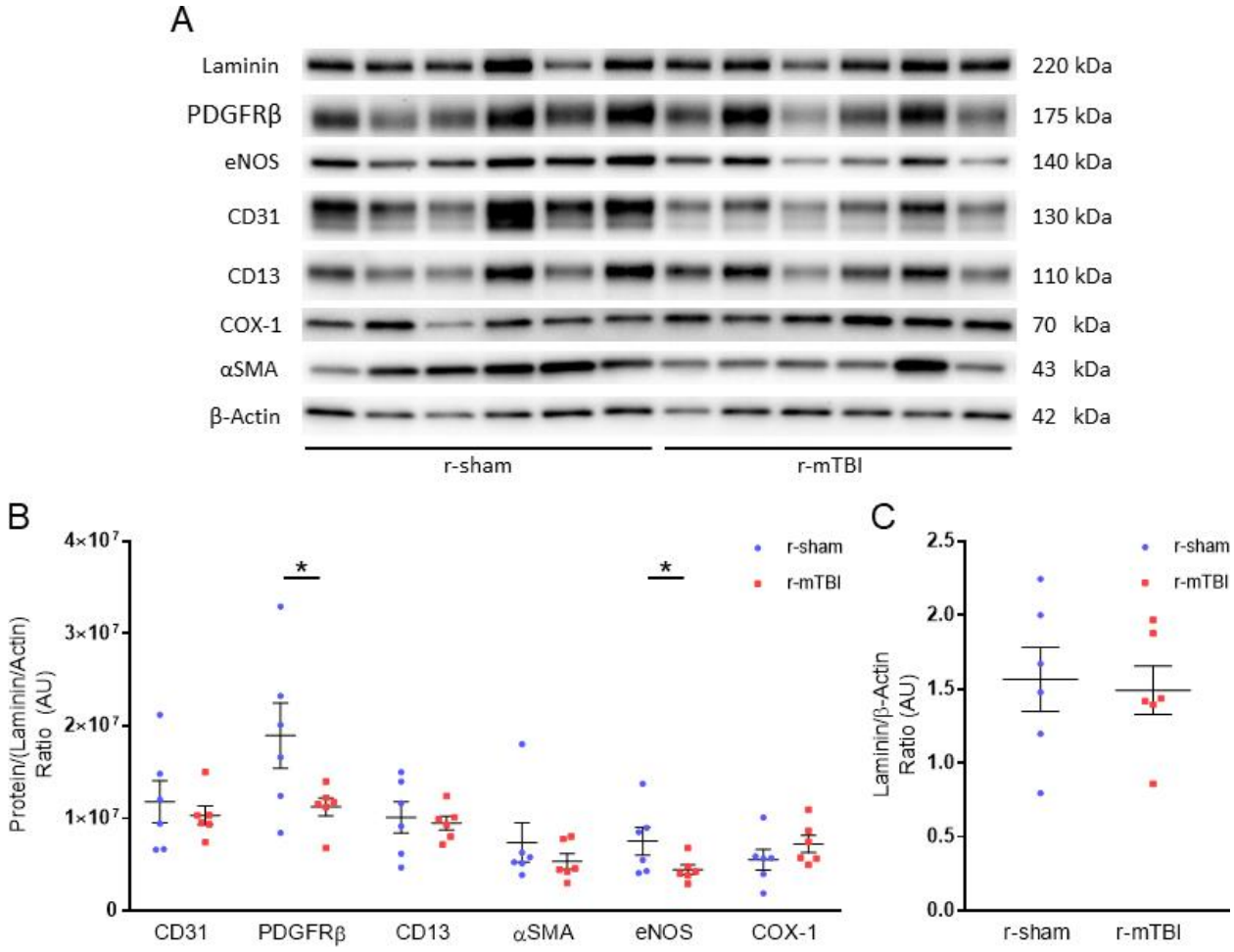

Figure 3.3. Western immunoblot analyses of cerebrovascular cellular and functional markers in cortical vascular-enriched fractions at 3 months following r-mTBI. Representative images of western blot bands shown in (A) were analyzed via densitometry to compile the graphs shown in (B) and (C). Expression of laminin, CD31, CD13, αSMA, and COX-1 were not altered in cortical vascular fractions of r-mTBI mice, as compared to r-sham, at 3 months post-injury (B, P>0.05, unpaired student t-test), however, the expression of the receptor complex PDGFRβ, and endothelial nitric oxide synthase (eNOS) were significantly decreased in r-mTBI cortical vasculature, compared to the vascular fractions of r-sham controls (B, P<0.05, unpaired student t-test). There was a trend toward increase in levels of cyclo-oxygenase 1 (COX-1) in the cortical cerebrovasculature of r-mTBI mice, versus that of r-sham controls, however, this change was not significant (C, P = 0.0532, unpaired student t-test). The mean density of the Laminin/β-Actin ratio did not differ across groups (C, P>0.05, unpaired student t-test). *Wild type mice; 6 r-Sham and 6 r-mTBI. Values expressed as AU. Error bars represent ± SEM. All densitometry values for individual bands in (A) were normalized to the Laminin/β-Actin value for their respective lane and this ratio used for statistical analysis in (B). Values for individual lanes for Laminin/β-Actin in (C) were not normalized to any other band. No statistical significance between groups unless otherwise stated by horizontal bars and text. Error bars represent ± SEM.*

3.3.4. Cerebrovascular Marker Dysregulation, Normalized to β-Actin, at 9 Months Post-Injury.

Western blot analysis of vascular fractions of cortical tissue isolated from r-sham and r-mTBI mice at 9 months post r-mTBI (15 months of age) showed no statistically significant difference between any vascular markers when comparing r-sham and r-mTBI mice (Figure 3.4, B, $P<0.05$, unpaired student t-test), however, there was a trend towards an increase in eNOS expression in r-mTBI mice, compared to r-sham animals at this post-injury time-point (Figure 3.4, B, $P = 0.0649$, unpaired student t-test). The average density of the loading control, β-Actin, bands was statistically greater in the r-mTBI mice, compared r-sham controls, at 9 months post-injury, potentially indicating that the cerebrovasculature in r-mTBI animals exhibited a proportionately increased cellular density than r-sham mice at this time-point post-injury (Figure 3.4, C, $P<0.01$, unpaired student t-test).

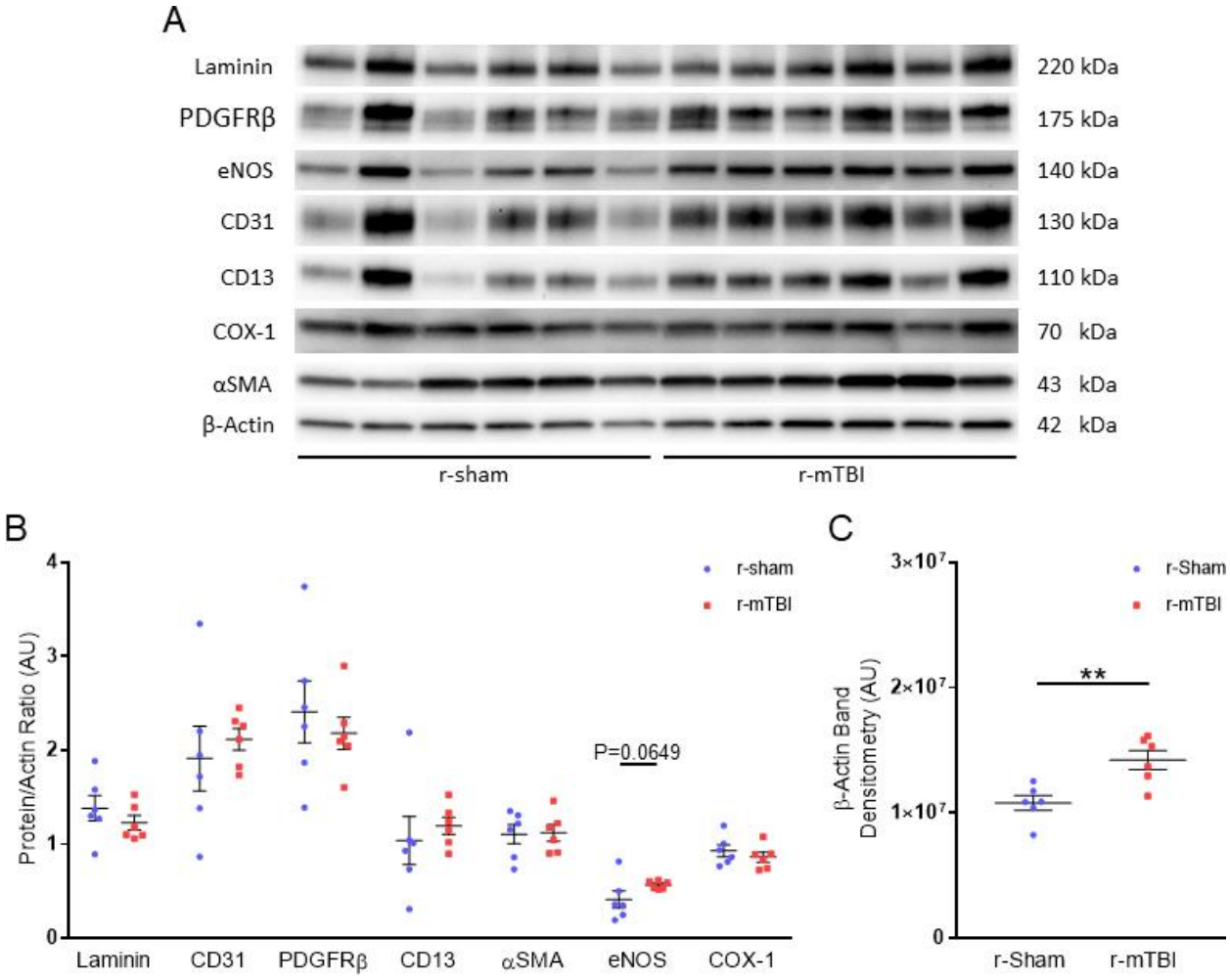

Figure 3.4. Western immunoblot analyses of cerebrovascular cellular and functional markers in cortical vascular-enriched fractions at 9 months following r-mTBI. Representative images of western blot bands shown in (A) were analyzed via densitometry to compile the graphs shown in (B) and (C). r-mTBI did not result in a change in expression in any vascular cellular or functional marker at 9 months post-injury in r-mTBI mice, compared to r-sham, however, there was a trend in increase in expression of eNOS in r-mTBI, with respect to r-sham (B, P = 0.0649, unpaired student t-test). There was a statistically significant increase in the mean intensity of the loading control protein β-Actin in r-mTBI mice, compared with r-sham animals (C, P<0.01, unpaired student t-test). *Wild type mice; 6 r-Sham and 6 r-mTBI. Values expressed as AU. Error bars represent ± SEM. All densitometry values for individual bands in (A) were normalized to the β-Actin value for their respective lane and this ratio used for statistical analysis in (B). Values for individual lanes for β-Actin in (C) were not normalized to any other band. No statistical significance between groups unless otherwise stated by horizontal bars and text. Error bars represent ± SEM.*

3.3.5. Cerebrovascular Marker Dysregulation, Normalized to the Laminin/β-Actin Ratio, at 9 Months Post-Injury.

When normalized to their respective Laminin/β-Actin ratio for each lane, western blot analysis of vascular fractions of cortical tissue isolated from r-sham and r-mTBI mice at 9 months post r-mTBI (15 months of age) showed a statistically significant increase in all vascular markers when comparing r-sham and r-mTBI mice (Figure 3.5, B, $P>0.05$, unpaired student t-test). The average density of the loading control, the Laminin/β-Actin ratio, was not statistically different in the r-mTBI mice, compared r-sham controls, at 9 months post-injury, indicating that the cerebrovasculature in r-mTBI animals exhibited a proportionately similar density to r-sham mice at this time-point post-injury (Figure 3.5, C, $P<0.01$, unpaired student t-test).

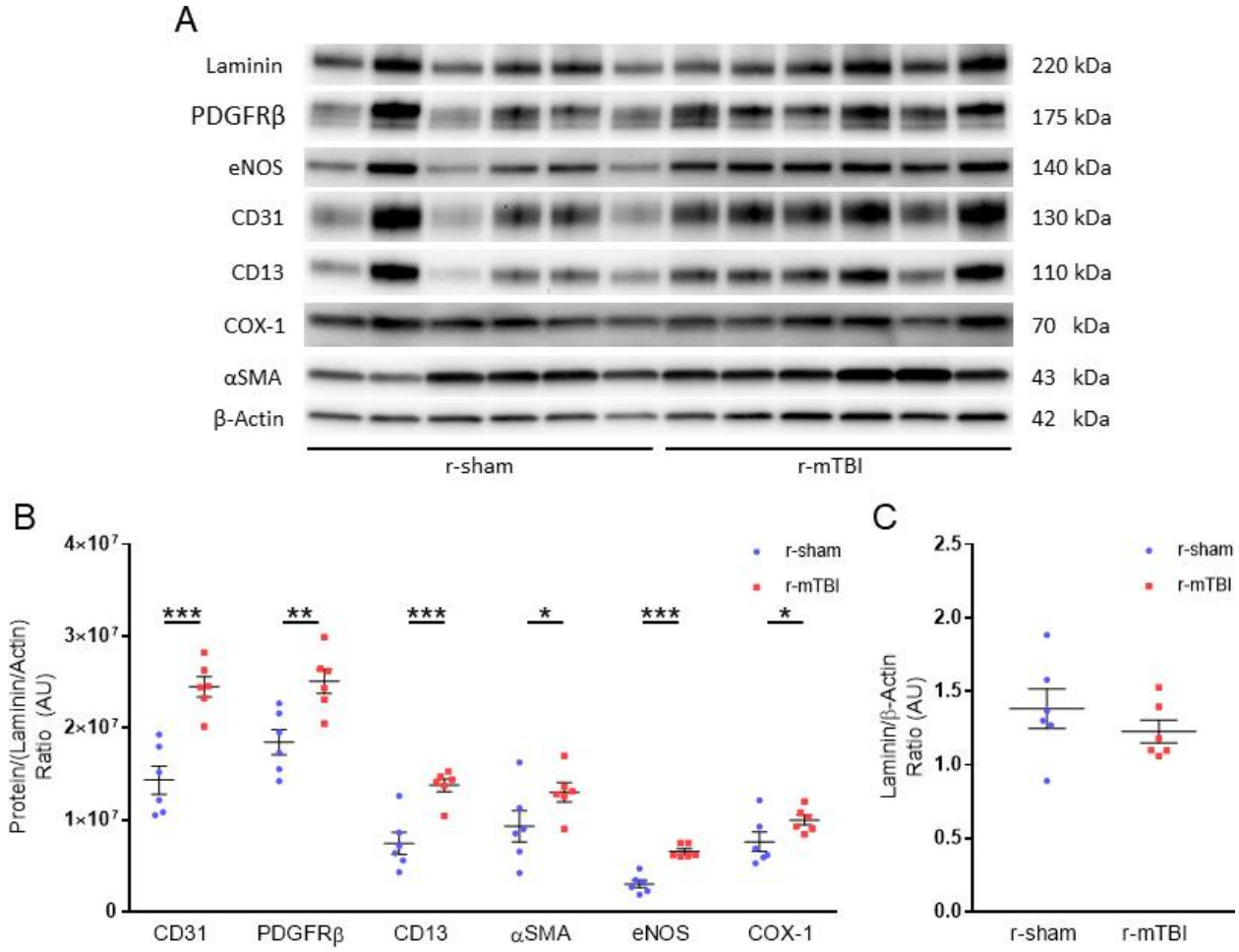

Figure 3.5. Western immunoblot analyses of cerebrovascular cellular and functional markers in cortical vascular-enriched fractions at 9 months following r-mTBI. Representative images of western blot bands shown in (A) were analyzed via densitometry to compile the graphs shown in (B) and (C). r-mTBI resulted in a statistically significant increase in expression in all vascular cellular and functional markers at 9 months post-injury in r-mTBI mice, compared to r-sham, however, there was a trend in increase in expression of eNOS in r-mTBI, with respect to r-sham (B, $P<0.05$, unpaired student t-test). There was no statistically significant difference in the mean intensity of the loading control, Laminin/β-Actin ratio, in r-mTBI mice, compared with r-sham animals (C, $P>0.05$, unpaired student t-test). *Wild type mice; 6 r-Sham and 6 r-mTBI. Values expressed as AU. Error bars represent ± SEM. All densitometry values for individual bands in (A) were normalized to the Laminin/β-Actin ratio value for their respective lane and this ratio used for statistical analysis in (B). Values for individual lanes for Laminin/β-Actin in (C) were not normalized to any other band. No statistical significance between groups unless otherwise stated by horizontal bars and text. Error bars represent ± SEM.*

3.3.6. Blood Brain Barrier Penetrance at 3 and 9 months Following Head Injury

Western blot analysis of vascular fractions of cortical tissue isolated from r-sham and r-mTBI mice at 3 and 9 months post r-mTBI (9 and 15 months of age, respectively) showed no statistically significant difference between any endothelial tight junction markers analyzed across r-sham and r-mTBI mice (Figure 3.6, A and B, $P<0.05$, unpaired student t-test).

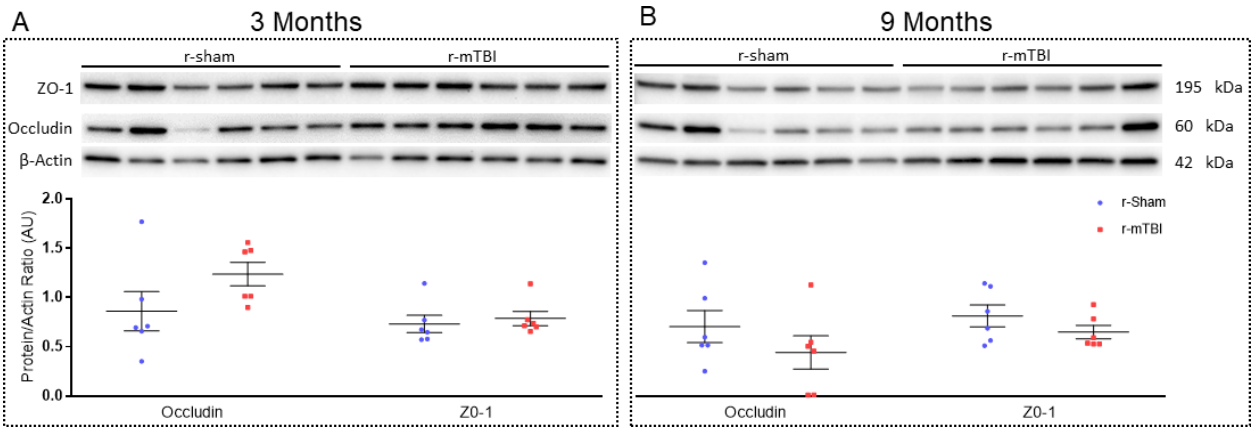

Figure 3.6. Western immunoblot analysis of markers of BBB integrity at 3 and 9 months post-r-mTBI. Expression of the endothelial tight junction protein Occludin and Zonula Occludens 1 (ZO-1) in the cortical vasculature of r-mTBI mice was not statistically different to that of r-sham control mice at either 3 months or 9 months post-injury (A and B, respectively, $P>0.05$, unpaired student t-test). *Values expressed as AU. Error bars represent ± SEM. All densitometry values for individual bands in (A) were normalized to the β-Actin value for their respective lane and this ratio used for statistical analysis in (B).*

3.3.7. Validation of Vascular-Enriched Fractions Prepared from Whole Cortical Brain Tissue

Laser confocal microscopic analysis of 4% paraformaldehyde-embedded vascular-enriched fractions of mouse cortical tissue demonstrated intact lectin-positive capillary segments, containing DAPI-positive cell nuclei and abluminal CD13-positive pericytes (Figure 3.7, A – D).

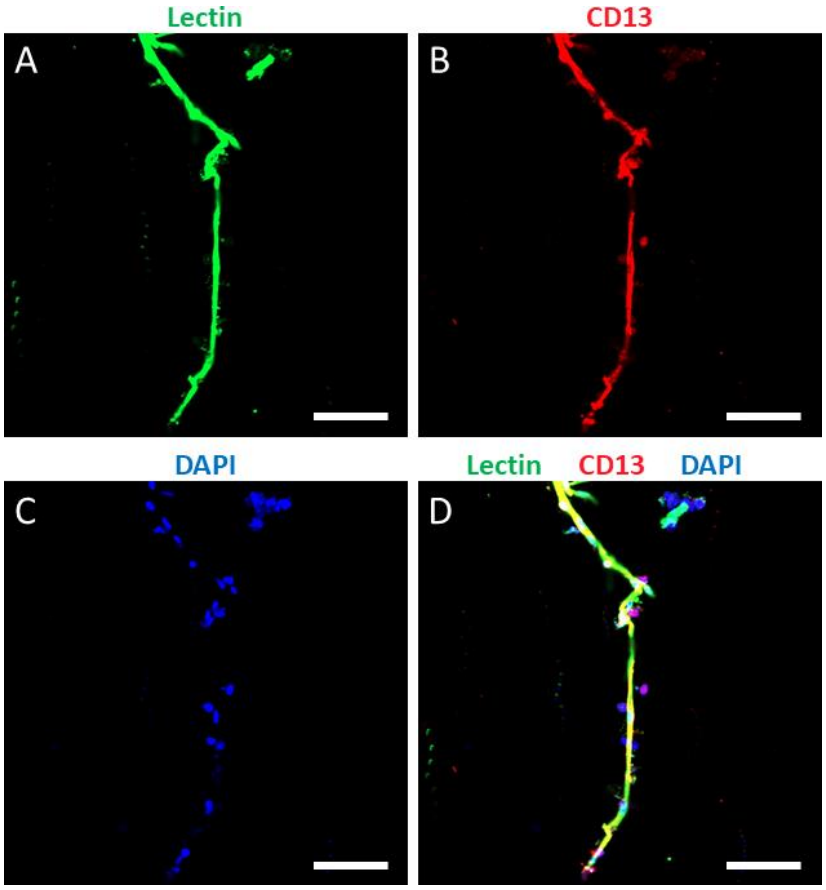

Figure 3.7. Qualitative laser confocal fluorescent microscope images of a single capillary vessel segment from a vascular-enriched mouse cortical tissue preparation. Fluorescent Dylight Lectin-positive capillary segments (A) covered with CD13-positive pericyte processes (B) and vascular associated nuclear staining (C) were identifiable in PFA-fixed vascular-enriched fractions from wild type mice. *Scale bars represent 50µm in length. Images taken using a Carl Zeiss Laser Scanning Confocal Microscope. DyLight 488 labelled Lycopersicon Esculentum (Tomato) Lectin; goat anti-mouse aminopeptidade N (CD13).*

3.4. Discussion

We have in this chapter built upon the studies illustrated in Chapter 2 and characterized a progressive and dysregulated response of the cerebrovascular matter to r-mTBI at an age and injury paradigm relevant to both human contact sports and military populations, in our animal model of repeat closed head trauma. Furthermore, we have shown these vascular-specific aberrations coincide with pronounced spatial memory deficits at both 3 months and 6 months post-last injury, suggesting a potential link between r-mTBI-induced neurobehavioral dysfunction and TCVI.

As discussed in Chapter 1, cerebrovascular pathophysiology is already known to be sufficient for development of neurodegenerative illness in human patients, as is the case with those suffering from the inherited disease CADASIL[123], and CBF impairment has been found to accompany MCI symptomatology prior to AD clinical presentation[128-130]. However, there is currently very little research asserting TCVI as being causative in the development of neurocognitive disability in animal models of chronic mild TBI. The lack of evidence in this regard is arguably due to the publication of whole brain histological and biochemical data without any attempt to correlate these with neurobehavioral assessment of injured animals. For example, a recent study undertaken by Gama Sosa and colleagues[193] reported an absence of chronic neuroinflammation in the majority of Long Evans rats exposed to repetitive low level blast injuries at as late as 40 weeks post-last blast mTBI. However, one rat, which demonstrated focal blast-induced hemorrhagic tears and adjacent blood clots at 16 weeks post-injury, also exhibited profound microglial activation and proliferation, presumably due to chronic vascular

degeneration and leakage[193]. As unorthodox as it was to examine a single animal outlier as a case study for showing TCVI to be sufficient for chronic neuropathology following r-mTBI, this result is compelling. However, like many other studies, this report by Gama Sosa and colleagues[193] did not have any behavioral assessment with which to validate their findings. Our study is, to the best of our knowledge, the first to report longitudinal and persistent behavioral impairment alongside evidence of cerebrovascular dysregulation in an animal model of r-mTBI.

There have been few other notable attempts at a longitudinal assessment of the cerebrovasculature following experimental mTBI, and as mentioned, none with compelling comrade behavioral outcome measures. Obenaus et al[194] have catalogued an acute rarefaction of global cerebrovasculature density at 1 day following a unilateral controlled cortical impact, and an apparent recovery of normal vascular density to baseline levels at 14 days post-injury in mice. The same group have also reported an increased vascularity in the corpus callosum in mice at 60 days following a single unilateral closed head mTBI. The increased white matter vascularity was inversely correlated with the Apparent Diffusion Coefficient (ADC), a measure of white matter integrity[195], on MRI in the cortex ipsilateral to injury, suggesting the angiogenic response of the vascular bed to TCVI may ultimately be deleterious[194]. Concordantly, Morgan et al[196] have shown signs of premature capillary outgrowth at as early as 2 days following injury in a rodent model of closed head acceleration mTBI, and a more moderate to severe fluid percussion injury in mice has been demonstrated to result in subacute increased vascularization at 14 days, but with continued global hypoperfusion[197]. All studies mentioned have used histological analyses, confined to discrete serial sections of brain tissue, to catalogue the neovascularization following mTBI in their rodent models. Using immunoblotting assessment of our vascular-enriched

fractions from r-sham and r-mTBI mice, which incorporates the whole of the cortical cerebrovasculature, we too report an apparent increased vessel density, as observed in the relative increase in housekeeper protein β-Actin, and further in the increased expression of all cerebral vascular markers normalized against the Laminin/β-Actin ratio, at the more chronic of the two time-points post-injury analyzed (Figure 3.4, C). This occurs months following a profound decrease in expression of PDGFRβ, a marker of pericytes, and endothelial Nitric Oxide Synthase (eNOS), a marker of endothelial cells, at the earlier time-point post-injury (Figures 3.2 and 3.3, B), a result which may be interpreted as representing a more acute rarefaction of the cerebrovasculature in our animal model. The fact that we do herein normalize to a housekeeper protein within group does mean that changes in mural cell and basement membrane markers, such as CD13 and laminin, respectively, across groups may be underestimated in our analysis, as the ubiquity of traditional neuronal housekeeping proteins such as β-Actin across the components of the cerebral vasculature is ill-defined. However, use of a cellular marker, such as β-Actin, comes with the advantage of heightened resolution of changes in functional receptor and cell-specific enzyme expression, as a function of cellularity. In this regard, the decreases in the receptor PDGFRβ throughout the cortex of r-mTBI mice at 3 months post-injury can be considered an indication of possible pericyte loss, a phenomenon characterized in humans following moderate to severe TBI[133,134] and shown to be causal in CBF impairment in mice[108,122,172,198-200]. The stark reduction of PDGFRβ expression in the vascular-enriched sample of r-mTBI tissue falls in line with work by Dore-Duffy et al[120], showing detachment and migration of pericytes away from the vessel wall following TBI in mice. In much the same way as PDGFRβ , the profound decrease we observed in the expression of eNOS, the key mediator of synthesis of

the vasodilator nitric oxide (NO)[201], at 3 months post-injury in the cortices of r-mTBI mice, relative to r-sham controls, could as realistically represent a pallor of the endothelium as much as a loss of function of this integral vasodilatory machinery[201]. Indeed, this hypothesis is supported by the fact that upregulation of NO activity in preclinical brain injury studies is coupled with beneficial angiogenic effects *in vivo*[202-204]. At 3 months post-injury, we have also observed a modest increase in cyclo-oxygenase-1 (COX-1), a prostaglandin endoperoxide synthase expressed by both neurons and astrocytes of the mammalian CNS, and responsible for generation of vasoactive prostaglandins from arachidonic acid (AA). Though not statistically significant, this result may indicate a compensatory mechanism in lieu of the relativistic decrease in eNOS throughout the cortex of injured animals at 3 months post r-mTBI. The fact that we have not seen a decrease in alpha-smooth muscle actin (αSMA), the most robust cellular marker for the smooth musculature of the CNS vasculature, at 3 months following r-mTBI in the current study is again explained by the tissue samples in this Chapter being representative of the vasculature, as opposed to the entire brain, as was the case in Chapter 2 and our previously published work[155]. Indeed, cortical levels of αSMA are seen to be elevated at 9 months post-injury, along with all other cerebral vascular markers analyzed, when normalized to the Laminin/β-Actin ratio. As far as we are aware, there is no study showing attenuated expression of smooth musculature throughout the cortex after experimental TBI in the rodent. It is possible that the decrease in αSMA signal in the brain homogenates of 22 month-old mice several months following r-mTBI (Chapter 2) reflected an increased capillary, versus arteriolar, neovascularization, and so, a relativistic false positive for a decrease in αSMA was observed. Future immunohistochemical work examining cerebral vessel coverage by αSMA is required to definitively answer this question.

The fact that the decrease in both PDGFRβ and eNOS expression is no longer apparent at the later 9 month post-injury time-point (Figures 3.4 and 3.5, B) is interesting for a number of reasons. PDGFRβ-positive pericytes are known to exhibit a biphasic loss and reactivity pattern following brain injury[117,205], and treatment of CCI-injured 3 month old mice with a carbon monoxide releasing molecule diminished pericyte death, increased levels of neural NO synthesis, and rescued behavioral deficit across a variety of assessments, including Y-maze and Morris Water Maze[119]. Our results showing a restoration of PDGFRβ in the cortices of r-mTBI mice to sham levels when normalized to the cellular housekeeper β-Actin, and an augmentation in PDGFRβ signal when further normalized to the vascular density Laminin/β-Actin ratio, and concomitant, albeit insignificant, augmentation of spatial memory, infers there may be a latent restorative repair mechanism of the r-mTBI cortex following cessation of injury to the brain, at 9 months post-injury. Indeed, the proposed neovascularization within the cortical tissue of injured mice at this time-point may be indicative of a reparative response to injury, as there has been success in preclinical treatment of TCVI via therapeutics with angiogenic properties; for example, atorvastatin administered within 1 hour following Lateral Fluid Percussion Injury (LFPI) in rats was demonstrated to increase the amount of circulating endothelial progenitor cells, and was correlated with improved perilesional vascular density and functional outcomes[206]. The exact preclinical relevance of the consistent signs of neovascularization in animal models of r-mTBI, shown in one interpretation of the 9 months post-injury immunoblot analyses here, as they pertain to the human TBI population is difficult to gage, as there have been no studies examining global vascular density and changes therein over time in human brain samples.

Another facet of vascular dysregulation following TBI which may contribute to alterations in CBF and may be detectable via the approach used in this study, is loss of blood brain barrier (BBB) integrity. BBB disruptions can include mild and transient openings or loss of tight junctions altogether, and impaired regulation of trans-endothelial and paracellular transport of ions and molecules[207,208]. Thee alterations in BBB penetration can lead to increased extravasation of peripherally-derived immune cells in to the intraparenchymal space, culminating in pronounced brain pathology and the persistence of neurological deficits. Evidence for the immediate injurious effects of mTBI on the BBB include a 2013 study by Abdul-Muneer et al[209], showing that young male Sprague-Dawley rats exposed to a single 123 KPa intensity mild Blast Shock Wave (BSW) exposure injury caused upregulation of markers of oxidative and nitrosative stress in brain capillaries, which progressed into BBB disruption, as reflected by downregulation of the tight junction protein occludin, and reduced histological expression of PDGFRβ, all at 1 to 24 hours post-injury[209]. The acute effects of this r-mTBI on BBB permeability were also accompanied by an elevation of plasma concentrations S100β and neuron-specific protein enolase for several hours following injury[209]. Many studies have also investigated the tight junction protein Zonnula Occluden 1 (ZO-1) in relation to BBB disruption following experimental TBI[210-212]. We did not observe any significant changes in either occludin or ZO-1 (Figure 3.6, A and B), indicating that endothelial cell tight junction integrity is also unscathed at this time-point post-injury. As we do not observe appreciable changes in either tight junctional marker, it is unlikely the chronic impairment of CBF or behavioral performance at these time-points would be due to changes in BBB integrity.

The biochemical and behavioral findings of this chapter confirm an early and persistent biological basis for TCVI in our animal model of repetitive head trauma and validate its timepoints for a longitudinal assessment of the possibly biphasic pathophysiology of TCVI, using a complementary *in vivo* imaging study. In the next chapter, we will aim to develop, validate and make use of a clinically-relevant imaging platform to assess the functional responsiveness of the cerebrovasculature and characterize the evolving vascular degeneration following repeat mild traumatic brain injury.

Chapter 4. Cerebrovascular reactivity is impaired in r-mTBI mice at chronic time-points post-injury.

4.1. Introduction.

It is clear from the past chapters that Traumatic Cerebral Vascular Injury (TCVI) plays a contributory, if not causative, pathological role in chronic r-mTBI related neurodegeneration in both animal models and human patients, manifesting as acute and chronic, regional and global CBF irregularities in mouse and man. The early appearance of aberrant CBF in American football players[138,141] and the finding that global and regional CBF is decreased in retired military personnel having sustained an injury, compared to non-injured military control individuals[213], point toward TCVI as an instigator and biomarker of chronic neurodegenerative illness in these populations, and volunteers the cerebrovascular mélange as an enticing therapeutic target or diagnostic marker. Although CBF impairment appears to be a near constantly observed sequelae across repeat mild, to moderate and severe TBI, in both retired military personnel and current and former contact sports players, resting CBF is not by itself a reliable indicator of cerebrovascular health, as its measurement is tightly coupled to the metabolic demands of the CNS, and so, indiscriminate of primary and secondary neuronal and other injuries following a mTBI. For example, a recent study using Fluorodeoxyglucose PET (FDG-PET), combined with a battery of neuropsychological and post concussive symptom rating scales, demonstrated that Veterans with a history of r-mTBI show a decreased metabolic rate of glucose in the cerebellum, vermis, pons and medial temporal lobe, compared to controls[214]. Likewise, a recent report has shown increased plasma levels of brain-derived creatine kinase B as a biomarker of r-mTBI in

professional boxers[215]. Such studies infer gross CNS metabolic dysregulation at acute and chronic time-points post injury, which will invariably alter patient CBF.

Recently, clinicians have instead favored cerebrovascular reactivity (CVR), a measure of cerebral blood vessel dilation in response to a vasoactive stimulus, as a more representative measure of TCVI in both acute and chronic mTBI in the human population[100]. The vasoactive stimulus most typically employed in the clinic is an increase in partial pressure of CO_2 ($paCO_2$), by means of briefly increasing the fractional inspired concentration of CO_2 ($FiCO_2$) from atmospheric levels (approximately 0.04%) to 5% CO_2 via a facemask, or voluntary breath hold[100], both termed hypercapnia. CVR can be measured non-invasively, by a variety of modalities, including transcanial doppler (TCD) ultrasonography, and Near Infrared Spectroscopy (NIRS). The imaging technique of choice is usually either Arterial Spin Labelling (ASL) or Blood Oxygenation Level Dependent (Bold) MRI. In the case of ASL, water molecules in a patient's peripheral carotid arterial blood are radio-labelled, and the dissipation of the radio-frequency spin as the blood circulates through the brain creates an MRI contrast, allowing an indirect measure of CBF in absolute units (cc/100g/min)[100]; MRI-BOLD allows real-time measurement of oxygen delivery and consumption via the paramagnetic properties of deoxyhemoglobin, and is the clinical gold standard for measurement of cerebral perfusion and metabolism. Both MRI ASL and BOLD CO_2 hypercapnic challenge are done using a facemask to moderate the mixture of inspired air the patient is breathing, in tandem with a capnograph, for measurement of end tidal CO_2 ($ETCO_2$). Using TCD in American football athletes acutely following concussion, Len et al have recently demonstrated an impairment of CVR, in the absence of impairment of resting Medial Cerebral Artery Blood velocity (MCAv), via voluntary breath hold and resultant hypercapnia and increased

MCAv[216]. Similarly, Mutch et al[217] have reported alterations in MRI BOLD CVR in response to hypercapnic challenge, in the absence of global resting state CBF or cerebrovascular anatomical differences, in 15 adolescents diagnosed with post concussive symptoms, compared to 17 healthy controls[217]. In addition to the above studies describing impaired CVR at chronic and acute times post mTBI[216,217], perturbed CVR has also been seen at a median of 25 months post-injury using hypercapnic challenge and BOLD/ASL MRI in human patients following a moderate to severe TBI, with poor discrimination of patient from control via the CBF metric alone[142]. As such, CVR analyses may be a valuable tool in evaluating head trauma, as global mean gray matter CVR is dramatically altered and strongly correlates with patient neurobehavioral outcome[142].

Given the prevalence of cerebrovascular reactivity as an early indicator and endophenotype in r-mTBI, and the apparent conformity of its signal across TBI populations and time-points post-injury, where otherwise there is only disparate and patient-specific regional and global resting CBF and neurobehavioral outcome, CVR represents a potential diagnostic tool and therapeutic target in the treatment of TCVI. All this said, r-mTBI related CVR deficit has yet to be demonstrated in a relevant animal at a chronic time-point post-injury, making it practically impossible to draw any conclusions about the mechanisms behind TCVI-induced CVR deficit, and how it pertains to evolution of r-mTBI related chronic illness. In this chapter, we developed a platform to evaluate CVR at chronic time-points post-injury in our mouse model of repetitive head trauma.

4.2. Materials and Methods.

4.2.1. Animals

Male C57BL/6 and transgenic ApoE3-FAD mice were housed under standard laboratory conditions (23 ± 1ºC, 50 ± 5% humidity, and 12 hour light/dark cycle) with free access to food and water throughout the study. We employed the EFAD mouse model, as these animals recapitulate some of the pathological characteristics observed in human AD[218]. These mice express the Swedish (K670N/M671L), Florida (I716V), and London (V717I) mutations) and PSEN1 (with M146L and L286V mutations), each of which is driven by the mouse Thy1 promoter. The transgenes inserted at a single locus, Chr3:6297836 (Build GRCm38/mm10), where they do not affect any known genes[219]. These mice display early and aggressive Cerebral Amyloid Angiopathy (CAA) within the walls of cerebral vessels[220]. The EFAD colony was established by crossing mice expressing five familial AD mutations (5xFAD) to homozygous apoE targeted replacement (apoE-TR) expressing the human apoE3 isoform[218]. The apoE-TR mice were created by gene targeting and carry one of the three human alleles (APOE2, APOE3, or APOE4) in place of the endogenous murine apoE gene[221]. These mice retain the endogenous regulatory sequences required for apoE production and express the human apoE protein at physiological levels. All mice are on a C57BL/6 background and additional details on the production and genetic background of these mice are described in the sources cited above. All experimental protocols involving animals were approved by the Institutional Animal Care and Use Committee of the Roskamp Institute. All procedures were carried out in accordance with the National Institute of Health Guide for the Care and Use of Laboratory Animals.

4.2.2. Injury Schedule

3-month-old animals were randomly assigned to one of two groups: repetitive mild Traumatic Brain Injury (r-mTBI, delivered twice each calendar week i.e. 1 hit approximately every 72 hours, over a period of 3 months) or repetitive Sham (r-Sham; animals underwent the same duration and frequency of anesthesia as r-mTBI animals). An electromagnetic impactor (Leica Instruments) was used to generate a closed head midline mTBI, using a 5.0mm diameter flat face tip, 5m/s strike velocity, 1.0mm strike depth, and a 200msec dwell time, as previously characterized[60]. The mice were euthanatized at 3 and 9 months after the final injury/anesthesia (6, and 15 months of age, respectively). The 3 and 9-month post last injury cohorts studied here were separate groups of animals, given an identical regime and intensity of r-mTBI.

4.2.3. Preparation of mouse cranial window

24 hours prior to hypercapnic challenge, the left hand side of the animal's skull was thinned to transparency, and a cranial window installed over the thinned surface, using an optimized and validated technique[222]. Briefly, the animal was anesthetized under 3.0% isoflurane, its head shaved, and the shaved scalp scrubbed with betadine, followed by three scrubs with 70% isopropyl alcohol. Isoflurane concentration was lowered to 2% immediately prior to surgery. Using a forceps and scissors, an incision was made to expose the whole dorsal surface of the skull, and the incision was trimmed laterally to either edge of the temporal muscles of the skull, and posterior to the muscles of the neck. The thin layer of periosteum over the surface of the skull was carefully removed using a scalpel blade, and the edges of the incision on the scalp were

sealed and glued to the underlying bone of the skull using the clear version of the C&B Metabond dental cement (Parkell Inc, NY, USA). A 4-40 stainless steel screw was fixed to the cerebellar base plate of the exposed skull using Loctite 401 superglue, and upon drying of the glue, the base of the setscrew was further fastened to the area by application of clear dental cement. Allowing 10 minutes for thorough drying of the dental cement, the animals head was then fixed in position using a custom-built fixation frame, comprising a 'TRB1' ball and socket, re-tapped at one end to fit a 4-40 setscrew, attached to a 'Ø 0.5" post' connected to another Ø 0.5" post by a 'SWC rotating clamp', and to an aluminum base plate (all products bought from ThorLabs, see Figure 2.1). For fixation of the head, the ball and socket were rotated clockwise to the 4-40" setscrew on the mouse's skull. The articulated rotating socket and arm allow for fine adjustments to the animal's head position, which, when perfectly flat, was made absolutely still by tightening of the nuts of the apparatus. With the mouse's head in position, and under a dissecting microscope, a high torque, low speed dental drill (EXL-M40, Osada, CA, USA) and 0.5mm carbon steel drill burrs (item number 19007-05, Fine Science Tools, FST, USA) were used to thin the skull of the animal. The drill was set to approximately 2000 rpm, and warm Artificial Cerebrospinal Fluid (ACSF; 125mM NaCl, 10mM Glucose, 10mM HEPES, 3.1mM CaCl2, 1.3 mM MgCl2, pH 7.4, all chemicals from Sigma, USA) was applied between thinning steps. The bone begins to flex to the touch of the drill when it becomes approximately 50µm thick, and application of ACSF allows visualization of pial vessels through the wet bone. The final thickness of the bone should be about 15-20µm thick, at which point the bone is dried with a gentle stream of air from a dust can, cryano-acrylate glue is applied to the whole of the exposed skull, and a custom-shaped glass coverslip is gently lowered over the layer of glue. More glue is applied at the edges of the coverslip until there are

no gaps or bubbles between the cover slip and skull. The animal is placed back in its cage on a heating pad to recover from surgery and monitored over the next 24 hours for signs of stress or discomfort.

4.2.4. In-vivo assessment of Cerebrovascular Reactivity

9 or 15-month old male C57BL6 mice were evaluated for cerebrovascular reactivity *in vivo,* at 3 or 9-months post-injury, respectively, using Laser Speckle Contrast Imaging (FLPI2, Moor Instruments). As a positive, age-matched control for the *in vivo* experiments, we used 9 month-old male transgenic Apolipoprotein E Familial Alzheimer's Disease (EFAD) mice, as these mice not only recapitulate some of the neuro-vascular pathology characteristic of AD[218], in which CVR is well known to be compromised[140,223-226], but also as the FAD mouse has been shown to exhibit a pronounced deficit in cerebrovascular reactivity to hypercapnic challenge *in-vivo*[227-230]. Mice were anesthetized under 3% isoflurane in 100% oxygen, and anesthesia maintained at 2% isoflurane in oxygen for all surgical procedures. Prior to the in-vivo experiment, animals had an external pin-port catheter (custom) introduced in to the left femoral artery, in order to obtain blood draws for arterial blood gas analysis prior to and following hypercapnic challenge. After having cannulated the femoral artery, the mouse was orotracheally intubated, and connected to a ventilator (Mini-vent, Model 845, Harvard Apparatus), and Capnograph (Type 340, Harvard Apparatus), and the gas mixture was switched from 2% isoflurane in 100% Oxygen, to 1.1 - 1.5% Isoflurane in medical grade room air (21% O2, balance N2) for the duration of the experiment. The animal's body temperature was kept constant at 37 degrees Celsius using a body

temperature regulated homeothermic infrared heat pad and mean arterial blood pressure (MABP) was recorded constantly using a non-invasive tail-cuff monitor (CODA, Kent Scientific). The tidal volume and respiratory rate analog settings on the mini-vent were manipulated to keep the animal's baseline end-tidal CO_2 ($ETCO_2$) readings between 35 and 38 mmHg, and MABP, body temperature, respiratory rate, tracheal pressure, ET CO_2, and airflow recordings were monitored and recorded throughout the experiment via PowerLab/LabChart (AD Instruments. Upon establishment of steady baseline physiological readings, a 50-60µL blood draw was made from the femoral artery for baseline Arterial Blood Gas (ABG) analysis. 2 minutes following the blood draw, the laser speckle camera was placed directly perpendicular to the cranial window and images were collected at a frequency of 1Hz for the duration of the experiment. Following 60 seconds of steady baseline readings the gas mixture was switched from 1.1-1.5% Isoflurane in medical grade room air, to 1.5% isoflurane in a custom mix of 21% O_2, 5% CO_2, and balance N_2, for 60 seconds. Following the 60 seconds of hypercapnic challenge, the inhalation gas was switched back to 1.1-1.5% isoflurane in medical grade room air, and a further 4 minutes of 1 second recordings were collected, after which a second 50-60µL blood draw was made from the femoral artery, for ABG analysis, using the iSTAT®1 Vetscan (Abaxis, CA, USA). Any animal displaying a base excess outside of -4 to +4, a HCO_3^- (bicarbonate) level of less than 18mM/L, a pH of less than 3.5, or more than 4.5, or a saturated O_2 (sO_2) level of less than 90% before or after hypercapnic challenge was omitted from the study. Likewise, any mice displaying irregular breathing, as per their Labchart recordings, during any part of the experiment, or displaying an average MABP below 60mmHg, were not included in the analysis. After one or more successful hypercapnic challenges had been completed, the isoflurane was increased to 3% for

approximately 30 seconds, and the animal was extubated, removed from the experimental setup, and sacrificed under heavy isoflurane anesthesia.

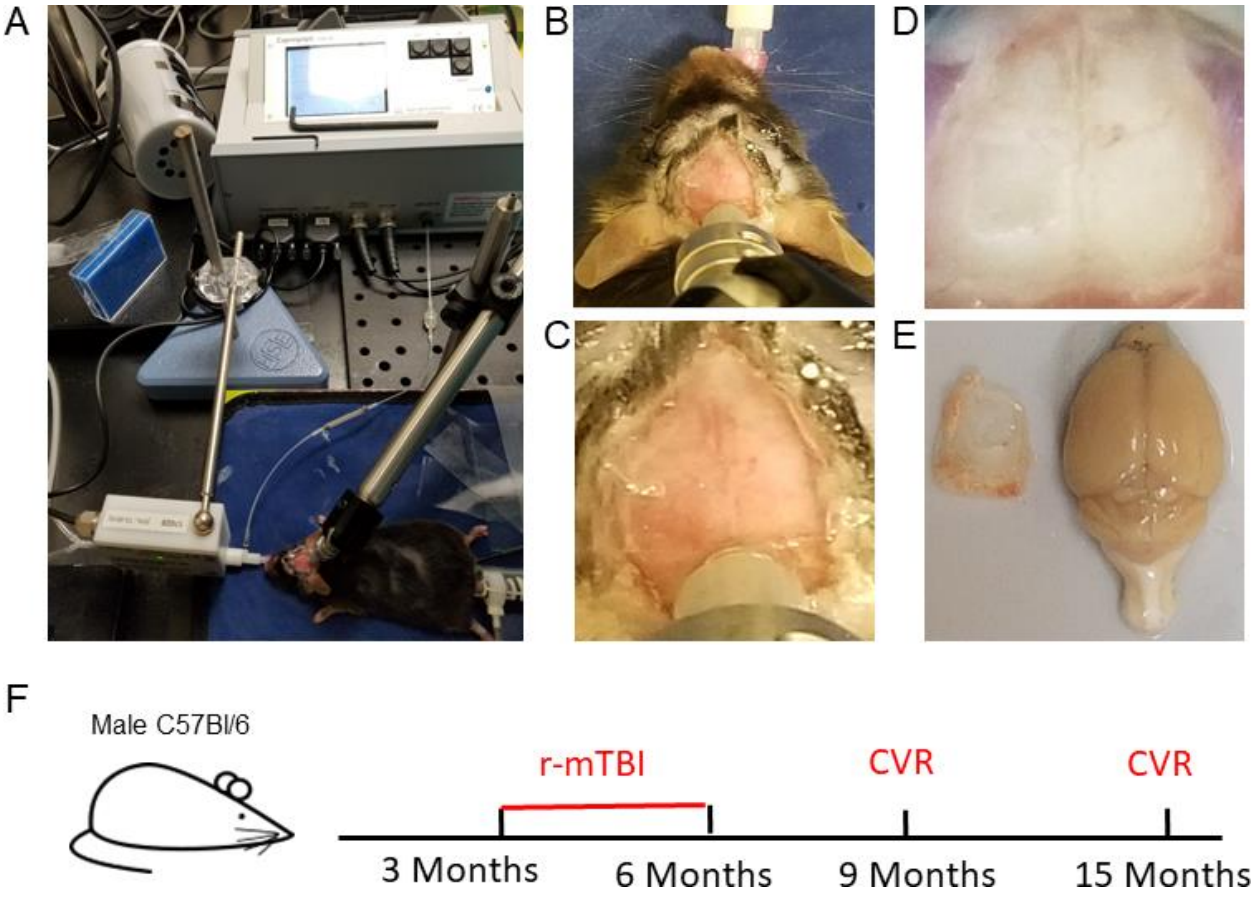

Figure 4.1. Experimental preparation of male C57BL/6 mice prior to in-vivo assessment of cerebrovascular reactivity. 24 hours prior to hypercapnic challenge, the skull was bilaterally thinned to transparency, and a cranial window installed over the thinned surface (B). A close-up inset of the cranial window in (B) is shown in (C). Immediately prior to the in-vivo experiment, the animal was anesthetized and the left femoral artery was dissected and cannulated with an external pin-port connected cannula (for measurement of arterial blood gas values during the experiment). The animal was then orotracheally intubated and ventilated with medical grade room air and 1.1 - 1.5% Isoflurane. The head was fixed in position via a custom fixation apparatus, with a setscrew attached to the baseplate of the animal's skull (installed at the time of thinning), mean blood pressure was monitored using a non-invasive tail cuff blood pressure monitor, and body temperature and end-tidal CO2 readings maintained at 37 °C ad 35 – 37 mmHg, respectively. Images D and E show the thinned and transparent surface of the skull of the animal depicted in (B) and (C) following animal sacrifice and trans-cardial perfusion with Phosphate Buffered Saline. The schematic shown in (F) depicts the timeline of the study, and the timepoints at which assessment of CVR was conducted.

4.2.5. In-vivo Imaging Analysis

The Moor FLPI2 image files (each 6 minutes in length), comprising 360 images taken at 1 second intervals, under the high resolution, low speed, spatial setting on the camera setup menu, were analyzed using the dedicated Moor Image Review software. A region of interest (ROI) measuring 0.3mm^2 was placed at a location within the area of thinned skull of the animal proximal to, and approximately 1.5mm from, the midline suture, and devoid of any large vessels, which may be meningeal or pial in nature, and so may not correspond to the brain parenchyma from which measurements were intended to be made. A second 0.3mm^2 ROI was placed at a similarly parenchyma-like region approximately 2.5mm distal to the midline, within the area of thinned skull. All image files from animals within the same time-point were set to the same threshold, and the image files scrolled through to correct for any head or camera movement during the experiment. If there was shifting of the image due to movement, the software's "Shift Image" application was used to correct it. Both proximal and distal ROIs were exported as separate graph Excel files, the flux data normalized to the 60 seconds' worth of baseline immediately prior to hypercapnic challenge, and so, expressed as percentage change from baseline (see Figure 4.2). Every image file's correlative Labchart was downsized by a factor of 100, and all continuous physiological parameter data for that experiment were plotted parallel to the flux data.

4.2.6. Statistical Analysis.

For the measurement of CBF, all Area Under Curve (AUC) and Cerebrovascular Reactivity Index (CVRx) data were tested for normality using skewness and kurtosis, and the effect of r-mTBI

analyzed across groups at proximal or distal ROIs using One-way ANOVA, and multiple comparisons t-test with Tukey post-hoc analysis. A given effect was considered significant at $p<0.05$, and indicated by asterisks in the Figures. Error bars represent the standard error of the mean. Statistical analyses were performed using JMP 11.1.1 (SAS) and graphs were created using GraphPad Prism 5.0.

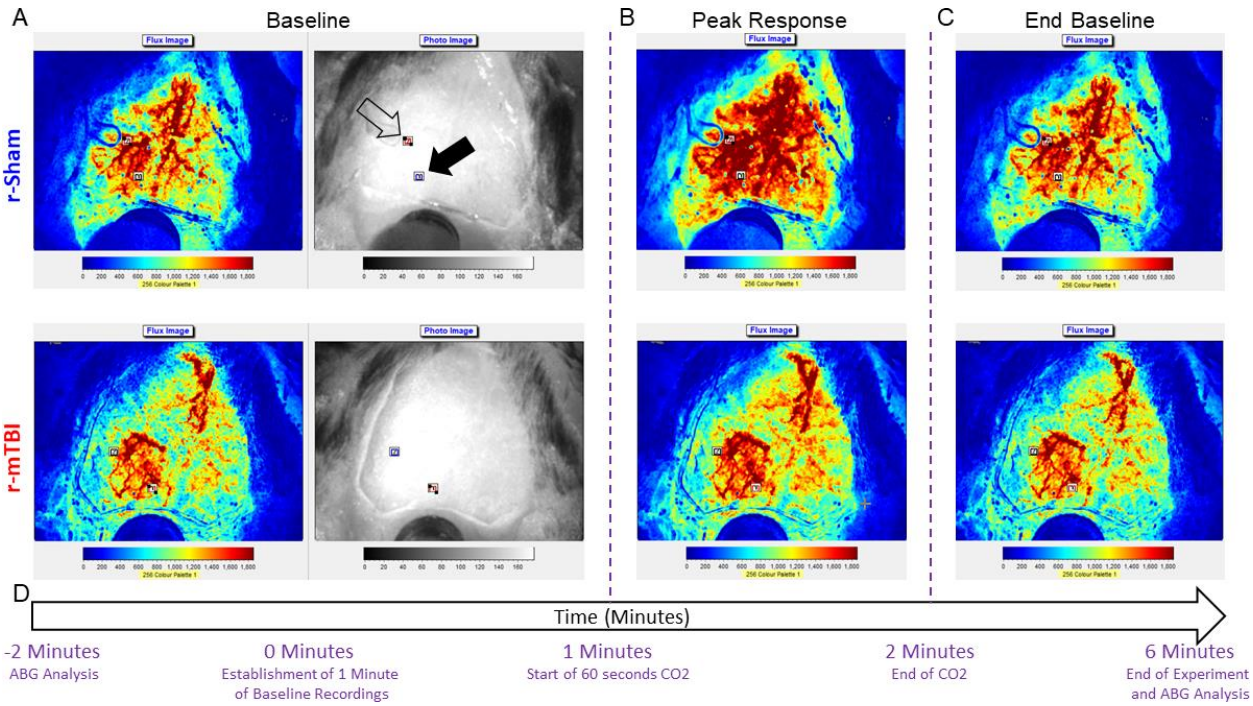

Figure 4.2. Time course of experimental assessment of cerebrovascular reactivity in male C57BL/6 mice. Representative laser speckle contrast flux and bright field images taken from the dorsal view by the Moor FLPI2 Laser Speckle Contrast Imager of fixed heads of a r-sham and r-mTBI mouse as viewed during the 60 second baseline immediately prior to hypercapnic challenge (A, first and second images from left, respectively, of top and bottom panels), during the peak response to hypercapnia (B, third image, top and bottom panel), and during the final return to baseline flux (C, fourth image, top and bottom). The time course of the experiment with relation to the representative images is shown in (D). Two 0.3mm squared rectangular regions of interest (ROIs) were positioned over areas of the cranial window with no obvious large arteries or transparency occlusion, with one ROI being positioned proximal to the midline site of injury (A, top panel, second image, closed arrowhead) and the second being positioned distally to the midline site of injury (A, top panel, second image, open arrowhead). The flux data for the entirety of the experiment duration for each mouse was normalized to the 60 second baseline of the animal, and ABG analysis was evaluated immediately before and after the experiment (D).

4.3. Results

4.3.1. Validation of In Vivo Assessment of Cerebrovascular Reactivity

The cerebrovascular reactivity of 9 month wild mice in response to inhalation of 5% CO2 in medical grade room air for 60 seconds, and concomitant transient increase in $ETCO_2$ to 55-60mmHg, was markedly decreased in ApoE3FAD mutant mice, compared to r-sham controls. The mean response of CBF from ROIs both proximal and distal to the midline site of injury of 9 month old r-sham and ApoE3FAD mice (Figure 4.3, A and B, respectively) was analyzed using both area under the curve (Figure 4.3, C) and the CVRx, a more clinically relevant index of CVR compared to the AUC, expressed by further normalizing the peak response percentage change in CBF from baseline, to the peak change in $ETCO_2$ from baseline for each animal. AUC analysis demonstrates a significantly greater response of r-sham mice, compared to ApoE3FAD controls, at both proximal and distal ROI locations (Figure 4.3, C; one-tailed student t-test, $P<0.05$), and CVRx analysis showed a decrease in peak CBF response, normalized to peak change in $ETCO_2$, of ApoE3FAD positive controls, relative to r-sham mice, at both the proximal and distal ROI (Figure 4.3, D, one-tailed student t-test, $P<0.05$).

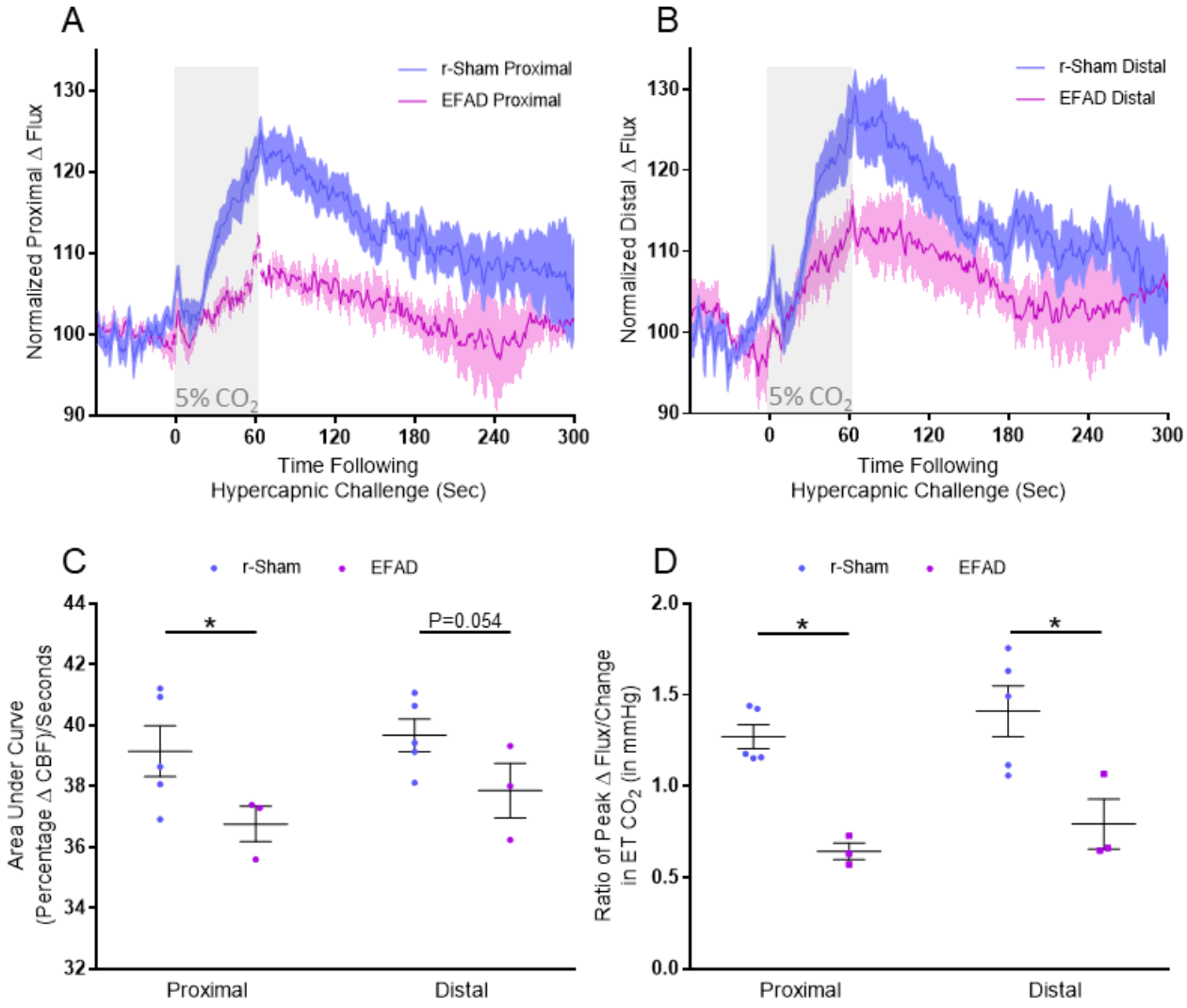

Figure 4.3. Cerebrovascular reactivity at 9 months of age. CO_2 evoked responses of the cerebrovasculature of positive control ApoE3FAD mutant mice are diminished, as compared to the responses of C57BL/6 mice, at 9 months post-injury. Representative traces of CBF flux, as measured by laser speckle contrast imaging, show a reduced mean response in CBF at ROIs both proximal (A) and distal (B) to the site of injury, in the brains of age-matched positive control ApoE3FAD mice, versus r-sham controls, following 60 seconds of 5% $C0_2$ hypercapnic challenge. The area under the curve (C, AUC) and peak response of each individual mouse, normalized to the animal's peak change in $ETCO_2$ (D, CVRx) were both analyzed using a one-tailed student t-test, within ROI and between groups. The AUC of the proximal ROI CBF of ApoE3FAD mice was significantly less than that or age-matched r-sham animals (Student's t-test, $P<0.05$). The AUC of the distal ROI CBF was not significantly different between ApoE3FAD and r-sham mice, however, there was a trend towards significance (One-tailed Student t-test, $P=0.054$). There was a statistically significant difference in CVRx ratio between groups at the proximal and distal ROIs at 9 months of age (Student t-test, $P<0.05$), with a significantly lower value in CVRx of ApoE3FAD mice of 0.64 ± 0.04, compared to a value of 1.27 ± 0.06 for age-matched r-sham controls (Student t-test; r-Sham vs ApoE3FAD, $P<0.05$). *R-sham mice; n = 5 per group. ApoE3FAD; n = 3 per group. CVRx; % Peak Response in CBF/Change in $ETCO_2$ (mmHg). Statistical analysis was conducted using a one-tailed student t-test analysis*

4.3.2. Cerebrovascular Reactivity at 3 Months Post-Injury

The cerebrovascular reactivity of 9 month old mice in response to inhalation of 5% CO_2 in medical grade room air for 60 seconds, and concomitant transient increase in $ETCO_2$ to 55-60mmHg, was markedly decreased in r-mTBI mice, compared to r-sham controls, at 3 months post-last mTBI. The mean response of CBF from ROIs both proximal and distal to the midline site of injury of 9 month old r-sham and r-mTBI mice (Figure 4.4, A and B, respectively) was analyzed using both area under the curve (Figure 4.4, C) and the CVRx, a more clinically relevant index of CVR compared to the AUC, expressed by further normalizing the peak response percentage change in CBF from baseline, to the peak change in $ETCO_2$ from baseline for each animal. The AUC analysis demonstrates a significantly greater response of r-sham mice, compared to r-mTBI (Figure 4.4, C; two-tailed student t-test, $P<0.05$), and CVRx analysis showed a decrease in peak CBF response, normalized to peak change in $ETCO_2$, of r-mTBI mice, relative to r-sham controls, at both the proximal and distal ROI (Figure 4.4, D, Student t-test, $P<0.05$).

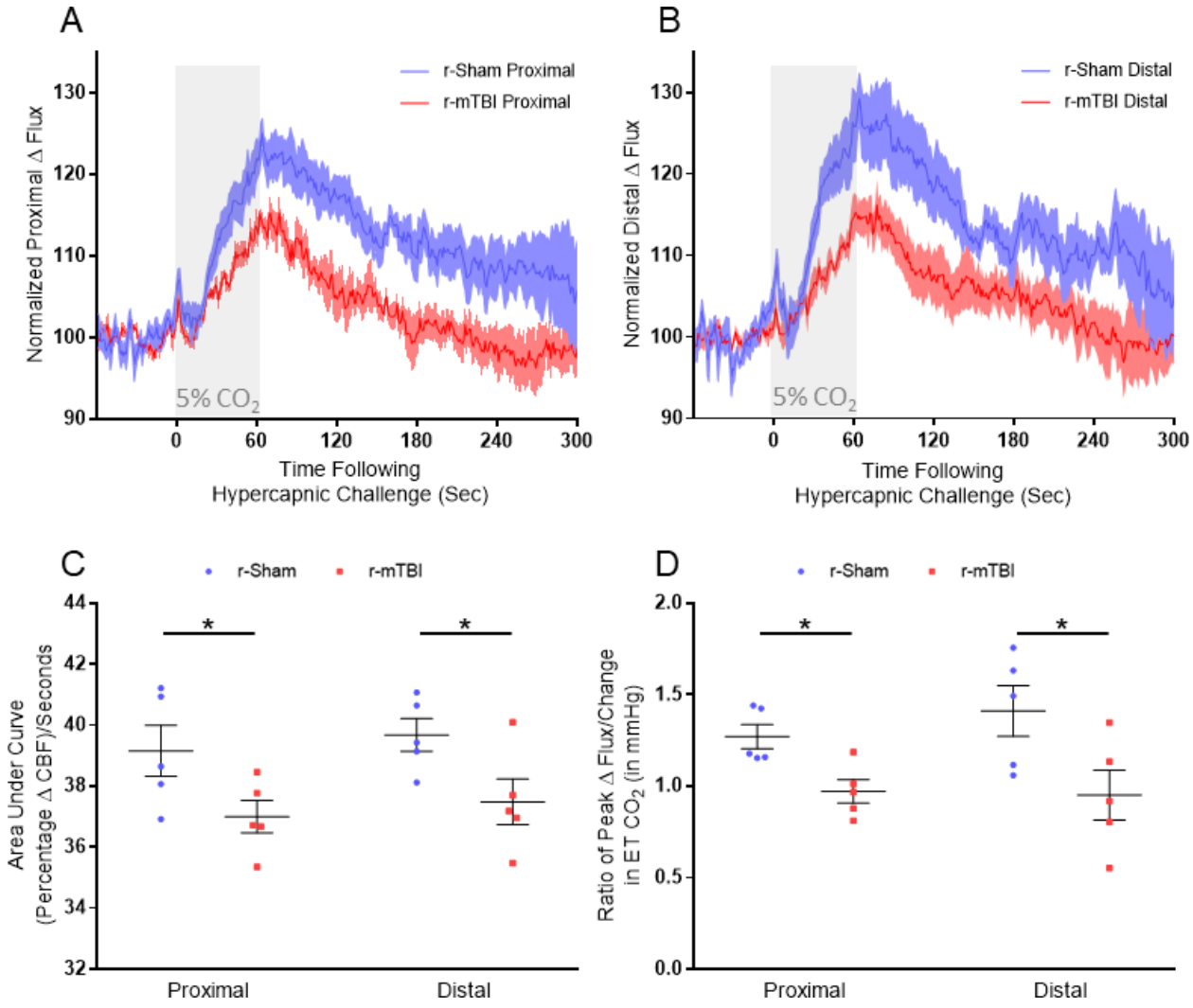

Figure 4.4. Cerebrovascular reactivity at 3 months post-injury. CO_2 evoked responses of the cerebrovasculature of C57BL/6 mice are diminished at 3 months post-injury. Representative traces of CBF flux, as measured by laser speckle contrast imaging, show a reduced mean response in CBF at ROIs both proximal (A) and distal (B) to the site of injury, in the brains of both r-mTBI mice, versus r-sham controls, following 60 seconds of 5% $C0_2$ hypercapnic challenge. The area under the curve (C, AUC) and peak response of each individual mouse, normalized to the animal's peak change in $ETCO_2$ (D, CVRx) were both analyzed using a one-tailed student t-test analysis. The AUC of both the proximal and distal ROI CBF of r-mTBI mice were significantly less than that of r-sham controls (C, two-tailed student t-test, $P<0.05$). There was a statistically significant difference in CVRx ratio between groups at both the proximal and distal ROIs at 3 months post-injury (D, two-tailed student t-test, $P<0.05$), with a significantly lower value in proximal CVRx of r-mTBI mice of 0.97 ± 0.06, compared to a value of 1.27 ± 0.06 for r-sham controls (D, two-tailed student t-test; r-sham vs r-mTBI, $P<0.05$), and a significantly lower value of distal CVRx of r-mTBI mice of 0.95 ± 0.13, compared to a value of 1.11 ± 0.13 (D, two-tailed student t-test, $P<0.05$). *R-sham and r-mTBI mice; n = 5 per group. CVRx; % Peak Response in CBF/Change in $ETCO_2$ (mmHg). Statistical analysis was conducted using one-tailed student t-test.*

4.3.3. Cerebrovascular Reactivity at 9 Months Post-Injury

The cerebrovascular reactivity of 14-15 months old mice in response to inhalation of 5% CO_2 for 60 seconds, and concomitant transient increase in $ETCO_2$ to 55-60mmHg, was markedly decreased in 14-15 months old r-mTBI mice, compared to r-sham controls, at 9 months post-last mTBI. The mean response of CBF from ROIs both proximal and distal to the midline site of injury of 15 month old r-sham and r-mTBI mice (Figure 4.4, A and B, respectively) was analyzed using both area of curve (AUC, Figure 4.5, C) and the CVRx, a more clinically relevant index of CVR compared to the AUC, expressed by further normalizing the peak response percentage change in CBF from baseline, to the peak change in $ETCO_2$ from baseline for each animal. AUC analysis demonstrates a statistically significant decrease in AUC of r-mTBI mice, compared to r-sham controls (Figure 4.5, C; Student t-test, $P>0.05$), however, CVRx analysis shows no correlate decrease in peak CBF response, normalized to peak change in ETCO2, of r-mTBI animals, relative to r-sham controls, at the proximal or distal ROI (Figure 4.5, D, Student t-test, $P<0.05$), but a trend towards a decrease at the proximal ROI (Figure 4.5, D, $P = 0.14$).

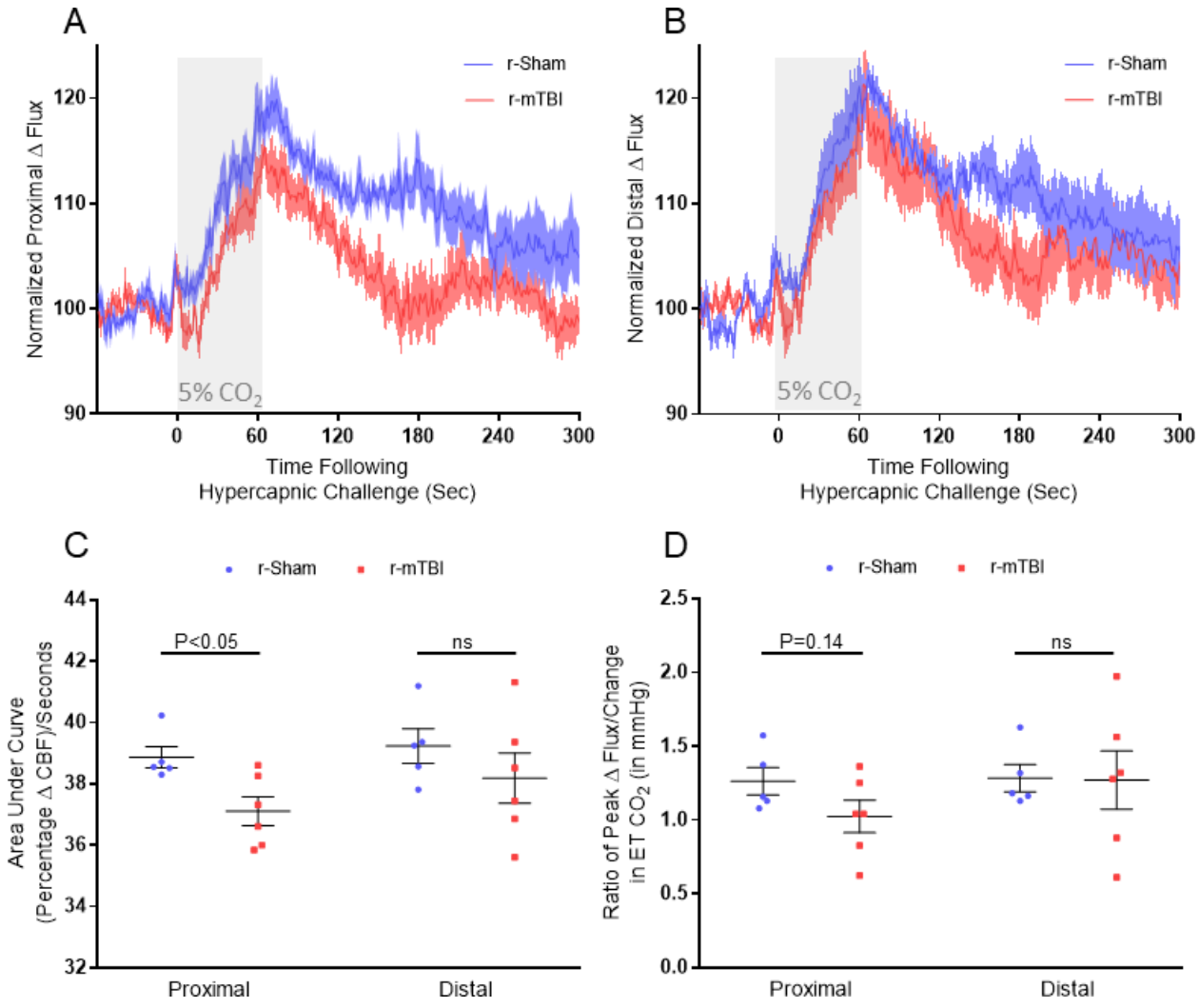

Figure 4.5. Cerebrovascular reactivity at 9 months post-injury. CO_2 evoked responses of the cerebrovasculature of C57BL/6 mice at 9 months post-injury. Representative traces of CBF flux, as measured by laser speckle contrast imaging, showed the response in CBF at ROIs both proximal (A) and distal (B) to the site of injury, in the brains of r-mTBI mice, versus r-sham controls, following 60 seconds of 5% $C0_2$ hypercapnic challenge, at 9 months post-injury. The area under curve (C, AUC) and peak response of each individual mouse, normalized to the animal's peak change in $ETCO_2$ (D, CVRx) were both analyzed within ROI using a two-tailed student t-test. There was a statistically significant decrease in AUC of r-mTBI mice, compared to r-sham controls, at the proximal ROI at 9 months post-injury (C, two-tailed student t-test, P<0.01). There was no statistically significant difference in CVRx between groups at either the proximal or distal ROI at 9 months post-injury (D, One-way ANOVA, P>0.05). Neither the AUC, nor the CVRx analysis of the distal ROI reported statistically significant difference between r-sham and r-mTBI at 9 months post-injury (P = 0.14, Student t-test). *Wild type mice; r-sham, n = 5, r-mTBI, n = 6. CVRx; % Peak Response in CBF/Change in ETCO2 (mmHg). Statistical analysis was conducted using One-way ANOVA and Tukey HSD post-hoc analysis.*

4.3.4. Physiological Parameters Affecting Cerebrovascular Reactivity

The mean $ETCO_2$ and MABP recordings for the first 60 seconds of baseline prior to hypercapnic challenge onset, the timepoint corresponding to the peak $ETCO_2$ value reached, and the last 60 seconds of baseline before the end of the experiment, were analyzed for each group at both 3 months (Figure 4.6, C) and 9 months (Figure 4.6, D) post-injury. $ETCO_2$ values at peak were significantly higher than those at baseline levels in r-sham, r-mTBI, and ApoE3FAD groups (One-way ANOVA, $P<0.001$). $ETC0_2$ values for r-sham, r-mTBI, and ApoE3FAD mice were no different between baseline and final baseline (Figure 4.6, C, One-way ANOVA, $P>0.05$). There was no difference in $ETCO_2$ or MABP between r-sham, r-mTBI, and ApoE3FAD groups at either initial baseline, or the final baseline, at 3 months post-injury (Figure 4.6, C, one-way ANOVA, multiple comparisons t-test). However, there was a statistically significantly lower peak $ETCO_2$ reading of 56.38 ± 0.26 mmHg in r-mTBI mice, compared to a value of 58.03 ± 0.37 mmHg for r-sham controls (Figure 4.6, C, top panel, one-way ANOVA, multiple comparisons t-test, $P<0.05$), but no difference between r-sham or r-mTBI peak ETCO2 value and the ApoE3FAD group value of 56 ± 1.14 mmHg, at 3 months. The difference in peak $ETCO_2$ level reached at 3 months was not accompanied by a difference in MABP across groups. At 9 months post-injury, $ETCO_2$ values at peak response were significantly higher than those at baseline levels in r-sham and r-mTBI groups (Figure 4.6, D, One-way ANOVA, $P<0.001$). There was no statistically significant difference in $ETCO_2$ or MABP across groups at baseline, peak, or final baseline during the experiment at 9 months, however, there was a significantly greater $ETCO_2$ value at final baseline of 37.92 ± 1.37 mmHg for r-mTBI mice, compared to baseline value of 36.73 ± 0.34 mmHg (Figure 4.6, D, One-way ANOVA, P = 0 0453).

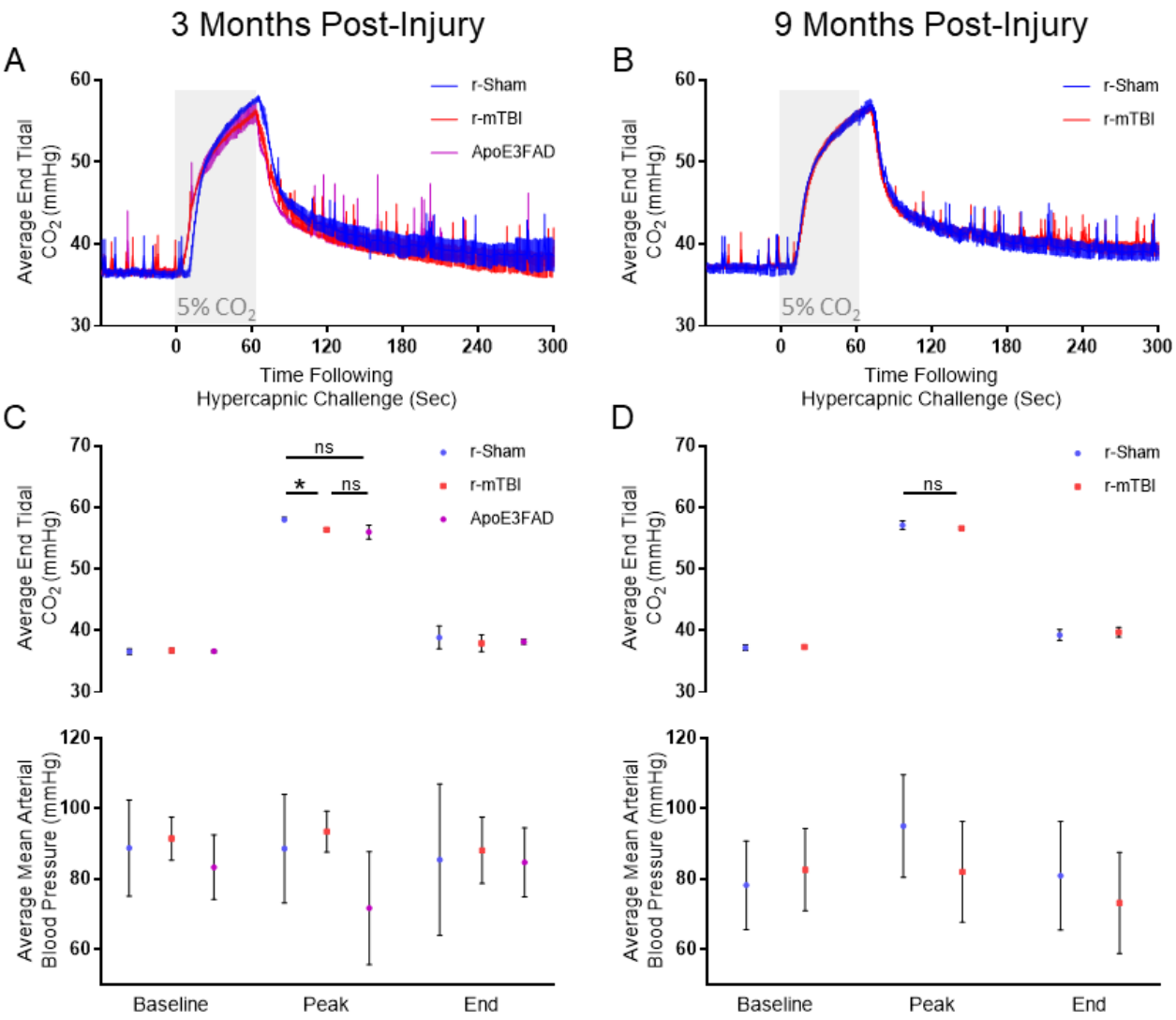

Figure 4.6. Physiological parameters at initial baseline, peak response to hypercapnic challenge, and final baseline prior to end of experiment, in C57BL/6 mice at 3 and 9 months post-injury. A and B show representative traces of the $ETCO_2$ increase, as recorded by capnography, in r-sham and r-mTBI mice, in response to hypercapnic challenge, at 3 and 9 months post-injury, respectively. $ETCO_2$ and MABP values corresponding to the peak $ETCO_2$ time-point, and continuous 60 second blocks of data from the initial and final baselines of the experiment were analyzed via one-way ANOVA (C, and D). $ETCO_2$ values for r-sham, r-mTBI, and ApoE3FAD mice were no different between baseline and final baseline (Figure 4.5, C, One-way ANOVA, $P>0.05$). There was no difference in $ETCO_2$ or MABP between r-sham, r-mTBI, and ApoE3FAD groups at either initial baseline, or the final baseline, at 3 months post-injury (C, one-way ANOVA, $P>0.05$), however, there was a statistically significantly lower peak $ETCO_2$ in r-mTBI mice, compared to r-sham controls (C, one-way ANOVA, $P<0.05$), but no difference between r-sham or r-mTBI peak $ETCO_2$ and ApoE3FAD $ETCO_2$, at 3 months. Peak $ETCO_2$ response was significantly greater in comparison to baseline values, in r-sham and r-mTBI groups at 9 months post-injury (D, One-way ANOVA, $P<0.001$). There was no statistically significant difference in $ETCO_2$ or MABP between groups at baseline, peak, or final baseline at 9 months, however, there was a significantly greater $ETCO_2$ value at final baseline for r-mTBI mice, compared to initial baseline (D, One-way ANOVA, P = 0 0453). *3 months; wild type mice, n = 5 per group. ApoE3FAD; n = 3 per group. 9 months; wild type mice, r-sham, n = 5; r-mTBI, n = 6. Statistical analysis was conducted using One-way ANOVA and multiple comparisons with Wilcoxon t-test.*

4.4. Discussion

The recapitulation of relevant and early occurring physiological hallmarks in preclinical animal models of neurodegenerative disease is a prerequisite for successful understanding of, and therapeutic action against, deleterious biological mechanisms. In this report, using our mouse model of r-mTBI related chronic neurodegenerative illness, we have emulated clinical studies in the human r-mTBI population[142,143,231] and demonstrated a severe deficit in cerebrovascular reactivity at chronic time-points post-injury, coinciding with dysregulation of vascular cellular and functional markers and neurobehavioral deficit, as demonstrated in Chapter 3.

Despite the preponderance of TCVI throughout the preclinical TBI literature, and across near moderate to severe head trauma[186,232] and CTE-like human case report[41,46], relatively few pre-clinical studies have characterized TCVI at a chronic time-point post-last injury, and none in tandem with clinically relevant in-vivo physiological recording, and neurobehavioral and vascular-directed biochemical analyses. This is perhaps due to the only recent emergence of CVR deficit as an endophenotype of both acute and chronic mTBI in civilian, military, and athlete populations alike. However, this is most likely due to the difficulty in conducting controlled in-vivo experiments in general, and a clinically representative in-vivo hypercapnic challenge in particular, on laboratory rodents across an age range comparable to the time typical of r-mTBI related neuropsychological and pathological manifestation in humans. Our animal model has already been shown to mimic some signs of the pathognomonic CTE-like neuropathology in the human population, such as cortical pTau accumulation and neuroinflammation, when the injury

paradigm is administered to hTau mice[62], and has herein been further validated in replicating the TCVI-specific CVR deficit in human patients.

Although CVR deficit has been implicated as a symptom of many neurodegenerative diseases, including the inheritable small vessel disease CADASIL[148,233] and AD[140], recent work by a number of research groups has galvanized CVR as a forerunner in TCVI diagnosis, and potentially as a treatment outcome metric, in the field of human TBI. Recent studies by Diaz-Arrastia and colleagues[100,142,143,231] have demonstrated global, whole gray, and white matter CVR deficit in moderate-to-severe TBI patients over as chronic a timeframe as 6 months to 8 years following injury, typically as a result of automotive accident[100,142,143,231]. Amyot et al reported patchy "moth-eaten" multifocal BOLD MRI-assessed regions of CVR deficit throughout the gray matter of brains of these 27 moderate-to-severe TBI patients, in comparison with 15 healthy controls, and a correlation of global gray matter CVR, but not CBF, defect with chronic TBI symptoms, such as fatigue, irritability, and depressed mood, in these patients[142], but no correlation between CVR or CBF and neuropsychological symptoms across healthy and TBI groups. Interestingly, neuropsychological score, as assessed by the wide range achievement test (WRAT) scores and the Rivermead post-concussive symptoms questionnaire, showed a trend towards correlation between individual TBI CVR and individual Rivermeaad score, as compared to healthy age and gender matched controls, where no such correlation existed[142]. The group further expanded on these data in this same group of patients by demonstrating that regions of parenchymal tissue distant from areas of encephalomalacia and gross tissue damage, as identified through FLAIR MRI, exhibited resting CBF comparable to healthy control brain, but showed a CVR deficit via BOLD MRI hypercapnia, insinuating that normal appearing areas of tissue with apparently

adequate vessel density and resting state perfusion are still damaged enough to have decreased response to vasoactive stimulus[142,143]. Moreover, while the study cited the largest decreases in CVR and CBF to occur within regions of structural MRI-identified encephalomalacia, and exaggerated and decreased mean diffusivity (MD) and fractional anisotropy (FA), respectively, the magnitude of functional loss was not consistent between imaging modalities, indicating that vascular and structural tissue damage, traditionally identified via MD and FA, may be separate endophenotypes of chronic TBI within an individual[143]. Indeed, the fact that the above studies cited CVR deficit diffusely and distinct to the structural lesions exemplifies the relative redundancy of structural MRI based methods in the assessment of TCVI. Perhaps most interesting of the findings from this cohort of patients is the study by Haber et al[143] is that, when comparing lesion-negative whole brain CVR from TBI patients with marked encephalomalacia, to whole brain CVR from those patients without detectable parenchymal lesion, there was no difference in response, indicating that , although this is a moderate-to-severe TBI cohort, gross tissue damage may not be necessary for the diffuse TCVI associated pathophysiology seen here, and in lesser severities of TBI.

Though the above studies[142,143,231], and the work carried out by the aforementioned group in general, could be argued to be the most comprehensive of longitudinal CVR analyses conducted thus far in the human TBI population, the prevalence of CVR perturbation is not limited to the chronic phase following the more severe forms of injury, and has been seen across a range of studies of athletes at varying times following mTBI. One such study, mentioned previously, by Mutch et al[144,217], has demonstrated patient-specific alterations in global CVR via BOLD MRI hypercapnic challenge in 15 sports related concussion (SRC) patients of 13 – 21 years old, with

structurally-normal brain scans, at time-points of 7-279 days following onset of symptoms, compared to 17 healthy control subjects. Although there was no detectable difference in whole-brain resting CBF between SRC patients and healthy controls at either initial or follow-up MRI testing, there was an initial mean global decrease in CVR across the 6 SRC patients on average, compared to healthy subjects. Additionally, all 6 SRC patients displayed ongoing and individual patient-to-patient signature regional CVR increases and decreases, at both initial examination and following symptom resolution[144,217]. A follow-up study by the same group, examining 15 SRC subjects in a more acute-to-subacute phase following concussion, and required to be symptomatic at rest, or demonstrating a symptom-limited threshold during aerobic treadmill training[234], were shown to exhibit a predominant pattern of increased CVR, relative to a brain atlas from 27 healthy control participants,

The above findings of altered CVR in adolescent PCS following r-mTBI have been corroborated in older individuals. Using NIRS and TCD, Bailey et al[235] have shown that the magnitude of decreased CVR in boxers, of 27 years and older, correlated directly with both the number of mTBIs sustained and the degree of neuropsychological deficit at chronic time-points post injury. Seemingly contradictory data from a report by Svaldi et al[145] shows only a transient CVR deficit in asymptomatic 18 year old female soccer players following a single season of play, and correlating with number and degree of high acceleration events (HAEs), as assessed by hypercapnic breath hold fMRI, and xPatch head acceleration sensors. Individual CVR returned to baseline pre-season levels within 2 month following end of season for all participants, however, it was reported that the players exhibiting greatest correlation between magnitude of CVR impairment and HAEs were those experiencing the highest proportion of HAEs over 50g in

force[145]. The fact that both symptomatic boxers[235] and asymptomatic soccer players[145,146] exhibit decreased CVR, assessed via different imaging modalities, supports the use of CVR as an imaging biomarker of TCVI across mTBI populations. Furthermore, the apparent recovery of normal CVR in the female athletes mentioned, as compared to the ongoing deficit in said boxers, is possibly due to comparatively greater load and frequency of mTBIs attained during a boxing season, as compared with that over a season of soccer. As mentioned, those soccer players sustaining greatest load of higher force HAEs demonstrated worst CVR, indicating there may be a threshold of mTBIs needed for prolonged CVR perturbation in humans, much as is the case in animal models of r-mTBI, where, typically, the highest frequencies of repeat closed head impact head trauma have resulted in AT8-positive and pTau accumulation[62,63]. Regardless, the previous reports posit CVR analyses as a definitive alternate non-invasive and sensitive approach for examining r-mTBI in the human population.

To ascertain whether there was an observable effect of r-mTBI on CVR in our animal model, and if so, whether it was similarly representative of behavioral and pathological burden, we employed laser speckle contrast imaging, at a high temporal resolution of 1 Hz acquisition, to measure CBF flux in relation to baseline readings, in response to hypercapnic challenge (Figure 4.2). The high temporal resolution of this approach allows for a representative analysis of peak vasodilatory response of the cerebrovasculature to increased arterial paCO2 concentration, however, the method is also limited in terms of the depth of parenchymal tissue analyzed, approximated to be no more than 500µm below the surface of the brain. The results of this report can thus be considered reflective of superficial gray matter CVR changes. The stability and reproducibility of the experimental design is demonstrated in Figure 4.5, whereby there was no

difference in MABP or $ETCO_2$, the two main determinants of CBF alongside paO_2 and neuronal function, at baseline between groups at either time-point evaluated. Additionally, the animals' physiology, on average, demonstrated the ability to eliminate supra-normal physiological levels of paCO2 (Figure 4.5, A and B). We further validated the in-vivo experiment by assessing CVR in age-matched ApoE3FAD mice, which express 5 familial AD mutations[218], and confirmed both a lower AUC and CVRx of peak response in these transgenic mice, compared to either r-sham or r-mTBI animals (Figure 4.3). EFAD mice were chosen as a positive signal for functional hyperemic deficit on account of published data demonstrating transgenic mice harboring FAD mutations to exhibit decreased CVR in response to hypercapnia[227,236,237], much as is the case in the AD population[140,223,225,226,228]. In fact, one study by Shin et al[229] describes a progressive age-dependent decrease in both CBF flux value and CVRx ratio in the Tg2576 mouse, compared to age-matched wild type mice, at 3, 8, and 15 months of age, indicating the impact that just one FAD mutation has on CVR. The same study also shows decreased CVR response with age within the wild type group[229], similar to the decreased response we see in sham mice at 9 months post-injury (15 months of age), compared to sham mice at 3 months post-injury (Figures 4.3 & 4.4, A and C) when exposed to hypercapnia. Indeed, it is worth noting that the modest difference in CVRx between r-sham and r-mTBI mice at 9 months post-injury (15 months of age) in our study may have been significant had it not been for the confounding age-dependent decrease in CVR at this time-point. The difference in peak $ETCO_2$ levels between r-sham and both r-mTBI mice and E3FAD controls at 3 months post-injury should not be considered to be driving the CVRx difference between groups, as this is controlled for by normalization of percentage change in flux

to the change in $ETCO_2$ readings when generating the CVRx value (Figures 4.3, D, and 4.4, D), as is frequently done in the clinic.

In agreement with the aforementioned human TBI studies, we report a significant and profound multifocal (both proximal and distal to the site of injury, Figures 4.3 and 4.4) reduction in CVRx at the chronic 3 month post-injury time-point in our animal model of r-mTBI. As mentioned, this CVR deficit is likely to be central and representative of TCVI in the r-mTBI mice, and not driven by peripheral physiological determinants, as mice with signs of alkalosis, acidosis, sub-normal bicarbonate, or saturated O_2 concentrations less than 95% prior to hypercapnic challenge were not included in the analyses. The difference in CVR at both time-points analyzed seems to be less exaggerated at the ROI distal to the site of r-mTBI, with apparent restoration of normal function at 9 months post-last injury (Figure 4.4, D), alongside a trend in persistent CVRx deficit in tissue nearest the impact area (Figure 4.4, D, $P = 0.07$). While this apparent restoration in vascular function may be a false negative, as mentioned in regards to the possible confounding effects of age at this time-point, if taken as representative, the seemingly transient nature of the CVRx impairment seen here can be interpreted in one of two ways; either the CVRx sequelae of r-mTBI induced TCVI in our animal model is short-lived, and shows a propensity to resolve following reprieve from trauma, or the effect at the more chronic 9 months following r-mTBI is more global, and requires a much larger sampling of a greater depth of tissue, as has been used in identification of chronic human TBI CVR dysfunction[142,143,231], than was possible in this study. Both interpretations of this data would agree with the literature at large, as our biochemical analyses from Chapter 2 show a possible biphasic reaction of the cerebrovasculature to injury, akin to the compensatory response seen across animal models of TCVI[100], which could account

for the disappearance of CVR deficit with age in our animals, much as with the human population of athletes[145,146,217,238]. Likewise, studies investigating moderate to severe TBIs[142,143] postulate a CVR deficit detectable only by global CVR analyses at the more chronic time-point post-injury, and so, elusive to the localized ROI measurements in this study.

Only one other study has examined CVR deficit in a mouse model of repetitive head trauma. Adams et al[239] have administered 3 unilateral closed head impacts to Thy1-ChR2 mice at 3 day intervals and assessed CVR in repetitively injured mice and controls at 2 weeks post-injury via ASL, and inhalation of 10% CO_2 for 60 seconds for evocation of hypercapnic challenge[239]. Although this group reported a severe decrease in CVR in the cortex ipsilateral to injury, the study has several caveats, not least of all the high incidence of attrition within the TBI group of mice within 2 weeks post-injury, the use of a greater percentage of CO_2 above than that used in the clinic, and the lack of data on MABP and $ETCO_2$ at baseline or peak levels in mice during the experiment. As such, the effects seen in the study may be regarded as somewhat representative of CVR deficit following a moderate to severe TBI, but certainly not applicable in the context of repetitive mild head trauma.

In summary, we have in this Chapter for the first time shown a functional physiological deficit by the cerebral vasculature following repeat mild head trauma coinciding with cerebrovascular-specific pathology and neurobehavioral decline in an animal model of r-mTBI. These findings not only recapitulate those seen across a spectrum of mTBI patients in the human population, but also provides the first evidence of a causative role for TCVI in preclinical r-mTBI related

pathogenesis, and justification for the use of CVR measurements as a prospective diagnostic and therapeutic metric in research.

Chapter 5. Discussion and Conclusions.

5.1. Overview.

Traumatic brain injury is a major cause of chronic disability worldwide, and despite the incidence and impact of the so-called 'silent epidemic' of mild TBI, there is an unmet need to understand the biological mechanisms underpinning onset and evolution of TBI-related neurodegeneration in both human patients and animal models of the disease. Researchers attempting to emulate the pathological sequelae most typically seen in r-mTBI patients have failed to reproduce many of the trademark pathological lesions seen at autopsy of those diagnosed with CTE or dying in the acute to subacute phase following a mTBI, and so, the validity of relying upon these hallmarks of repetitive injury-related disease that are seemingly monogamous for the human condition is speculative at best. Ergo, validation of a physiological biomarker common across the spectrum of mTBIs both developed in various animal models, and sustained by human patients, would eliminate the reliance of the preclinical field on neuropathological end-points of longitudinal studies, and represent an *in vivo* diagnostic alternative in mouse and man. Currently available clinical imaging modalities such as pseudo carotid Arterial Spin Labelling (pcASL) are especially sensitive to changes in vascular perfusion, commonly seen in chronic TBI. Traumatic Cerebral Vascular Injury (TCVI) is a non-invasively demonstrable endophenotype which manifests as a lack of cerebrovascular reactivity (CVR) *in vivo* in human patients and is shared across the spectrum of r-mTBI in mouse and man. However, this physiological deficit, typical of TCVI, has until now eluded measurement in preclinical models of r-mTBI.

5.2. Summary of Findings.

Given the heterogenous nature of the head trauma accrued by the more than 2.5 million patients each year in the United States alone, early occurring and injury-specific biomarkers will be paramount in the development of therapeutic strategies, as they can demonstrate target engagement, or lack thereof, with the hypothesized mechanism of injury, and provide proof of principle by indication of efficacy on a preclinical screening platform. Arguably the most immediate central phenomena following TBI and meeting the criteria of a non-invasively quantifiable biomarker is a decrease or abnormal patient cerebral blood flow (CBF). A greater proportion of moderate-to-severe TBI patients have marked reduction in resting state CBF within 12 hours following head injury[240], and individuals with a history of r-mTBI demonstrate alterations in regional and global brain perfusion many days and weeks following traumatic insult[138,141]. Severe TBI is known to result in potentially fatal ischemia through vasospasm and hypoperfusion[135], and so, therapeutic intervention to augment CBF acutely is predicted to have clinical benefit[241]. However, there is currently no cerebrovascular oriented therapy considered protective against chronic r-mTBI symptoms, chiefly because so little is known regarding the vascular mechanics underlying its pathogenesis. For this reason, we aimed to conduct the first characterization of chronic cerebrovascular pathophysiology in an animal model of repetitive mild traumatic brain injury[155]. Our model recapitulated the long-term decrement in cognition, and neuroinflammatory phenotype archetypal of murine model CTE-like neurodegeneration, alongside vascular marker and, most importantly, CBF decrement, seen in individuals suspected at risk for development of the pathognomonic pTau pathology of CTE. These findings provide rationale for using this model as a validation of the preclinical relevance of the CVR

endophenotype seen in the mTBI population, and a potential alternative and more mechanistically telling outcome measure to Tau pathology.

Over the course of this thesis, we have designed and validated a sensitive and relatively non-invasive experiment to elucidate the degree of CVR in our relevant animal model of r-mTBI and demonstrated a deficit in CVR representative of that seen across select studies of chronic TBI in human patients. Specifically, we have identified a chronic CVR pathophysiology, akin to the profile of cerebrovascular responsiveness seen under similar conditions and experimental interrogation in a proportion of studies conducted on human athletes[145,146,238]. Furthermore, we have demonstrated evidence of a parallel biphasic TCVI pathology occurring at the time-points of *in vivo* analysis, providing a biological mechanistic rationale for the observed physiological phenomena, adding further credence to the significance of TCVI as a distinct endophenotype of chronic TBI-related illness, and bridging a gap in knowledge in the literature.

The exact cause of CVR deficit in human TBI is not understood, though it is believed to be due to an inherent inability of the cerebral vessels to react normally to vasoactive stimuli, rather than a decreased presence of the vessels themselves[143]. This hypothesis is supported by several studies in animal models, one such example being a report by Wei et al[242], using cranial windows to visualize pial vessels and parenchymal vasculature as we did, to show that while Fluid Percussion Injury mTBI in rats elicited a pronounced decrease in CVR via hypercapnic challenge for up to 3 weeks post-injury, the degree of deficit in response to either hypercapnia or topical application of acetylcholine was quantitatively greater than that observed with application of the nitric oxide donor Sodium Nitroprusside (SNP)[242]. This result indicates that the smooth

musculature of the endothelium retains the ability to respond to NO in this animal model of chronic TBI, however, the signaling mechanisms governing NO production itself seem impaired[242]. This hypothesis is mirrored in our findings at 3 months post-injury in our own model of chronic r-mTBI, whereby profoundly reduced expression of eNOS, without concomitant decrease in markers of vascular mural or endothelial cellularity, throughout the cortices of r-mTBI mice is seen in unison with CVR decrease in response to hypercapnia. The results of our study and of Wei et al[242] falls in line with the proposed mechanistic modus operandi, recently proposed[231], for the augmentation of chronic CVR deficit in moderate-to-severe TBI patients by treatment with Sildenafil, a PDE5 inhibitor, which indirectly increases the vasodilatory effects of NO *in vivo*[231]. Kenney et al[231] demonstrated that a single oral 25mg dose of sildenafil is sufficient to potentiate CVR in TBI patients exhibiting both global and regional CVR deficit in lesioned and normal appearing gray matter tissue. Once again, the CVR in these patients is seen to be compromised in areas exhibiting normal resting CBF, indicating intact and functional vessel density. Furthermore, patients receiving a twice daily dose of 25mg sildenafil for a course of 8 weeks showed improved CVR, relative to baseline, with two patients self-reporting increased processing speed and concentration. The lack of an overall effect of prolonged treatment with sildenafil on neurocognitive parameters in these patients beyond self-report may have been as much due to small sample sizes as to the very late time-point analyzed. However, the studies of both Kenney et al[231], and Wei and colleagues[242] provide proof of concept for the targetability and therapeutic efficacy of treatment of TCVI via CVR analyses *in vivo*.

The next most prescient finding of our study was the fact that alterations in normalized CVR index appear to dissipate by the second, most chronic time-point post-injury analyzed in our

r-mTBI paradigm. This can be interpreted as the cerebrovasculature's latent plasticity and adaptability in the response to TCVI, as seen in animal models of r-mTBI[171,194-197,206,211], and is encouraging in the context of prospective prophylactic and other therapeutic interventions. However, marked neurobehavioral impairment was still observed, despite the modest resolution in CVR deficit (P = 0.14), perhaps indicating that, as detrimental as TCVI may be early on in disease pathogenesis, the poly-pathological burden of white matter tract damage and neuroinflammation endured through to chronic time-points post-injury alongside vascular pathology may be sufficient to continue to advance disease progression despite possible TCVI/CVR recovery. It should be noted that the modest resolution in CVR signal at 9 months post-injury in our animal model may have been statistically significant were it not for a possible masking effect of decreased vascular responsiveness in the sham animals at this very chronic time-point post-injury, such as is possible and has been noted by a separate group[229]. This is not necessarily a disparaging result, as early treatment of TCVI with angiogenic therapeutics has been shown to ameliorate cognitive symptoms in animal models of brain injury, with one group reporting improved neurologic recovery following experimental ischemic stroke with Sildenafil treatment[204]. Another team has recently demonstrated that infusion of the vascular-associated sulfonlylurea urea pathway antagonist Gilbenclamide, following polytraumatic CCI and hemorrhagic shock injury in wild type mice, results in decreased cerebral edema[243]. Statins, 3-hydroxy-3-methyl-glutaryl-coenzyme A (HMG-CoA) reductase inhibitors, prescribed universally for treatment of high cholesterol and lowering of incidence of vascular and cardiac-related adverse events in the human population, have shown great promise in treatment of mTBI preclinically, with one study by Xu et al[244] showing acute treatment following CCI in wild type

mice to have neuroinflammatory and neurobehavioral outcome benefits. Tong and Hamel[245] have shown that chronic treatment of 18 month old Transforming Growth Factor-β 1 (TGF-1) mice, considered a model of cerebrovascular disease, with Simvastatin managed to restore nitric oxide levels to baseline *in vivo* and to rescue Acetylcholine-induced deficit in cerebrovascular reactivity *ex vivo*[245]. The same group previously confirmed synergistic rescue of impaired spatial memory, as assessed by Morris Water Maze, and cerebrovascular reactivity deficit in response to the Acetylcholine and Calcitonin Gene-Related Peptide (CGRP) stimulation *ex vivo* in cerebral arteries from double transgenic FAD mice following treatment with Simvastatin[228]. Most importantly, these neurocognitive and physiological improvements occurred without obvious resolution of amyloid pathology, and only in adult treated mice, and not aged animals[228]. The reversal of both cognitive and CVR deficits by statins at an earlier stage of neuropathology in animal models of Alzheimer's disease, taken together with the above success in rescue of vascular responsiveness and behavioral phenotype in animal models of TBI, suggest that treatment of TCVI early on may have broad spectrum therapeutic efficacy past just vascular health, and independent of other persistent co-pathology. Our animal model and current optimized experimental setup is the first attempt in the field of preclinical neurotrauma research to investigate vascular health and physiology following r-mTBI and is ideal for testing of these hypotheses. The findings from this thesis support the involvement of TCVI as a key pathology of chronic r-mTBI-related neurodegeneration in both the human population of mTBI survivors and our animal model thereof. Furthermore, the results described herein are the first to resemble the physiological *in vivo* endophenotype of TCVI of the human population in the preclinical arena

and demonstrate sound mechanistic basis for compromised cerebrovascular health and responsiveness following repeat head trauma.

5.3. Future Directions

As with any novel approach, the sensitivity and application of the *in vivo* methodology outlined in this thesis can be advanced upon. Though replicate cohorts of age matched male mice were used for the two time-points at which CVR and neurobehavioral assessment was conducted, and the results can thus be assumed to be representative of those had the same animals been analyzed across all metrics, future investigations will involve the longitudinal and repeated CVR and cognitive testing in each biological replicate mouse. This approach will give greater insight in to individual animal to animal variability in response to injury and allow for longitudinal treatments, with the benefit of sensitive and telling multivariate analyses of each biological replicate across time. In addition, the CVR index of each animal can be measured against the animal's Barnes Maze probe memory assessment in both treated and untreated sham and TBI mice, in an aim to answer whether the degree of CVR deficit correlates directly with learning and memory impairment.

The complement biochemical analyses to the *in vivo* data herein, though in agreement with relevant studies in the field, incorporated the whole of the cortical vasculature, and so, arteriolar or capillary-specific alterations in mural cellular or functional markers may have been underestimated. Future research will build upon this more global biochemical assessment by examining high magnification confocal images of immunohistochemically stained cortical vessels

for the same markers as were examined in Chapter 3, to determine whether the downregulation seen for cellular markers, such as PDGFRβ, was representative of a decreased pericyte population, or a decreased presence of the receptor itself, relative to mural cell count. Another complement technique, alongside the immunoblot analyses from Chapter 3, to further interrogate the extent, if any, of BBB permeability throughout the cortices of r-mTBI mice would be the inclusion of a low molecular weight fluorescent dye in to the femoral artery catheter perfusate following the hypercapnic challenge, immediately prior to euthanasia. This would allow cerebral vascular circulation and *in vivo* imaging of dye extravasation from the vessels via fluorescent microscopy, and post mortem confocal microscopy of said fluorescent marker throughout the parenchyma, as an indicator of BBB leakage.

Although the above histopathological approaches would address whether changes in the gross vascular density and structure may be partly responsible for the diminished CVR seen following r-mTBI, they would not provide insight in to the underlying signaling pathways, or aberrations therein, mediating vessel dilation in response to increased arterial pCO_2. The transient activation of the intracellular pathways leading to production of vasodilatory substances, such as NO and Prostaglandin E_2, is likely to subside, and vasoactive mediator concentrations probable to return to baseline physiological levels soon after cessation of hypercapnia. Additionally, the biological mechanisms governing the chemosensory response of the cerebral vasculature to hypercapnia are thought to be multi-faceted and are not very well defined in health, let alone in a neurodegenerative disease state such as chronic head trauma-related illness. Nonetheless, it is essential to dissect the molecular cascade upstream of hypercapnia-elicited CVR in both the healthy and r-mTBI rodent if we are to adequately

understand and target the pathogenesis of this aspect of TCVI, and due to the short-lived signaling involved, this would be best done in real time in an intact cranial window imaging setup used in this and a few other studies. Recent such efforts by other groups have demonstrated the astrocytic release of COX-1 derived PGE_2 to be in part responsible for the cerebral vasodilation in response to hypercapnia[246] in the rodent, and the aforementioned studies by Wei et al[242] have shown facilitation of CVR in both lateral fluid percussion-injured animals and control sham rats upon administration of Sodium Nitroprusside (SNP), implicating Nitric Oxide as a key potentiator of CVR *in vivo*, much as has been shown by the work of Kenney et al[143] in chronic TBI in human patients. Ergo, there may be several vasodilators, released from more than one mural or endothelial cell type acting synergistically to initiate and facilitate CVR in the cerebral cortex.

The most obvious future experiment may be to eliminate each potential vasoactive substance one at a time, such as has been done with regards to Adenosine in a study by Miekisiak et al[247], which demonstrates a similar CVR response to hypercapnia, as measured by laser Doppler Flowmetry, in anesthetized, intubated and artificially ventilated wild type and age-matched Adenosine A_{2A} receptor knockout mice, suggesting that Adenosine may not be essential to induction or facilitation of hypercapnia-induced hyperemia[247], and so, not a compelling line of inquiry or therapeutic candidate in the study of physio-normal vasoreactivity or r-mTBI related CVR impairment, respectively. The most pronounced CVR deficit in our animal model of r-mTBI was seen at 3 months post-injury, coinciding with an apparent decrease in cortical expression of eNOS, suggesting either a downregulation of the essential NO-producing enzyme. This interpretation would agree with the data presented by both Wei et al[242] and Haber and colleagues[143,231], invoking an intact endothelium, but a reduced permissive action of NO during

hypercapnia. To test if this is the case in our animal model, we could expose the 9 month old sham and r-mTBI mice to two sequential hypercapnic challenges separated by a femoral artery catheter infusion of SNP, in order to normalize NO activity between groups. Under this experimental setup, if the decrease in CVR is solely endothelium-dependent, and not caused by other factors, such as smooth muscle loss, or vasoactive signaling dysfunction separate to NO, then the CVR response should be rescued in r-mTBI mice, compared to sham. The SNP administration could also be coupled with a pretreatment, following the first hypercapnic stimulus, of 2,4-diamino hydroxyl pyrimidine (DAHP), a specific inhibitor of guanosine triphosphate cyclohydrolase (GCH1), the rate-limiting enzyme in the *de novo* biosynthesis of tetrahydrobiopterin (BH4)[248], an essential co-factor for eNOS activity[249]. This pretreatment would ensure depletion of endogenous NO reserves and activity, and in so doing, aid in normalizing the response across biological replicates.

The decrease in PDGFRβ expression, without a concomitant decrease in the aminopeptidase N marker CD13, arguably a much more membranous ubiquitously expressed marker of pericytes, might suggest a downregulation of receptor function with little or no decrease in pericytic cellularity or vessel coverage. This is an important finding with regards to the profound decrease in CVR at the 3 months post-injury time-point, as, not only is PDGFRβ receptor expression loss implicated in cerebrovascular dysregulation in AD, but pericytes and smooth muscle cells are known to secrete, and express receptors for, the potent vasoconstrictor Endothelin-1 (ET-1) *in vivo* following TBI[121], and inhibition of ET-1 signaling following experiment TBI has been shown to protect against hypoperfusion[181], so it is possible that an enhanced ET-1 mediated tone may be in part responsible for the decreased CVR in response to hypercapnia seen at the earlier of

the two chronic time-points. The first future experiment to determine the role of ET-1 would be to assess concentrations of this vasoconstrictor in the cortices of sham and r-mTBI mice via immunoblot and ELISA analyses. An in vivo approach to further confirm the role of ET-1, if any, in dampening of the CVR response in the cortices of r-mTBI mice would be to replicate the cohort and paradigm and give two hypercapnic challenges separated by a treatment, analogous to the above proposed SNP, but to instead administer an intracerebral ventricular infusion of antisense ET-1 oligodeoxynucleotides before the second of the two consecutive hypercapnic challenges. A restoration of CVR to sham levels would indicate an involvement of aberrant ET-1 tone in the blunting of vascular responsiveness to hypercapnia.

The recent observations of CVR impairment as an easily detectable and early occurring *in vivo* physiological symptom, if not biomarker, of mild TBI have been recapitulated here in this report. However, it has also been reported that, although CVR deficit can be targeted and rescued in chronic TBI in human patients, this amelioration of vascular responsiveness is not accompanied by neurological improvement as assessed by standardized clinical tests[231], a result which begs the question whether resolution of CVR insult will be of any biological or clinical relevance if patients are treated acutely following head trauma. Moreover, as the interrogation of cerebral vasoreactivity in the human TBI population is a relatively new field of research, there has yet to be a post mortem confirmation of TCVI or CTE-like pathology in patients with a history of mild head trauma and concurrent aberrant CVR readings. The in vivo platform presented here offers the first opportunity to assess the therapeutic implications of CVR restoration acutely post-injury on chronic r-mTBI-related neuropathological and behavioral outcome in an animal model also displaying CTE-like symptoms. Although CVR is seen to improve with time following injury in our

animal model, as it is in some reports of sports related CVR impairment, even a transient inability of the cerebral vasculature to react to the metabolic demands of the brain could lead to cortical infarcts and ischemia, which are frequently reported across moderate to severe degrees of TBI in human patients[31,250-252], and indeed, in the cortices of the patients exhibiting rescued CVR upon treatment with the Phosphodiesterase 5 (PDE5) inhibitor, Sildenafil[143,231], one of the many FDA-approved and tolerable drugs believed to be protective against ischemic injury[253]. We have not thus far investigated ischemia in our animal models of r-mTBI, however, Bolton et al[254] have reported ischemic injury and neuronal degeneration in wild type mice at an acute time-point post-injury using our lab's original r-mTBI model[59], and so, it is conceivable that ischemia and concomitant neuronal injury may occur downstream of compromised CVR, contributing to the neurobehavioral deficits in learning and memory at 3 and 9 months post-injury in our chronic r-mTBI paradigm described here. A pertinent future experiment would thus be to have a longitudinal treatment of the r-sham and r-mTBI animals with Sildenafil, and vehicle, coupled with survival CVR analyses and Barnes Maze learning and memory assessment at both an acute and chronic time-point post-injury, and a detailed immunohistochemical assessment of diffuse ischemic brain injury. Such an experiment will give both a proof of concept confirmation that CVR can be rescued with therapeutic intervention and will also determine whether CVR normalization translates in to meaningful symptom resolution.

5.4. Concluding Remarks

It is clear from the recent literature pertaining to the frequency of occurrence of CVR perturbations across multiple mild and moderate TBI patient populations that measurement of cerebral vascular responsiveness may represent a more compelling and clinically feasible alternative biomarker to conventional less validated and post mortem analyses. The fact that CVR detriment appears transiently in asymptomatic contact sports athletes suffering repeat mTBIs, persisting in others experiencing a greater burden of TBI intensity and frequency, and chronic TBI-related cognitive disability, implicates this easily assessable and robust physiological biomarker as an endophenotype of underlying TCVI, and so, a candidate criterium for patient diagnosis and stratification in to cerebral vascular directed clinical trials.

A review of what is currently understood about the response of the cerebral vasculature to TBI, alongside parallel neuropathology and symptom onset, in both human patients and animal models thereof, suggests that there is an acute rarefaction of the cerebrovasculature following a critical load of TBI, and a chronic neovascularization or normalization, which perhaps represents a latent reparative mechanism to compensate for the infringed vasoreactivity and capacity of the cerebral vessels to supply adequate perfusion (Figure 5.1). The results from this thesis corroborate these insights from other studies and clinical observations, recapitulating the persistently compromised CVR seen in symptomatic human patients, in unison with chronic learning and memory impairment. The hypothesized TCVI progression (Figure 5.1) may allow for early therapeutic intervention with drugs such as Sildenafil, which can potentiate CVR, and facilitate adequate perfusion for prophylactic angiogenic and neuroprotective effect in

individuals identified by CVR assessment as being at risk for development of chronic TVBI-related illness.

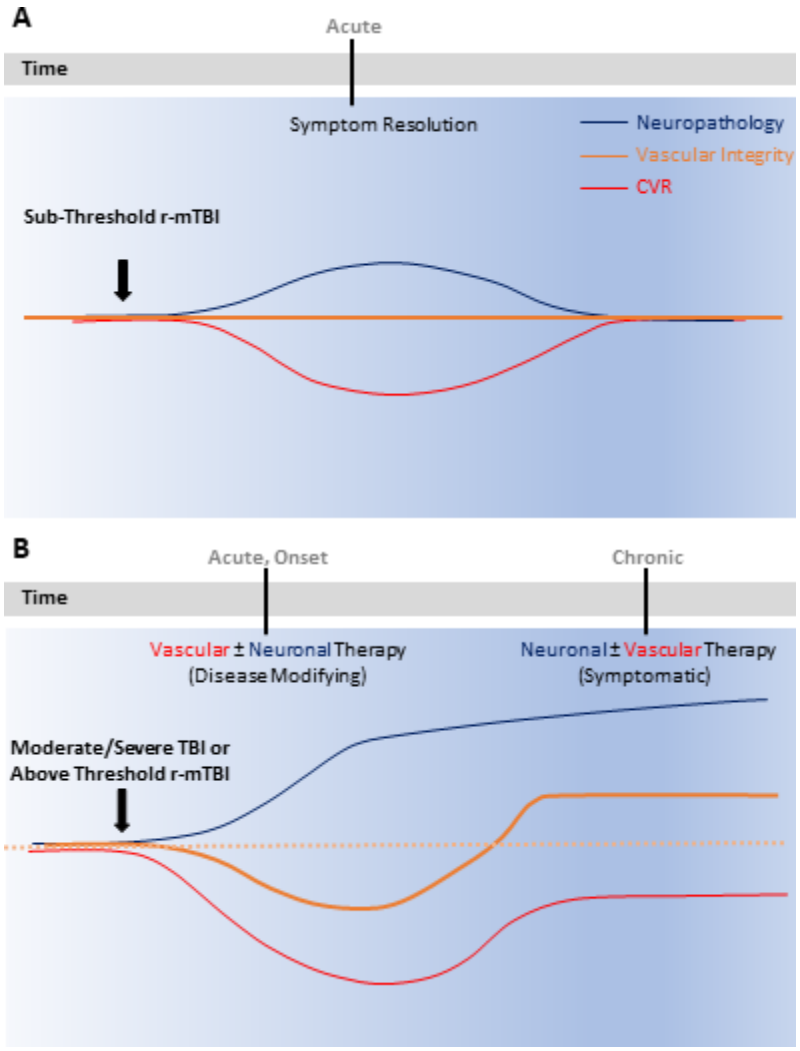

Figure 5.1. Cerebrovascular response to injury. Hypothesized timeline of the degree and direction of Traumatic Cerebral Vascular Injury (TCVI) and Cerebral Vascular Reactivity (CVR) alongside neurodegenerative and symptomatic sequelae following repetitive mild, or moderate-to-severe head trauma. Whereas cerebral vascular reactivity (CVR) deficit is observed in human patients following both a mild TBI with or without transient post-concussive symptoms (A), prolonged CVR impairment is observed at chronic time points post-injury in conjunction with chronic TBI-related neurocognitive and neurodegenerative illness (B), with all current preclinical animal model vascular interrogation indicating a parallel biphasic response of the cerebral vascular tissue density and vasoactive capacity to injury (B). Reports of an initial rarefaction in the vascular network, followed by a chronic neovascularization may indicate a latent recovery of the cerebral vessel network in response to TBI to compensate for diminished hyperemic response seen post-injury (B), and may represent a therapeutic window of vascular-directed prophylactic therapy before chronic neurodegenerative and neuroinflammatory pathologies fully manifest.

5.5. Acknowledgements

I would like to thank Dr Matilde Balbi, Centre for Biomedical Sciences, University of Vancouver, British Columbia, Canada, CA, for her assistance and insight in to development of the hypercapnic challenge technique. I would also like to thank Dr Andy Shih, University of Charleston, for his help in developing the skull thinning and cranial window technique used for the CVR analysis in mice. I would also like to express my gratitude to Ms Margaret Baldwin for her help in developing the skill set necessary for femoral artery catheter implantation and Arterial Blood Gas analyses.

This work was supported by the Office of the Assistant Secretary of Defense for Health Affairs, through the DoD Alzheimer's Research Program Convergence Science Research Award under Award No. W81XWH-15-PRARP-CSRA, and the National Institute on Aging of the National Institutes of Health under award number R01AG041971, and the Roskamp Foundation. The opinions, interpretations, conclusions and recommendations are not necessarily endorsed by the Department of Defense. The content does not necessarily represent the official views of the National Institutes of Health or the United States Government.

Chapter 6. Bibliography

1. Taylor CA, Bell JM, Breiding MJ, Xu L. Traumatic Brain Injury-Related Emergency Department Visits, Hospitalizations, and Deaths - United States, 2007 and 2013. MMWR Surveill Summ 2017;66(9):1-16.
2. Langlois JA, Rutland-Brown W, Wald MM. The epidemiology and impact of traumatic brain injury: a brief overview. J Head Trauma Rehabil 2006;21(5):375-8.
3. Langlois JA, Marr A, Mitchko J, Johnson RL. Tracking the silent epidemic and educating the public: CDC's traumatic brain injury-associated activities under the TBI Act of 1996 and the Children's Health Act of 2000. J Head Trauma Rehabil 2005;20(3):196-204.
4. McMahon P, Hricik A, Yue JK, Puccio AM, Inoue T, Lingsma HF, Beers SR, Gordon WA, Valadka AB, Manley GT and others. Symptomatology and functional outcome in mild traumatic brain injury: results from the prospective TRACK-TBI study. J Neurotrauma 2014;31(1):26-33.
5. Vanderploeg RD, Curtiss G, Luis CA, Salazar AM. Long-term morbidities following self-reported mild traumatic brain injury. J Clin Exp Neuropsychol 2007;29(6):585-98.
6. Alexander MP. Mild traumatic brain injury: pathophysiology, natural history, and clinical management. Neurology 1995;45(7):1253-60.
7. Cassidy JD, Carroll LJ, Peloso PM, Borg J, von Holst H, Holm L, Kraus J, Coronado VG, Injury WHOCCTFoMTB. Incidence, risk factors and prevention of mild traumatic brain injury: results of the WHO Collaborating Centre Task Force on Mild Traumatic Brain Injury. J Rehabil Med 2004(43 Suppl):28-60.
8. Ryu WH, Feinstein A, Colantonio A, Streiner DL, Dawson DR. Early identification and incidence of mild TBI in Ontario. Can J Neurol Sci 2009;36(4):429-35.
9. Kushner D. Mild traumatic brain injury: toward understanding manifestations and treatment. Arch Intern Med 1998;158(15):1617-24.
10. Zaloshnja E, Miller T, Langlois JA, Selassie AW. Prevalence of long-term disability from traumatic brain injury in the civilian population of the United States, 2005. J Head Trauma Rehabil 2008;23(6):394-400.
11. Greenwald BD, Ambrose AF, Armstrong GP. Mild brain injury. Rehabil Res Pract 2012;2012:469475.
12. Ruff RM, Iverson GL, Barth JT, Bush SS, Broshek DK, Policy NAN, Planning C. Recommendations for diagnosing a mild traumatic brain injury: a National Academy of Neuropsychology education paper. Arch Clin Neuropsychol 2009;24(1):3-10.
13. Carroll LJ, Cassidy JD, Holm L, Kraus J, Coronado VG, Injury WHOCCTFoMTB. Methodological issues and research recommendations for mild traumatic brain injury: the WHO Collaborating Centre Task Force on Mild Traumatic Brain Injury. J Rehabil Med 2004(43 Suppl):113-25.
14. Bailes JE, Petraglia AL, Omalu BI, Nauman E, Talavage T. Role of subconcussion in repetitive mild traumatic brain injury. J Neurosurg 2013;119(5):1235-45.
15. Mannix R, Iverson GL, Maxwell B, Atkins JE, Zafonte R, Berkner PD. Multiple prior concussions are associated with symptoms in high school athletes. Ann Clin Transl Neurol 2014;1(6):433-8.
16. Vynorius KC, Paquin AM, Seichepine DR. Lifetime Multiple Mild Traumatic Brain Injuries Are Associated with Cognitive and Mood Symptoms in Young Healthy College Students. Front Neurol 2016;7:188.
17. Lipton ML, Kim N, Zimmerman ME, Kim M, Stewart WF, Branch CA, Lipton RB. Soccer heading is associated with white matter microstructural and cognitive abnormalities. Radiology 2013;268(3):850-7.
18. Webbe FM, Ochs SR. Recency and frequency of soccer heading interact to decrease neurocognitive performance. Appl Neuropsychol 2003;10(1):31-41.

19. Witol AD, Webbe FM. Soccer heading frequency predicts neuropsychological deficits. Arch Clin Neuropsychol 2003;18(4):397-417.
20. Menon DK, Schwab K, Wright DW, Maas AI, Demographics, Clinical Assessment Working Group of the I, Interagency Initiative toward Common Data Elements for Research on Traumatic Brain I, Psychological H. Position statement: definition of traumatic brain injury. Arch Phys Med Rehabil 2010;91(11):1637-40.
21. Okie S. Traumatic brain injury in the war zone. N Engl J Med 2005;352(20):2043-7.
22. Warden D. Military TBI during the Iraq and Afghanistan wars. J Head Trauma Rehabil 2006;21(5):398-402.
23. Huang MX, Nichols S, Robb-Swan A, Angeles-Quinto A, Harrington DL, Drake A, Huang CW, Song T, Diwakar M, Risbrough VB and others. MEG Working Memory N-Back Task Reveals Functional Deficits in Combat-Related Mild Traumatic Brain Injury. Cereb Cortex 2018.
24. Mac Donald CL, Barber J, Jordan M, Johnson AM, Dikmen S, Fann JR, Temkin N. Early Clinical Predictors of 5-Year Outcome After Concussive Blast Traumatic Brain Injury. JAMA Neurol 2017;74(7):821-829.
25. MacDonald CL, Johnson AM, Nelson EC, Werner NJ, Fang R, Flaherty SF, Brody DL. Functional status after blast-plus-impact complex concussive traumatic brain injury in evacuated United States military personnel. J Neurotrauma 2014;31(10):889-98.
26. Narayan RK, Michel ME, Ansell B, Baethmann A, Biegon A, Bracken MB, Bullock MR, Choi SC, Clifton GL, Contant CF and others. Clinical trials in head injury. J Neurotrauma 2002;19(5):503-57.
27. Raghupathi R, McIntosh TK. Pharmacotherapy for traumatic brain injury: a review. Proc West Pharmacol Soc 1998;41:241-6.
28. Marklund N, Hillered L. Animal modelling of traumatic brain injury in preclinical drug development: where do we go from here? Br J Pharmacol 2011;164(4):1207-29.
29. Doppenberg EM, Bullock R. Clinical neuro-protection trials in severe traumatic brain injury: lessons from previous studies. J Neurotrauma 1997;14(2):71-80.
30. Millspaugh J, A. Dementia Pugilistica. US Naval Med. Bull. 1937;35,:261-297.
31. McKee AC, Daneshvar DH, Alvarez VE, Stein TD. The neuropathology of sport. Acta Neuropathol 2014;127(1):29-51.
32. Breen E, Steele G, Jr., Mercurio AM. Role of the E-cadherin/alpha-catenin complex in modulating cell-cell and cell-matrix adhesive properties of invasive colon carcinoma cells. Ann Surg Oncol 1995;2(5):378-85.
33. Trapp BD, Hauer PE. Amyloid precursor protein is enriched in radial glia: implications for neuronal development. J Neurosci Res 1994;37(4):538-50.
34. Aloisi F. Immune function of microglia. Glia 2001;36(2):165-79.
35. Bye N, Habgood MD, Callaway JK, Malakooti N, Potter A, Kossmann T, Morganti-Kossmann MC. Transient neuroprotection by minocycline following traumatic brain injury is associated with attenuated microglial activation but no changes in cell apoptosis or neutrophil infiltration. Exp Neurol 2007;204(1):220-33.
36. Czigner A, Mihaly A, Farkas O, Buki A, Krisztin-Peva B, Dobo E, Barzo P. Kinetics of the cellular immune response following closed head injury. Acta Neurochir (Wien) 2007;149(3):281-9.
37. Goldstein LE, Fisher AM, Tagge CA, Zhang XL, Velisek L, Sullivan JA, Upreti C, Kracht JM, Ericsson M, Wojnarowicz MW and others. Chronic traumatic encephalopathy in blast-exposed military veterans and a blast neurotrauma mouse model. Sci Transl Med 2012;4(134):134ra60.
38. Smith DH, Johnson VE, Stewart W. Chronic neuropathologies of single and repetitive TBI: substrates of dementia? Nat Rev Neurol 2013;9(4):211-21.

39. Omalu BI, DeKosky ST, Hamilton RL, Minster RL, Kamboh MI, Shakir AM, Wecht CH. Chronic traumatic encephalopathy in a national football league player: part II. Neurosurgery 2006;59(5):1086-92; discussion 1092-3.
40. Omalu BI, DeKosky ST, Minster RL, Kamboh MI, Hamilton RL, Wecht CH. Chronic traumatic encephalopathy in a National Football League player. Neurosurgery 2005;57(1):128-34; discussion 128-34.
41. McKee AC, Stern RA, Nowinski CJ, Stein TD, Alvarez VE, Daneshvar DH, Lee HS, Wojtowicz SM, Hall G, Baugh CM and others. The spectrum of disease in chronic traumatic encephalopathy. Brain 2013;136(Pt 1):43-64.
42. Gardner A, Iverson GL, McCrory P. Chronic traumatic encephalopathy in sport: a systematic review. Br J Sports Med 2014;48(2):84-90.
43. Hazrati LN, Tartaglia MC, Diamandis P, Davis KD, Green RE, Wennberg R, Wong JC, Ezerins L, Tator CH. Absence of chronic traumatic encephalopathy in retired football players with multiple concussions and neurological symptomatology. Front Hum Neurosci 2013;7:222.
44. Lowe VJ, Wiste HJ, Senjem ML, Weigand SD, Therneau TM, Boeve BF, Josephs KA, Fang P, Pandey MK, Murray ME and others. Widespread brain tau and its association with ageing, Braak stage and Alzheimer's dementia. Brain 2018;141(1):271-287.
45. Mez J, Daneshvar DH, Kiernan PT, Abdolmohammadi B, Alvarez VE, Huber BR, Alosco ML, Solomon TM, Nowinski CJ, McHale L and others. Clinicopathological Evaluation of Chronic Traumatic Encephalopathy in Players of American Football. JAMA 2017;318(4):360-370.
46. McKee AC, Cairns NJ, Dickson DW, Folkerth RD, Keene CD, Litvan I, Perl DP, Stein TD, Vonsattel JP, Stewart W and others. The first NINDS/NIBIB consensus meeting to define neuropathological criteria for the diagnosis of chronic traumatic encephalopathy. Acta Neuropathol 2016;131(1):75-86.
47. Viano DC, Hamberger A, Bolouri H, Saljo A. Concussion in professional football: animal model of brain injury--part 15. Neurosurgery 2009;64(6):1162-73; discussion 1173.
48. Hamberger A, Viano DC, Saljo A, Bolouri H. Concussion in professional football: morphology of brain injuries in the NFL concussion model--part 16. Neurosurgery 2009;64(6):1174-82; discussion 1182.
49. Angoa-Perez M, Kane MJ, Briggs DI, Herrera-Mundo N, Viano DC, Kuhn DM. Animal models of sports-related head injury: bridging the gap between pre-clinical research and clinical reality. J Neurochem 2014;129(6):916-31.
50. Kane MJ, Angoa-Perez M, Briggs DI, Viano DC, Kreipke CW, Kuhn DM. A mouse model of human repetitive mild traumatic brain injury. J Neurosci Methods 2012;203(1):41-9.
51. Mannix R, Meehan WP, Mandeville J, Grant PE, Gray T, Berglass J, Zhang J, Bryant J, Rezaie S, Chung JY and others. Clinical correlates in an experimental model of repetitive mild brain injury. Ann Neurol 2013;74(1):65-75.
52. Kondo A, Shahpasand K, Mannix R, Qiu J, Moncaster J, Chen CH, Yao Y, Lin YM, Driver JA, Sun Y and others. Antibody against early driver of neurodegeneration cis P-tau blocks brain injury and tauopathy. Nature 2015;523(7561):431-436.
53. Cheng JS, Craft R, Yu GQ, Ho K, Wang X, Mohan G, Mangnitsky S, Ponnusamy R, Mucke L. Tau reduction diminishes spatial learning and memory deficits after mild repetitive traumatic brain injury in mice. PLoS One 2014;9(12):e115765.
54. Kilbourne M, Kuehn R, Tosun C, Caridi J, Keledjian K, Bochicchio G, Scalea T, Gerzanich V, Simard JM. Novel model of frontal impact closed head injury in the rat. J Neurotrauma 2009;26(12):2233-43.

55. Ren Z, Iliff JJ, Yang L, Yang J, Chen X, Chen MJ, Giese RN, Wang B, Shi X, Nedergaard M. 'Hit & Run' model of closed-skull traumatic brain injury (TBI) reveals complex patterns of post-traumatic AQP4 dysregulation. J Cereb Blood Flow Metab 2013;33(6):834-45.
56. Huber BR, Meabon JS, Martin TJ, Mourad PD, Bennett R, Kraemer BC, Cernak I, Petrie EC, Emery MJ, Swenson ER and others. Blast exposure causes early and persistent aberrant phospho- and cleaved-tau expression in a murine model of mild blast-induced traumatic brain injury. J Alzheimers Dis 2013;37(2):309-23.
57. Huber BR, Meabon JS, Hoffer ZS, Zhang J, Hoekstra JG, Pagulayan KF, McMillan PJ, Mayer CL, Banks WA, Kraemer BC and others. Blast exposure causes dynamic microglial/macrophage responses and microdomains of brain microvessel dysfunction. Neuroscience 2016;319:206-20.
58. Meabon JS, Huber BR, Cross DJ, Richards TL, Minoshima S, Pagulayan KF, Li G, Meeker KD, Kraemer BC, Petrie EC and others. Repetitive blast exposure in mice and combat veterans causes persistent cerebellar dysfunction. Sci Transl Med 2016;8(321):321ra6.
59. Mouzon B, Chaytow H, Crynen G, Bachmeier C, Stewart J, Mullan M, Stewart W, Crawford F. Repetitive mild traumatic brain injury in a mouse model produces learning and memory deficits accompanied by histological changes. J Neurotrauma 2012;29(18):2761-73.
60. Mouzon BC, Bachmeier C, Ferro A, Ojo JO, Crynen G, Acker CM, Davies P, Mullan M, Stewart W, Crawford F. Chronic neuropathological and neurobehavioral changes in a repetitive mild traumatic brain injury model. Ann Neurol 2014;75(2):241-54.
61. Mouzon B, Bachmeier C, Ojo J, Acker C, Ferguson S, Crynen G, Davies P, Mullan M, Stewart W, Crawford F. Chronic White Matter Degeneration, But No Tau Pathology at One-Year Post-Repetitive Mild Traumatic Brain Injury in a Tau Transgenic Model. J Neurotrauma 2018.
62. Ojo JO, Mouzon B, Algamal M, Leary P, Lynch C, Abdullah L, Evans J, Mullan M, Bachmeier C, Stewart W and others. Chronic Repetitive Mild Traumatic Brain Injury Results in Reduced Cerebral Blood Flow, Axonal Injury, Gliosis, and Increased T-Tau and Tau Oligomers. J Neuropathol Exp Neurol 2016;75(7):636-55.
63. Petraglia AL, Plog BA, Dayawansa S, Dashnaw ML, Czerniecka K, Walker CT, Chen M, Hyrien O, Iliff JJ, Deane R and others. The pathophysiology underlying repetitive mild traumatic brain injury in a novel mouse model of chronic traumatic encephalopathy. Surg Neurol Int 2014;5:184.
64. Edwards G, 3rd, Moreno-Gonzalez I, Soto C. Amyloid-beta and tau pathology following repetitive mild traumatic brain injury. Biochem Biophys Res Commun 2017;483(4):1137-1142.
65. Risling M, Davidsson J. Experimental animal models for studies on the mechanisms of blast-induced neurotrauma. Front Neurol 2012;3:30.
66. Turner RC, Lucke-Wold BP, Logsdon AF, Robson MJ, Dashnaw ML, Huang JH, Smith KE, Huber JD, Rosen CL, Petraglia AL. The Quest to Model Chronic Traumatic Encephalopathy: A Multiple Model and Injury Paradigm Experience. Front Neurol 2015;6:222.
67. Tweedie D, Rachmany L, Rubovitch V, Zhang Y, Becker KG, Perez E, Hoffer BJ, Pick CG, Greig NH. Changes in mouse cognition and hippocampal gene expression observed in a mild physical- and blast-traumatic brain injury. Neurobiol Dis 2013;54:1-11.
68. Luo J, Nguyen A, Villeda S, Zhang H, Ding Z, Lindsey D, Bieri G, Castellano JM, Beaupre GS, Wyss-Coray T. Long-term cognitive impairments and pathological alterations in a mouse model of repetitive mild traumatic brain injury. Front Neurol 2014;5:12.
69. Ojo JO, Mouzon BC, Crawford F. Repetitive head trauma, chronic traumatic encephalopathy and tau: Challenges in translating from mice to men. Exp Neurol 2015.
70. Uryu K, Laurer H, McIntosh T, Pratico D, Martinez D, Leight S, Lee VM, Trojanowski JQ. Repetitive mild brain trauma accelerates Abeta deposition, lipid peroxidation, and cognitive impairment in a transgenic mouse model of Alzheimer amyloidosis. J Neurosci 2002;22(2):446-54.

71. Yoshiyama Y, Uryu K, Higuchi M, Longhi L, Hoover R, Fujimoto S, McIntosh T, Lee VM, Trojanowski JQ. Enhanced neurofibrillary tangle formation, cerebral atrophy, and cognitive deficits induced by repetitive mild brain injury in a transgenic tauopathy mouse model. J Neurotrauma 2005;22(10):1134-41.
72. Braak H, Zetterberg H, Del Tredici K, Blennow K. Intraneuronal tau aggregation precedes diffuse plaque deposition, but amyloid-beta changes occur before increases of tau in cerebrospinal fluid. Acta Neuropathol 2013;126(5):631-41.
73. Andorfer C, Acker CM, Kress Y, Hof PR, Duff K, Davies P. Cell-cycle reentry and cell death in transgenic mice expressing nonmutant human tau isoforms. J Neurosci 2005;25(22):5446-54.
74. Xie L, Kang H, Xu Q, Chen MJ, Liao Y, Thiyagarajan M, O'Donnell J, Christensen DJ, Nicholson C, Iliff JJ and others. Sleep drives metabolite clearance from the adult brain. Science 2013;342(6156):373-7.
75. Sullan MJ, Asken BM, Jaffee MS, DeKosky ST, Bauer RM. Glymphatic system disruption as a mediator of brain trauma and chronic traumatic encephalopathy. Neurosci Biobehav Rev 2018;84:316-324.
76. Iliff JJ, Chen MJ, Plog BA, Zeppenfeld DM, Soltero M, Yang L, Singh I, Deane R, Nedergaard M. Impairment of glymphatic pathway function promotes tau pathology after traumatic brain injury. J Neurosci 2014;34(49):16180-93.
77. Weller RO, Subash M, Preston SD, Mazanti I, Carare RO. Perivascular drainage of amyloid-beta peptides from the brain and its failure in cerebral amyloid angiopathy and Alzheimer's disease. Brain Pathol 2008;18(2):253-66.
78. Roman G, Pascual B. Contribution of neuroimaging to the diagnosis of Alzheimer's disease and vascular dementia. Arch Med Res 2012;43(8):671-6.
79. Masdeu JC, Kreisl WC, Berman KF. The neurobiology of Alzheimer disease defined by neuroimaging. Curr Opin Neurol 2012;25(4):410-20.
80. Kantarci K, Jack CR, Jr. Neuroimaging in Alzheimer disease: an evidence-based review. Neuroimaging Clin N Am 2003;13(2):197-209.
81. Wilson L, Stewart W, Dams-O'Connor K, Diaz-Arrastia R, Horton L, Menon DK, Polinder S. The chronic and evolving neurological consequences of traumatic brain injury. Lancet Neurol 2017;16(10):813-825.
82. Sidaros A, Engberg AW, Sidaros K, Liptrot MG, Herning M, Petersen P, Paulson OB, Jernigan TL, Rostrup E. Diffusion tensor imaging during recovery from severe traumatic brain injury and relation to clinical outcome: a longitudinal study. Brain 2008;131(Pt 2):559-72.
83. Newcombe VF, Correia MM, Ledig C, Abate MG, Outtrim JG, Chatfield D, Geeraerts T, Manktelow AE, Garyfallidis E, Pickard JD and others. Dynamic Changes in White Matter Abnormalities Correlate With Late Improvement and Deterioration Following TBI: A Diffusion Tensor Imaging Study. Neurorehabil Neural Repair 2016;30(1):49-62.
84. Haberg AK, Olsen A, Moen KG, Schirmer-Mikalsen K, Visser E, Finnanger TG, Evensen KA, Skandsen T, Vik A, Eikenes L. White matter microstructure in chronic moderate-to-severe traumatic brain injury: Impact of acute-phase injury-related variables and associations with outcome measures. J Neurosci Res 2015;93(7):1109-26.
85. Kraus MF, Susmaras T, Caughlin BP, Walker CJ, Sweeney JA, Little DM. White matter integrity and cognition in chronic traumatic brain injury: a diffusion tensor imaging study. Brain 2007;130(Pt 10):2508-19.
86. Hayes JP, Logue MW, Sadeh N, Spielberg JM, Verfaellie M, Hayes SM, Reagan A, Salat DH, Wolf EJ, McGlinchey RE and others. Mild traumatic brain injury is associated with reduced cortical thickness in those at risk for Alzheimer's disease. Brain 2017;140(3):813-825.

87. Quigley H, Colloby SJ, O'Brien JT. PET imaging of brain amyloid in dementia: a review. Int J Geriatr Psychiatry 2011;26(10):991-9.
88. Small GW, Kepe V, Ercoli LM, Siddarth P, Bookheimer SY, Miller KJ, Lavretsky H, Burggren AC, Cole GM, Vinters HV and others. PET of brain amyloid and tau in mild cognitive impairment. N Engl J Med 2006;355(25):2652-63.
89. Verhoeff NP, Wilson AA, Takeshita S, Trop L, Hussey D, Singh K, Kung HF, Kung MP, Houle S. In-vivo imaging of Alzheimer disease beta-amyloid with [11C]SB-13 PET. Am J Geriatr Psychiatry 2004;12(6):584-95.
90. Klunk WE, Engler H, Nordberg A, Bacskai BJ, Wang Y, Price JC, Bergstrom M, Hyman BT, Langstrom B, Mathis CA. Imaging the pathology of Alzheimer's disease: amyloid-imaging with positron emission tomography. Neuroimaging Clin N Am 2003;13(4):781-9, ix.
91. Klunk WE, Engler H, Nordberg A, Wang Y, Blomqvist G, Holt DP, Bergstrom M, Savitcheva I, Huang GF, Estrada S and others. Imaging brain amyloid in Alzheimer's disease with Pittsburgh Compound-B. Ann Neurol 2004;55(3):306-19.
92. Choi SR, Schneider JA, Bennett DA, Beach TG, Bedell BJ, Zehntner SP, Krautkramer MJ, Kung HF, Skovronsky DM, Hefti F and others. Correlation of amyloid PET ligand florbetapir F 18 binding with Abeta aggregation and neuritic plaque deposition in postmortem brain tissue. Alzheimer Dis Assoc Disord 2012;26(1):8-16.
93. Gardner RC, Yaffe K. Epidemiology of mild traumatic brain injury and neurodegenerative disease. Mol Cell Neurosci 2015;66(Pt B):75-80.
94. Wooten DW, Guehl NJ, Verwer EE, Shoup TM, Yokell DL, Zubcevik N, Vasdev N, Zafonte RD, Johnson KA, El Fakhri G and others. Pharmacokinetic Evaluation of the Tau PET Radiotracer (18)F-T807 ((18)F-AV-1451) in Human Subjects. J Nucl Med 2017;58(3):484-491.
95. Braak H, Braak E. Neuropathological stageing of Alzheimer-related changes. Acta Neuropathol 1991;82(4):239-59.
96. Dickstein DL, Pullman MY, Fernandez C, Short JA, Kostakoglu L, Knesaurek K, Soleimani L, Jordan BD, Gordon WA, Dams-O'Connor K and others. Cerebral [(18) F]T807/AV1451 retention pattern in clinically probable CTE resembles pathognomonic distribution of CTE tauopathy. Transl Psychiatry 2016;6(9):e900.
97. Mitsis EM, Riggio S, Kostakoglu L, Dickstein DL, Machac J, Delman B, Goldstein M, Jennings D, D'Antonio E, Martin J and others. Tauopathy PET and amyloid PET in the diagnosis of chronic traumatic encephalopathies: studies of a retired NFL player and of a man with FTD and a severe head injury. Transl Psychiatry 2014;4:e441.
98. Barrio JR, Small GW, Wong KP, Huang SC, Liu J, Merrill DA, Giza CC, Fitzsimmons RP, Omalu B, Bailes J and others. In vivo characterization of chronic traumatic encephalopathy using [F-18]FDDNP PET brain imaging. Proc Natl Acad Sci U S A 2015;112(16):E2039-47.
99. Gandy S, DeKosky ST. [18F]-T807 tauopathy PET imaging in chronic traumatic encephalopathy. F1000Res 2014;3:229.
100. Kenney K, Amyot F, Haber M, Pronger A, Bogoslovsky T, Moore C, Diaz-Arrastia R. Cerebral Vascular Injury in Traumatic Brain Injury. Exp Neurol 2015.
101. Besancon E, Guo S, Lok J, Tymianski M, Lo EH. Beyond NMDA and AMPA glutamate receptors: emerging mechanisms for ionic imbalance and cell death in stroke. Trends Pharmacol Sci 2008;29(5):268-75.
102. Golding EM. Sequelae following traumatic brain injury. The cerebrovascular perspective. Brain Res Brain Res Rev 2002;38(3):377-88.
103. Golding EM, Robertson CS, Bryan RM, Jr. The consequences of traumatic brain injury on cerebral blood flow and autoregulation: a review. Clin Exp Hypertens 1999;21(4):299-332.

104. Pappius HM, Dadoun R, McHugh M. The effect of p-chlorophenylalanine on cerebral metabolism and biogenic amine content of traumatized brain. J Cereb Blood Flow Metab 1988;8(3):324-34.
105. Tan CO, Meehan WP, 3rd, Iverson GL, Taylor JA. Cerebrovascular regulation, exercise, and mild traumatic brain injury. Neurology 2014;83(18):1665-72.
106. Hill RA, Tong L, Yuan P, Murikinati S, Gupta S, Grutzendler J. Regional Blood Flow in the Normal and Ischemic Brain Is Controlled by Arteriolar Smooth Muscle Cell Contractility and Not by Capillary Pericytes. Neuron 2015;87(1):95-110.
107. Lassen NA. Cerebral blood flow and oxygen consumption in man. Physiol Rev 1959;39(2):183-238.
108. Hall CN, Reynell C, Gesslein B, Hamilton NB, Mishra A, Sutherland BA, O'Farrell FM, Buchan AM, Lauritzen M, Attwell D. Capillary pericytes regulate cerebral blood flow in health and disease. Nature 2014;508(7494):55-60.
109. Peppiatt CM, Howarth C, Mobbs P, Attwell D. Bidirectional control of CNS capillary diameter by pericytes. Nature 2006;443(7112):700-4.
110. Mishra A, Reynolds JP, Chen Y, Gourine AV, Rusakov DA, Attwell D. Astrocytes mediate neurovascular signaling to capillary pericytes but not to arterioles. Nat Neurosci 2016;19(12):1619-1627.
111. Harraz OF, Longden TA, Dabertrand F, Hill-Eubanks D, Nelson MT. Endothelial GqPCR activity controls capillary electrical signaling and brain blood flow through PIP2 depletion. Proc Natl Acad Sci U S A 2018;115(15):E3569-E3577.
112. Longden TA, Dabertrand F, Koide M, Gonzales AL, Tykocki NR, Brayden JE, Hill-Eubanks D, Nelson MT. Capillary K(+)-sensing initiates retrograde hyperpolarization to increase local cerebral blood flow. Nat Neurosci 2017;20(5):717-726.
113. Grant RI, Hartmann DA, Underly RG, Berthiaume AA, Bhat NR, Shih AY. Organizational hierarchy and structural diversity of microvascular pericytes in adult mouse cortex. J Cereb Blood Flow Metab 2017:271678X17732229.
114. Lee J, Wu W, Boas DA. Early capillary flux homogenization in response to neural activation. J Cereb Blood Flow Metab 2016;36(2):375-80.
115. Uhlirova H, Kilic K, Tian P, Thunemann M, Desjardins M, Saisan PA, Sakadzic S, Ness TV, Mateo C, Cheng Q and others. Cell type specificity of neurovascular coupling in cerebral cortex. Elife 2016;5.
116. Hillman EM. Coupling mechanism and significance of the BOLD signal: a status report. Annu Rev Neurosci 2014;37:161-81.
117. Zehendner CM, Sebastiani A, Hugonnet A, Bischoff F, Luhmann HJ, Thal SC. Traumatic brain injury results in rapid pericyte loss followed by reactive pericytosis in the cerebral cortex. Sci Rep 2015;5:13497.
118. Chaigneau E, Oheim M, Audinat E, Charpak S. Two-photon imaging of capillary blood flow in olfactory bulb glomeruli. Proc Natl Acad Sci U S A 2003;100(22):13081-6.
119. Choi YK, Maki T, Mandeville ET, Koh SH, Hayakawa K, Arai K, Kim YM, Whalen MJ, Xing C, Wang X and others. Dual effects of carbon monoxide on pericytes and neurogenesis in traumatic brain injury. Nat Med 2016;22(11):1335-1341.
120. Dore-Duffy P, Owen C, Balabanov R, Murphy S, Beaumont T, Rafols JA. Pericyte migration from the vascular wall in response to traumatic brain injury. Microvasc Res 2000;60(1):55-69.
121. Dore-Duffy P, Wang S, Mehedi A, Katyshev V, Cleary K, Tapper A, Reynolds C, Ding Y, Zhan P, Rafols J and others. Pericyte-mediated vasoconstriction underlies TBI-induced hypoperfusion. Neurol Res 2011;33(2):176-86.
122. Kisler K, Nelson AR, Rege SV, Ramanathan A, Wang Y, Ahuja A, Lazic D, Tsai PS, Zhao Z, Zhou Y and others. Pericyte degeneration leads to neurovascular uncoupling and limits oxygen supply to brain. Nat Neurosci 2017;20(3):406-416.

123. Stanimirovic DB, Friedman A. Pathophysiology of the neurovascular unit: disease cause or consequence? J Cereb Blood Flow Metab 2012;32(7):1207-21.
124. Marchesi VT. Alzheimer's disease and CADASIL are heritable, adult-onset dementias that both involve damaged small blood vessels. Cell Mol Life Sci 2014;71(6):949-55.
125. Gardner RC, Burke JF, Nettiksimmons J, Goldman S, Tanner CM, Yaffe K. Traumatic brain injury in later life increases risk for Parkinson disease. Ann Neurol 2015;77(6):987-95.
126. Plassman BL, Havlik RJ, Steffens DC, Helms MJ, Newman TN, Drosdick D, Phillips C, Gau BA, Welsh-Bohmer KA, Burke JR and others. Documented head injury in early adulthood and risk of Alzheimer's disease and other dementias. Neurology 2000;55(8):1158-66.
127. Schofield PW, Logroscino G, Andrews HF, Albert S, Stern Y. An association between head circumference and Alzheimer's disease in a population-based study of aging and dementia. Neurology 1997;49(1):30-7.
128. Ruitenberg A, den Heijer T, Bakker SL, van Swieten JC, Koudstaal PJ, Hofman A, Breteler MM. Cerebral hypoperfusion and clinical onset of dementia: the Rotterdam Study. Ann Neurol 2005;57(6):789-94.
129. Snowdon DA, Greiner LH, Mortimer JA, Riley KP, Greiner PA, Markesbery WR. Brain infarction and the clinical expression of Alzheimer disease. The Nun Study. JAMA 1997;277(10):813-7.
130. Hirao K, Ohnishi T, Hirata Y, Yamashita F, Mori T, Moriguchi Y, Matsuda H, Nemoto K, Imabayashi E, Yamada M and others. The prediction of rapid conversion to Alzheimer's disease in mild cognitive impairment using regional cerebral blood flow SPECT. Neuroimage 2005;28(4):1014-21.
131. Hartmann DA, Underly RG, Grant RI, Watson AN, Lindner V, Shih AY. Pericyte structure and distribution in the cerebral cortex revealed by high-resolution imaging of transgenic mice. Neurophotonics 2015;2(4):041402.
132. Stein SC, Chen XH, Sinson GP, Smith DH. Intravascular coagulation: a major secondary insult in nonfatal traumatic brain injury. J Neurosurg 2002;97(6):1373-7.
133. Castejon OJ. Ultrastructural pathology of cortical capillary pericytes in human traumatic brain oedema. Folia Neuropathol 2011;49(3):162-73.
134. Castejon OJ. Ultrastructural alterations of human cortical capillary basement membrane in human brain oedema. Folia Neuropathol 2014;52(1):10-21.
135. Ostergaard L, Engedal TS, Aamand R, Mikkelsen R, Iversen NK, Anzabi M, Naess-Schmidt ET, Drasbek KR, Bay V, Blicher JU and others. Capillary transit time heterogeneity and flow-metabolism coupling after traumatic brain injury. J Cereb Blood Flow Metab 2014;34(10):1585-98.
136. Berger RP, Adelson PD, Pierce MC, Dulani T, Cassidy LD, Kochanek PM. Serum neuron-specific enolase, S100B, and myelin basic protein concentrations after inflicted and noninflicted traumatic brain injury in children. J Neurosurg 2005;103(1 Suppl):61-8.
137. Gill J, Latour L, Diaz-Arrastia R, Motamedi V, Turtzo C, Shahim P, Mondello S, DeVoto C, Veras E, Hanlon D and others. Glial fibrillary acidic protein elevations relate to neuroimaging abnormalities after mild TBI. Neurology 2018;91(15):e1385-e1389.
138. Slobounov SM, Walter A, Breiter HC, Zhu DC, Bai X, Bream T, Seidenberg P, Mao X, Johnson B, Talavage TM. The effect of repetitive subconcussive collisions on brain integrity in collegiate football players over a single football season: A multi-modal neuroimaging study. Neuroimage Clin 2017;14:708-718.
139. Ahn MJ, Sherwood ER, Prough DS, Lin CY, DeWitt DS. The effects of traumatic brain injury on cerebral blood flow and brain tissue nitric oxide levels and cytokine expression. J Neurotrauma 2004;21(10):1431-42.
140. Yezhuvath US, Lewis-Amezcua K, Varghese R, Xiao G, Lu H. On the assessment of cerebrovascular reactivity using hypercapnia BOLD MRI. NMR Biomed 2009;22(7):779-86.

141. Amen DG, Willeumier K, Omalu B, Newberg A, Raghavendra C, Raji CA. Perfusion Neuroimaging Abnormalities Alone Distinguish National Football League Players from a Healthy Population. J Alzheimers Dis 2016.
142. Amyot F, Kenney K, Moore C, Haber M, Turtzo LC, Shenouda C, Silverman E, Gong Y, Qu BX, Harburg L and others. Imaging of Cerebrovascular Function in Chronic Traumatic Brain Injury. J Neurotrauma 2018;35(10):1116-1123.
143. Haber M, Amyot F, Kenney K, Meredith-Duliba T, Moore C, Silverman E, Podell J, Chou YY, Pham DL, Butman J and others. Vascular Abnormalities within Normal Appearing Tissue in Chronic Traumatic Brain Injury. J Neurotrauma 2018;35(19):2250-2258.
144. Mutch WAC, Ellis MJ, Ryner LN, McDonald PJ, Morissette MP, Pries P, Essig M, Mikulis DJ, Duffin J, Fisher JA. Patient-Specific Alterations in CO2 Cerebrovascular Responsiveness in Acute and Sub-Acute Sports-Related Concussion. Front Neurol 2018;9:23.
145. Svaldi DO, Joshi C, McCuen EC, Music JP, Hannemann R, Leverenz LJ, Nauman EA, Talavage TM. Accumulation of high magnitude acceleration events predicts cerebrovascular reactivity changes in female high school soccer athletes. Brain Imaging Behav 2018.
146. Svaldi DO, McCuen EC, Joshi C, Robinson ME, Nho Y, Hannemann R, Nauman EA, Leverenz LJ, Talavage TM. Cerebrovascular reactivity changes in asymptomatic female athletes attributable to high school soccer participation. Brain Imaging Behav 2017;11(1):98-112.
147. Liem MK, Lesnik Oberstein SA, Haan J, Boom R, Ferrari MD, Buchem MA, Grond J. Cerebrovascular reactivity is a main determinant of white matter hyperintensity progression in CADASIL. AJNR Am J Neuroradiol 2009;30(6):1244-7.
148. Singhal S, Markus HS. Cerebrovascular reactivity and dynamic autoregulation in nondemented patients with CADASIL (cerebral autosomal dominant arteriopathy with subcortical infarcts and leukoencephalopathy). J Neurol 2005;252(2):163-7.
149. Fujiwara Y, Mizuno T, Okuyama C, Nagakane Y, Watanabe-Hosomi A, Kondo M, Kuriyama N, Tokuda T, Matsushima S, Nishimura T and others. Simultaneous impairment of intracranial and peripheral artery vasoreactivity in CADASIL patients. Cerebrovasc Dis 2012;33(2):128-34.
150. Cantin S, Villien M, Moreaud O, Tropres I, Keignart S, Chipon E, Le Bas JF, Warnking J, Krainik A. Impaired cerebral vasoreactivity to CO2 in Alzheimer's disease using BOLD fMRI. Neuroimage 2011;58(2):579-87.
151. Patel DR, Fidrocki D, Parachuri V. Sport-related concussions in adolescent athletes: a critical public health problem for which prevention remains an elusive goal. Transl Pediatr 2017;6(3):114-120.
152. Bieniek KF, Ross OA, Cormier KA, Walton RL, Soto-Ortolaza A, Johnston AE, DeSaro P, Boylan KB, Graff-Radford NR, Wszolek ZK and others. Chronic traumatic encephalopathy pathology in a neurodegenerative disorders brain bank. Acta Neuropathol 2015;130(6):877-89.
153. Tagge CA, Fisher AM, Minaeva OV, Gaudreau-Balderrama A, Moncaster JA, Zhang XL, Wojnarowicz MW, Casey N, Lu H, Kokiko-Cochran ON and others. Concussion, microvascular injury, and early tauopathy in young athletes after impact head injury and an impact concussion mouse model. Brain 2018;141(2):422-458.
154. https://clinicaltrials.gov/ct2/show/NCT01767311. A Placebo-controlled, Double-blind, Parallel-group, Bayesian Adaptive Randomization Design and Dose Regimen-finding Study to Evaluate Safety, Tolerability and Efficacy of BAN2401 in Subjects With Early Alzheimer's Disease. 2018.
155. Lynch CE, Crynen G, Ferguson S, Mouzon B, Paris D, Ojo J, Leary P, Crawford F, Bachmeier C. Chronic cerebrovascular abnormalities in a mouse model of repetitive mild traumatic brain injury. Brain Inj 2016;30(12):1414-1427.
156. Buckley EM, Miller BF, Golinski JM, Sadeghian H, McAllister LM, Vangel M, Ayata C, Meehan WP, 3rd, Franceschini MA, Whalen MJ. Decreased microvascular cerebral blood flow assessed by

diffuse correlation spectroscopy after repetitive concussions in mice. J Cereb Blood Flow Metab 2015;35(12):1995-2000.
157. Nomikos GG, Spyraki C. Influence of oestrogen on spontaneous and diazepam-induced exploration of rats in an elevated plus maze. Neuropharmacology 1988;27(7):691-6.
158. Algamal M, Ojo JO, Lungmus CP, Muza P, Cammarata C, Owens MJ, Mouzon BC, Diamond DM, Mullan M, Crawford F. Chronic Hippocampal Abnormalities and Blunted HPA Axis in an Animal Model of Repeated Unpredictable Stress. Front Behav Neurosci 2018;12:150.
159. Paris D, Quadros A, Humphrey J, Patel N, Crescentini R, Crawford F, Mullan M. Nilvadipine antagonizes both Abeta vasoactivity in isolated arteries, and the reduced cerebral blood flow in APPsw transgenic mice. Brain Res 2004;999(1):53-61.
160. Johnson VE, Stewart JE, Begbie FD, Trojanowski JQ, Smith DH, Stewart W. Inflammation and white matter degeneration persist for years after a single traumatic brain injury. Brain 2013;136(Pt 1):28-42.
161. Ramlackhansingh AF, Brooks DJ, Greenwood RJ, Bose SK, Turkheimer FE, Kinnunen KM, Gentleman S, Heckemann RA, Gunanayagam K, Gelosa G and others. Inflammation after trauma: microglial activation and traumatic brain injury. Ann Neurol 2011;70(3):374-83.
162. Hsu ET, Gangolli M, Su S, Holleran L, Stein TD, Alvarez VE, McKee AC, Schmidt RE, Brody DL. Astrocytic degeneration in chronic traumatic encephalopathy. Acta Neuropathol 2018.
163. Mouzon BC, Bachmeier C, Ojo JO, Acker CM, Ferguson S, Paris D, Ait-Ghezala G, Crynen G, Davies P, Mullan M and others. Lifelong behavioral and neuropathological consequences of repetitive mild traumatic brain injury. Ann Clin Transl Neurol 2018;5(1):64-80.
164. Livingston WS, Gill JM, Cota MR, Olivera A, O'Keefe JL, Martin C, Latour LL. Differential Gene Expression Associated with Meningeal Injury in Acute Mild Traumatic Brain Injury. J Neurotrauma 2017;34(4):853-860.
165. Russo MV, Latour LL, McGavern DB. Distinct myeloid cell subsets promote meningeal remodeling and vascular repair after mild traumatic brain injury. Nat Immunol 2018;19(5):442-452.
166. Roth TL, Nayak D, Atanasijevic T, Koretsky AP, Latour LL, McGavern DB. Transcranial amelioration of inflammation and cell death after brain injury. Nature 2014;505(7482):223-8.
167. Werner C, Engelhard K. Pathophysiology of traumatic brain injury. Br J Anaesth 2007;99(1):4-9.
168. Searcy JL, Le Bihan T, Salvadores N, McCulloch J, Horsburgh K. Impact of age on the cerebrovascular proteomes of wild-type and Tg-SwDI mice. PLoS One 2014;9(2):e89970.
169. Xiong Y, Mahmood A, Chopp M. Angiogenesis, neurogenesis and brain recovery of function following injury. Curr Opin Investig Drugs 2010;11(3):298-308.
170. Prakash R, Carmichael ST. Blood-brain barrier breakdown and neovascularization processes after stroke and traumatic brain injury. Curr Opin Neurol 2015;28(6):556-64.
171. Hayward NM, Tuunanen PI, Immonen R, Ndode-Ekane XE, Pitkanen A, Grohn O. Magnetic resonance imaging of regional hemodynamic and cerebrovascular recovery after lateral fluid-percussion brain injury in rats. J Cereb Blood Flow Metab 2011;31(1):166-77.
172. Bell RD, Winkler EA, Sagare AP, Singh I, LaRue B, Deane R, Zlokovic BV. Pericytes control key neurovascular functions and neuronal phenotype in the adult brain and during brain aging. Neuron 2010;68(3):409-27.
173. Fernandez-Klett F, Offenhauser N, Dirnagl U, Priller J, Lindauer U. Pericytes in capillaries are contractile in vivo, but arterioles mediate functional hyperemia in the mouse brain. Proc Natl Acad Sci U S A 2010;107(51):22290-5.
174. Kornfield TE, Newman EA. Regulation of blood flow in the retinal trilaminar vascular network. J Neurosci 2014;34(34):11504-13.
175. O'Farrell FM, Attwell D. A role for pericytes in coronary no-reflow. Nat Rev Cardiol 2014;11(7):427-32.

176. Yemisci M, Gursoy-Ozdemir Y, Vural A, Can A, Topalkara K, Dalkara T. Pericyte contraction induced by oxidative-nitrative stress impairs capillary reflow despite successful opening of an occluded cerebral artery. Nat Med 2009;15(9):1031-7.
177. Yamin R, Morgan KG. Deciphering actin cytoskeletal function in the contractile vascular smooth muscle cell. J Physiol 2012;590(17):4145-54.
178. Chow N, Bell RD, Deane R, Streb JW, Chen J, Brooks A, Van Nostrand W, Miano JM, Zlokovic BV. Serum response factor and myocardin mediate arterial hypercontractility and cerebral blood flow dysregulation in Alzheimer's phenotype. Proc Natl Acad Sci U S A 2007;104(3):823-8.
179. Merlini M, Wanner D, Nitsch RM. Tau pathology-dependent remodelling of cerebral arteries precedes Alzheimer's disease-related microvascular cerebral amyloid angiopathy. Acta Neuropathol 2016;131(5):737-52.
180. Armstead WM, Bohman LE, Riley J, Yarovoi S, Higazi AA, Cines DB. tPA-S(481)A prevents impairment of cerebrovascular autoregulation by endogenous tPA after traumatic brain injury by upregulating p38 MAPK and inhibiting ET-1. J Neurotrauma 2013;30(22):1898-907.
181. Petrov T. Amelioration of hypoperfusion after traumatic brain injury by in vivo endothelin-1 knockout. Can J Physiol Pharmacol 2009;87(5):379-86.
182. Salonia R, Empey PE, Poloyac SM, Wisniewski SR, Klamerus M, Ozawa H, Wagner AK, Ruppel R, Bell MJ, Feldman K and others. Endothelin-1 is increased in cerebrospinal fluid and associated with unfavorable outcomes in children after severe traumatic brain injury. J Neurotrauma 2010;27(10):1819-25.
183. DeGracia DJ, Kreipke CW, Kayali FM, Rafols JA. Brain endothelial HSP-70 stress response coincides with endothelial and pericyte death after brain trauma. Neurol Res 2007;29(4):356-61.
184. Torres-Platas SG, Comeau S, Rachalski A, Bo GD, Cruceanu C, Turecki G, Giros B, Mechawar N. Morphometric characterization of microglial phenotypes in human cerebral cortex. J Neuroinflammation 2014;11:12.
185. Oppenheimer DR. Microscopic lesions in the brain following head injury. J Neurol Neurosurg Psychiatry 1968;31(4):299-306.
186. Rodriguez-Baeza A, Reina-de la Torre F, Poca A, Marti M, Garnacho A. Morphological features in human cortical brain microvessels after head injury: a three-dimensional and immunocytochemical study. Anat Rec A Discov Mol Cell Evol Biol 2003;273(1):583-93.
187. Stein SC, Graham DI, Chen XH, Smith DH. Association between intravascular microthrombosis and cerebral ischemia in traumatic brain injury. Neurosurgery 2004;54(3):687-91; discussion 691.
188. Tomlinson BE. Brain-stem lesions after head injury. J Clin Pathol Suppl (R Coll Pathol) 1970;4:154-65.
189. Danaila L, Popescu I, Pais V, Riga D, Riga S, Pais E. Apoptosis, paraptosis, necrosis, and cell regeneration in posttraumatic cerebral arteries. Chirurgia (Bucur) 2013;108(3):319-24.
190. Alosco ML, Kasimis AB, Stamm JM, Chua AS, Baugh CM, Daneshvar DH, Robbins CA, Mariani M, Hayden J, Conneely S and others. Age of first exposure to American football and long-term neuropsychiatric and cognitive outcomes. Transl Psychiatry 2017;7(9):e1236.
191. Mouzon B, Saltiel N, Ferguson S, Ojo J, Lungmus C, Lynch C, Algamal M, Morin A, Carper B, Bieler G and others. Impact of age on acute post-TBI neuropathology in mice expressing humanized tau: a Chronic Effects of Neurotrauma Consortium Study. Brain Inj 2018;32(10):1285-1294.
192. Bachmeier C, Shackleton B, Ojo J, Paris D, Mullan M, Crawford F. Apolipoprotein E isoform-specific effects on lipoprotein receptor processing. Neuromolecular Med 2014;16(4):686-96.
193. Gama Sosa MA, De Gasperi R, Perez Garcia GS, Sosa H, Searcy C, Vargas D, Janssen PL, Perez GM, Tschiffely AE, Janssen WG and others. Lack of chronic neuroinflammation in the absence of focal hemorrhage in a rat model of low-energy blast-induced TBI. Acta Neuropathol Commun 2017;5(1):80.

194. Salehi A, Zhang JH, Obenaus A. Response of the cerebral vasculature following traumatic brain injury. J Cereb Blood Flow Metab 2017;37(7):2320-2339.
195. Wendel KM, Lee JB, Affeldt BM, Hamer M, Harahap-Carrillo IS, Pardo AC, Obenaus A. Corpus Callosum Vasculature Predicts White Matter Microstructure Abnormalities after Pediatric Mild Traumatic Brain Injury. J Neurotrauma 2018.
196. Morgan R, Kreipke CW, Roberts G, Bagchi M, Rafols JA. Neovascularization following traumatic brain injury: possible evidence for both angiogenesis and vasculogenesis. Neurol Res 2007;29(4):375-81.
197. Hayward NM, Yanev P, Haapasalo A, Miettinen R, Hiltunen M, Grohn O, Jolkkonen J. Chronic hyperperfusion and angiogenesis follow subacute hypoperfusion in the thalamus of rats with focal cerebral ischemia. J Cereb Blood Flow Metab 2011;31(4):1119-32.
198. Kisler K, Nelson AR, Montagne A, Zlokovic BV. Cerebral blood flow regulation and neurovascular dysfunction in Alzheimer disease. Nat Rev Neurosci 2017;18(7):419-434.
199. Nikolakopoulou AM, Zhao Z, Montagne A, Zlokovic BV. Regional early and progressive loss of brain pericytes but not vascular smooth muscle cells in adult mice with disrupted platelet-derived growth factor receptor-beta signaling. PLoS One 2017;12(4):e0176225.
200. Sagare AP, Bell RD, Zhao Z, Ma Q, Winkler EA, Ramanathan A, Zlokovic BV. Pericyte loss influences Alzheimer-like neurodegeneration in mice. Nat Commun 2013;4:2932.
201. Sessa WC. Molecular control of blood flow and angiogenesis: role of nitric oxide. J Thromb Haemost 2009;7 Suppl 1:35-7.
202. Ding G, Jiang Q, Li L, Zhang L, Zhang ZG, Ledbetter KA, Panda S, Davarani SP, Athiraman H, Li Q and others. Magnetic resonance imaging investigation of axonal remodeling and angiogenesis after embolic stroke in sildenafil-treated rats. J Cereb Blood Flow Metab 2008;28(8):1440-8.
203. Pifarre P, Prado J, Giralt M, Molinero A, Hidalgo J, Garcia A. Cyclic GMP phosphodiesterase inhibition alters the glial inflammatory response, reduces oxidative stress and cell death and increases angiogenesis following focal brain injury. J Neurochem 2010;112(3):807-17.
204. Zhang R, Wang Y, Zhang L, Zhang Z, Tsang W, Lu M, Zhang L, Chopp M. Sildenafil (Viagra) induces neurogenesis and promotes functional recovery after stroke in rats. Stroke 2002;33(11):2675-80.
205. Fernandez-Klett F, Potas JR, Hilpert D, Blazej K, Radke J, Huck J, Engel O, Stenzel W, Genove G, Priller J. Early loss of pericytes and perivascular stromal cell-induced scar formation after stroke. J Cereb Blood Flow Metab 2013;33(3):428-39.
206. Wang B, Sun L, Tian Y, Li Z, Wei H, Wang D, Yang Z, Chen J, Zhang J, Jiang R. Effects of atorvastatin in the regulation of circulating EPCs and angiogenesis in traumatic brain injury in rats. J Neurol Sci 2012;319(1-2):117-23.
207. Abbott NJ, Patabendige AA, Dolman DE, Yusof SR, Begley DJ. Structure and function of the blood-brain barrier. Neurobiol Dis 2010;37(1):13-25.
208. Obermeier B, Daneman R, Ransohoff RM. Development, maintenance and disruption of the blood-brain barrier. Nat Med 2013;19(12):1584-96.
209. Abdul-Muneer PM, Schuetz H, Wang F, Skotak M, Jones J, Gorantla S, Zimmerman MC, Chandra N, Haorah J. Induction of oxidative and nitrosative damage leads to cerebrovascular inflammation in an animal model of mild traumatic brain injury induced by primary blast. Free Radic Biol Med 2013;60:282-91.
210. Huang XT, Zhang YQ, Li SJ, Li SH, Tang Q, Wang ZT, Dong JF, Zhang JN. Intracerebroventricular transplantation of ex vivo expanded endothelial colony-forming cells restores blood-brain barrier integrity and promotes angiogenesis of mice with traumatic brain injury. J Neurotrauma 2013;30(24):2080-8.
211. Wang T, Meng Y, Zou DH, Li ZD, Chen YJ, Tao LY. [Expression of Zonula Occludens-1 in Cerebral Cortex Following Traumatic Brain Injury]. Fa Yi Xue Za Zhi 2015;31(2):85-7, 92.

212. Xu ZM, Yuan F, Liu YL, Ding J, Tian HL. Glibenclamide Attenuates Blood-Brain Barrier Disruption in Adult Mice after Traumatic Brain Injury. J Neurotrauma 2017;34(4):925-933.
213. Ponto LL, Brashers-Krug TM, Pierson RK, Menda Y, Acion L, Watkins GL, Sunderland JJ, Koeppel JA, Jorge RE. Preliminary Investigation of Cerebral Blood Flow and Amyloid Burden in Veterans With and Without Combat-Related Traumatic Brain Injury. J Neuropsychiatry Clin Neurosci 2015:appineuropsych15050106.
214. Peskind ER, Petrie EC, Cross DJ, Pagulayan K, McCraw K, Hoff D, Hart K, Yu CE, Raskind MA, Cook DG and others. Cerebrocerebellar hypometabolism associated with repetitive blast exposure mild traumatic brain injury in 12 Iraq war Veterans with persistent post-concussive symptoms. Neuroimage 2011;54 Suppl 1:S76-82.
215. Kilianski J, Peeters S, Debad J, Mohmed J, Wolf SE, Minei JP, Diaz-Arrastia R, Gatson JW. Plasma creatine kinase B correlates with injury severity and symptoms in professional boxers. J Clin Neurosci 2017;45:100-104.
216. Len TK, Neary JP, Asmundson GJ, Goodman DG, Bjornson B, Bhambhani YN. Cerebrovascular reactivity impairment after sport-induced concussion. Med Sci Sports Exerc 2011;43(12):2241-8.
217. Mutch WA, Ellis MJ, Ryner LN, Graham MR, Dufault B, Gregson B, Hall T, Bunge M, Essig M, Fisher JA and others. Brain magnetic resonance imaging CO2 stress testing in adolescent postconcussion syndrome. J Neurosurg 2016;125(3):648-60.
218. Youmans KL, Tai LM, Nwabuisi-Heath E, Jungbauer L, Kanekiyo T, Gan M, Kim J, Eimer WA, Estus S, Rebeck GW and others. APOE4-specific changes in Abeta accumulation in a new transgenic mouse model of Alzheimer disease. J Biol Chem 2012;287(50):41774-86.
219. Oakley H, Cole SL, Logan S, Maus E, Shao P, Craft J, Guillozet-Bongaarts A, Ohno M, Disterhoft J, Van Eldik L and others. Intraneuronal beta-amyloid aggregates, neurodegeneration, and neuron loss in transgenic mice with five familial Alzheimer's disease mutations: potential factors in amyloid plaque formation. J Neurosci 2006;26(40):10129-40.
220. Giannoni P, Arango-Lievano M, Neves ID, Rousset MC, Baranger K, Rivera S, Jeanneteau F, Claeysen S, Marchi N. Cerebrovascular pathology during the progression of experimental Alzheimer's disease. Neurobiol Dis 2016;88:107-17.
221. Sullivan PM, Mezdour H, Aratani Y, Knouff C, Najib J, Reddick RL, Quarfordt SH, Maeda N. Targeted replacement of the mouse apolipoprotein E gene with the common human APOE3 allele enhances diet-induced hypercholesterolemia and atherosclerosis. J Biol Chem 1997;272(29):17972-80.
222. Shih AY, Mateo C, Drew PJ, Tsai PS, Kleinfeld D. A polished and reinforced thinned-skull window for long-term imaging of the mouse brain. J Vis Exp 2012(61).
223. Yezhuvath US, Uh J, Cheng Y, Martin-Cook K, Weiner M, Diaz-Arrastia R, van Osch M, Lu H. Forebrain-dominant deficit in cerebrovascular reactivity in Alzheimer's disease. Neurobiol Aging 2012;33(1):75-82.
224. Glodzik L, Randall C, Rusinek H, de Leon MJ. Cerebrovascular reactivity to carbon dioxide in Alzheimer's disease. J Alzheimers Dis 2013;35(3):427-40.
225. Gao YZ, Zhang JJ, Liu H, Wu GY, Xiong L, Shu M. Regional cerebral blood flow and cerebrovascular reactivity in Alzheimer's disease and vascular dementia assessed by arterial spinlabeling magnetic resonance imaging. Curr Neurovasc Res 2013;10(1):49-53.
226. Viticchi G, Falsetti L, Buratti L, Luzzi S, Bartolini M, Acciarri MC, Provinciali L, Silvestrini M. Metabolic syndrome and cerebrovascular impairment in Alzheimer's disease. Int J Geriatr Psychiatry 2015;30(12):1164-70.
227. Park L, Koizumi K, El Jamal S, Zhou P, Previti ML, Van Nostrand WE, Carlson G, Iadecola C. Age-dependent neurovascular dysfunction and damage in a mouse model of cerebral amyloid angiopathy. Stroke 2014;45(6):1815-21.

228. Tong XK, Lecrux C, Rosa-Neto P, Hamel E. Age-dependent rescue by simvastatin of Alzheimer's disease cerebrovascular and memory deficits. J Neurosci 2012;32(14):4705-15.
229. Shin HK, Jones PB, Garcia-Alloza M, Borrelli L, Greenberg SM, Bacskai BJ, Frosch MP, Hyman BT, Moskowitz MA, Ayata C. Age-dependent cerebrovascular dysfunction in a transgenic mouse model of cerebral amyloid angiopathy. Brain 2007;130(Pt 9):2310-9.
230. Saito S, Yamamoto Y, Maki T, Hattori Y, Ito H, Mizuno K, Harada-Shiba M, Kalaria RN, Fukushima M, Takahashi R and others. Taxifolin inhibits amyloid-beta oligomer formation and fully restores vascular integrity and memory in cerebral amyloid angiopathy. Acta Neuropathol Commun 2017;5(1):26.
231. Kenney K, Amyot F, Moore C, Haber M, Turtzo LC, Shenouda C, Silverman E, Gong Y, Qu BX, Harburg L and others. Phosphodiesterase-5 inhibition potentiates cerebrovascular reactivity in chronic traumatic brain injury. Ann Clin Transl Neurol 2018;5(4):418-428.
232. Rostami E, Engquist H, Enblad P. Imaging of cerebral blood flow in patients with severe traumatic brain injury in the neurointensive care. Front Neurol 2014;5:114.
233. Pfefferkorn T, von Stuckrad-Barre S, Herzog J, Gasser T, Hamann GF, Dichgans M. Reduced cerebrovascular CO(2) reactivity in CADASIL: A transcranial Doppler sonography study. Stroke 2001;32(1):17-21.
234. Leddy JJ, Baker JG, Kozlowski K, Bisson L, Willer B. Reliability of a graded exercise test for assessing recovery from concussion. Clin J Sport Med 2011;21(2):89-94.
235. Bailey DM, Jones DW, Sinnott A, Brugniaux JV, New KJ, Hodson D, Marley CJ, Smirl JD, Ogoh S, Ainslie PN. Impaired cerebral haemodynamic function associated with chronic traumatic brain injury in professional boxers. Clin Sci (Lond) 2013;124(3):177-89.
236. Han BH, Zhou ML, Abousaleh F, Brendza RP, Dietrich HH, Koenigsknecht-Talboo J, Cirrito JR, Milner E, Holtzman DM, Zipfel GJ. Cerebrovascular dysfunction in amyloid precursor protein transgenic mice: contribution of soluble and insoluble amyloid-beta peptide, partial restoration via gamma-secretase inhibition. J Neurosci 2008;28(50):13542-50.
237. Papadopoulos P, Rosa-Neto P, Rochford J, Hamel E. Pioglitazone improves reversal learning and exerts mixed cerebrovascular effects in a mouse model of Alzheimer's disease with combined amyloid-beta and cerebrovascular pathology. PLoS One 2013;8(7):e68612.
238. Mutch WA, Ellis MJ, Ryner LN, Morissette MP, Pries PJ, Dufault B, Essig M, Mikulis DJ, Duffin J, Fisher JA. Longitudinal Brain Magnetic Resonance Imaging CO2 Stress Testing in Individual Adolescent Sports-Related Concussion Patients: A Pilot Study. Front Neurol 2016;7:107.
239. Adams C, Bazzigaluppi P, Beckett TL, Bishay J, Weisspapir I, Dorr A, Mester JR, Steinman J, Hirschler L, Warnking JM and others. Neurogliovascular dysfunction in a model of repeated traumatic brain injury. Theranostics 2018;8(17):4824-4836.
240. Soustiel JF, Glenn TC, Shik V, Boscardin J, Mahamid E, Zaaroor M. Monitoring of cerebral blood flow and metabolism in traumatic brain injury. J Neurotrauma 2005;22(9):955-65.
241. Inoue Y, Shiozaki T, Tasaki O, Hayakata T, Ikegawa H, Yoshiya K, Fujinaka T, Tanaka H, Shimazu T, Sugimoto H. Changes in cerebral blood flow from the acute to the chronic phase of severe head injury. J Neurotrauma 2005;22(12):1411-8.
242. Wei EP, Hamm RJ, Baranova AI, Povlishock JT. The long-term microvascular and behavioral consequences of experimental traumatic brain injury after hypothermic intervention. J Neurotrauma 2009;26(4):527-37.
243. Jha RM, Molyneaux BJ, Jackson TC, Wallisch JS, Park SY, Poloyac S, Vagni VA, Janesko-Feldman KL, Hoshitsuki K, Minnigh MB and others. Glibenclamide Produces Region-Dependent Effects on Cerebral Edema in a Combined Injury Model of Traumatic Brain Injury and Hemorrhagic Shock in Mice. J Neurotrauma 2018;35(17):2125-2135.

244. Xu X, Gao W, Cheng S, Yin D, Li F, Wu Y, Sun D, Zhou S, Wang D, Zhang Y and others. Anti-inflammatory and immunomodulatory mechanisms of atorvastatin in a murine model of traumatic brain injury. J Neuroinflammation 2017;14(1):167.
245. Tong XK, Hamel E. Simvastatin restored vascular reactivity, endothelial function and reduced string vessel pathology in a mouse model of cerebrovascular disease. J Cereb Blood Flow Metab 2015;35(3):512-20.
246. Howarth C, Sutherland B, Choi HB, Martin C, Lind BL, Khennouf L, LeDue JM, Pakan JM, Ko RW, Ellis-Davies G and others. A Critical Role for Astrocytes in Hypercapnic Vasodilation in Brain. J Neurosci 2017;37(9):2403-2414.
247. Miekisiak G, Yoo K, Sandler AL, Kulik TB, Chen JF, Winn HR. The role of adenosine in hypercarbic hyperemia: in vivo and in vitro studies in adenosine 2(A) receptor knockout and wild-type mice. J Neurosurg 2009;110(5):981-8.
248. Shanmuganathan MV, Krishnan S, Fu X, Prasadarao NV. Attenuation of biopterin synthesis prevents Escherichia coli K1 invasion of brain endothelial cells and the development of meningitis in newborn mice. J Infect Dis 2013;207(1):61-71.
249. Zhao Y, Vanhoutte PM, Leung SW. Vascular nitric oxide: Beyond eNOS. J Pharmacol Sci 2015;129(2):83-94.
250. Veenith TV, Carter EL, Geeraerts T, Grossac J, Newcombe VF, Outtrim J, Gee GS, Lupson V, Smith R, Aigbirhio FI and others. Pathophysiologic Mechanisms of Cerebral Ischemia and Diffusion Hypoxia in Traumatic Brain Injury. JAMA Neurol 2016;73(5):542-50.
251. Vespa PM. Brain Hypoxia and Ischemia After Traumatic Brain Injury: Is Oxygen the Right Metabolic Target? JAMA Neurol 2016;73(5):504-5.
252. Fehily B, Fitzgerald M. Repeated Mild Traumatic Brain Injury: Potential Mechanisms of Damage. Cell Transplant 2017;26(7):1131-1155.
253. Sallustio F, Diomedi M, Centonze D, Stanzione P. Saving the ischemic penumbra: potential role for statins and phosphodiesterase inhibitors. Curr Vasc Pharmacol 2007;5(4):259-65.
254. Bolton AN, Saatman KE. Regional neurodegeneration and gliosis are amplified by mild traumatic brain injury repeated at 24-hour intervals. J Neuropathol Exp Neurol 2014;73(10):933-47.